OPTIMAL CLUSTERING AND INTER-CLUSTER ROUTING IN LARGE-SCALE WIRELESS AD HOC AND SENSOR NETWORKS

A Dissertation
Presented to
The Academic Faculty

By

Deepa Phanish

In Partial Fulfillment
of the Requirements for the Degree
Doctor of Philosophy in the
School of Electrical and Computer Engineering

Georgia Institute of Technology

December 2017

OPTIMAL CLUSTERING AND INTER-CLUSTER ROUTING IN LARGE-SCALE WIRELESS AD HOC AND SENSOR NETWORKS

Approved by:

Professor Edward J. Coyle, Advisor
School of Electrical and Computer Engineering
Georgia Institute of Technology

Dr. Randal T. Abler
School of Electrical and Computer Engineering
Georgia Institute of Technology

Professor Raghupathy Sivakumar
School of Electrical and Computer Engineering
Georgia Institute of Technology

Professor Henry L. Owen III
School of Electrical and Computer Engineering
Georgia Institute of Technology

Professor Mostafa H. Ammar
School of Computer Science
Georgia Institute of Technology

Date Approved: November 13, 2017

To my parents and Phanish

ACKNOWLEDGEMENTS

First and foremost, I want to thank my advisor Prof. Edward J. Coyle for his invaluable support, guidance and encouragement throughout my Ph.D. study. Working with him has been a great learning experience. Discussions on both research and life over the years have certainly shaped my way of thinking. His optimistic outlook towards research, enthusiasm towards education and care towards students continue to inspire me. I want to thank him and Dr. Abler for providing me with the opportunity and guidance to interact with and mentor several undergraduate students through the Vertically Integrated Projects (VIP) program. I want to thank my other committee members Prof. Raghupathy Sivakumar, Prof. Henry Owen, and Prof. Mostafa Ammar. I want to thank Prof. George Riley for previously being on my committee. Their advice and comments have helped me to improve my dissertation. I also want to thank Prof. Bonnie Ferri for the interactions we had when I was teaching ECE 2020.

I have had the privilege to interact with many current and past members of the research group. I would like to acknowledge fellow graduate students Ghaith Matalkah, Paul Garver, Seksan Laitrakun, and Xinjun Dong. I would like to acknowledge all the undergraduate students in the VIP program who were part of the sensor networks team. In particular, I want to thank Tal Landes, and Jialin Wang (James) with whom I worked closely over several years. I want to thank Jaison George, my officemate over the last year for being a great company.

I am grateful to have a wonderful family. I would like to thank my parents and my sister for their love and support. They have nurtured my interests and always supported me in my endeavors. I also want to thank my parents-in-law for their continued support. Last but certainly not the least, I owe many thanks to my husband Phanish for sharing the joys and frustrations over these years. Apart from the useful discussions, firstly he kindled my interest for research and then continues to inspire me with his ideas everyday.

TABLE OF CONTENTS

LIST OF TABLES

LIST OF FIGURES

SUMMARY

A large number of small sensing devices connected together with low-power wireless transceivers can be used to effectively monitor various environments. However, these devices can have only limited energy reserves. Therefore, the network needs to be designed for energy-efficient gathering of the sensed signals and their integration. Clustering of nodes into groups can significantly save energy by aggregating local information to reduce the total communication cost. Further, multiple levels of clustering offers the scalability that is essential to large-scale ad hoc and sensor networks. The optimality of a multi-level network largely depends on two design variables: 1) The number of levels, and 2) The number of nodes operating at each level. We characterize these variables within a multi-hop, multi-level hierarchical network of variable size that gathers and aggregates data at each level. Our network communication cost model (EEHC-VA) is parameterized by the size of the data forwarded at each level. We minimize the communication cost to obtain the optimal probabilities of distributed and independent selection of level-(n+1) nodes from level-n nodes. Interestingly, we have identified intervals—based on the number of nodes and aggregated data sizes—within which single- or two-level hierarchies are optimal. The results have been numerically verified for a wide range of parameters and validated with network simulations. Finally, the impact of these results on the network architectures is discussed for selected applications and aggregation schemes.

When wireless networks are hierarchically clustered for energy-efficiency, the subsequent long-range communications from the central clusterheads cause large-scale interference and energy-hole problems around them. It is thus better to have packets forwarded via short-range multi-hop routes between the clusterheads at different levels of the hierarchy. In order to discover the most optimal routes that serve the purpose, we have analyzed the paths that minimize the inter-cluster routing delay within latticed clusters. Consequently, a low-delay, energy-balancing distributed algorithm for routing across clusters and between

levels is developed, which outperforms shortest path routing in high throughput networks. Further, a parametric study comprising large-scale network evaluations is performed by developing an NS-3 based simulator for clustered wireless networks.

Also, as a step towards achieving a large-scale deployable testbed, we discuss the design, development, and deployment of an inexpensive, power-efficient, clustered, and scalable wireless sensor network (WSN). The testbed operates in a harsh environment in which neither GPS nor internet connectivity are available. We use this testbed to collect real-time data during football games and other major events at Bobby Dodd stadium at Georgia Tech. The sensing devices in the testbed are synchronized without GPS or beacons, yet achieve sufficient accuracy to support modal analysis and detect if the stands are experiencing torsion. We have also developed a cognitive radio backhaul link to establish communication between the WSN in the stadium and a server in our lab. We present in detail the architecture, hardware components, and embedded software of the structural health monitoring platform. We also provide data collected during recent football games to verify the accuracy of the new synchronization algorithm and demonstrate that crowd behavior, such as rhythmic stomping, can be detected during a game.

CHAPTER 1
INTRODUCTION

Sensor and ad hoc networks have been of interest to researchers for over three decades. What originated in defense—as surveillance systems with a few devices—quickly gained importance when a wide range of unique applications were identified [1]. These wireless network applications span many fields, including automation, environment monitoring, event detection, signal estimation, localization, object tracking and classification [2]. Subsequent advances in micro-electro-mechanical systems (MEMS) technology have allowed for the realization of some of the aforementioned applications. Specifically, deployed and tested systems of $O100$) nodes include PinPtr, macroscope of redwood, MAX, CentWits, Cyclops, ZebraNet and VigilNet, as outlined in the review literature [3]. Following the evolution of projects like SmartDust [4], PicoRadio [5] and WINS [6] that attempted to build low-cost and reduced-size nodes, the latest efforts towards large-scale deployments include GreenOrb [7], Trio [8], WISEBED [9], SensLAB [10], and ExScal [11]. Notably, ExScal deployed nearly 1000 nodes performing intruder detection. See Reference [12] and the references therein for further details on recent developments. Indeed—with the conceptualization of the Internet of Things (IoT)—it is presently desirable to have dense networks with more than 10,000 nodes. Nevertheless, reliability, scalability and energy-efficiency of ad hoc and sensor networks continue to remain ongoing concerns. Novel and collaborative analytical, computational and experimental tools have to be developed to further the study and design of large scale sensor networks.

Extensive research efforts over the last several years have been directed towards building power-aware wireless sensor and ad hoc networks. These include finding low-power sensing technology, developing novel distributed signal processing schemes, and designing new protocols for channel access control, routing, security, and synchronization [13, 14,

15]. Clustering of nodes is of particular interest since it offers many advantages such as keeping communication local when appropriate and providing energy efficient strategies for collecting/distributing data from/to a large numbers of nodes [16]. Clusters provide the infrastructure necessary to employ novel schemes for distributed signal processing and aggregation [17].

The combination of clustering and the hierarchical routing it implies, offers scalability that is essential for the realization of large-scale networks. For the same reason, nearly all the aforementioned large-scale deployments are hierarchical in nature. With the ever growing size of microsensor networks, multi-level clusters will play a key role in solving issues related to both scalability and energy-efficiency [18, 19]. Further, when all the nodes including clusterheads are homogeneous and have the same range of communication, deployment is easier, interference problems are eased and the network can be truly scalable and reconfigurable. In this case, multiple levels coupled with well designed hop-by-hop routing schemes can also achieve more uniform energy expenditure, thereby circumventing the "energy hole" problem around the clusterheads [20] and improving the network lifetime.

1.1 Evolution of clustering algorithms

To date, several clustering algorithms have been designed for wireless sensor/ad-hoc networks, each incorporating new ideas that make a network more efficient, scalable and realizable. We refer the reader to the review articles [21, 18, 17, 16, 22, 19] for specific details. The earlier class of algorithms including the Linked Cluster Algorithm (LCA) [23], the Weighted Clustering Algorithm (WCA) [24], and the Distributed Clustering Algorithm (DCA) [25] were heuristic in nature, electing clusterheads based on node characteristics, node-id, number of neighbors, residual energy, transmission power etc. These algorithms had $O(n)$ complexity, where n is the number of nodes. They were followed by cluster optimization schemes, such as the Max-Min d-cluster algorithm [26] which minimizes the

total number of clusters in the network. These earlier schemes adopted the graph-theoretic approach in their network model.

Since the evolution of wireless sensor networks is restricted by limited energy reserves, the focus of the optimization schemes shifted towards minimizing the energy consumption and maximizing network lifetime. Such distributed clustering schemes of reduced complexity designed for data gathering networks include LEACH [27, 28], PEGASIS [29], ANDA [30] and HEED [31]. However, these models make significant assumptions about communication power-control capabilities and/or topology awareness. Furthermore, they generate one-hop clusters, which are not practical in large-scale microsensor networks on uneven terrain. For this reason, multi-hop clustering schemes like DWEHC [32] and M-LEACH [33] were developed. DWEHC assigns weights to nodes based on their energy reserve and proximity to their neighbors. The clusterheads are then elected based on these weights while assuming location awareness. M-LEACH minimizes the cost incurred by the electronics, amplifier and channel for transmitting and receiving data. Although multi-hop, both schemes consider only a single level of hierarchy. On the flip side, EEMC [34] considers multiple levels of hierarchy but single-hop clusters. EEMC also assumes location awareness at the nodes, power control capabilities, and equal data sizes at all the levels. These latter models use classical communication theory to model the energy cost being minimized.

The Energy Efficient Hierarchical Clustering (EEHC) [35] algorithm minimizes the communication cost within a multi-hop multi-level network without making assumptions on power control or location awareness (Table 1.1). EEHC offers a base model derived from stochastic geometry, an analytical approach recently applied to the study of wireless networks [36]. Unlike other approaches, stochastic geometry and random geometric graphs can account for the high level of uncertainty of node location, channel quality, etc. present in large wireless networks when compared to point-to-point systems.

Other recently evolving alternative approaches towards energy-efficient clustering—

Table 1.1: Comparison of Cluster Optimization Energy Models

Model	Levels of Hierarchy	Communication to Clusterhead	Communiation to Processing center	Power Control	Location awareness	Aggregation at the clusterhead
LEACH	single-level	single-hop	direct	yes	no	full
M-LEACH	single-level	multi-hop	direct	yes	no	full
EEMC	multi-level	single-hop	direct	yes	yes	full
EEHC	multi-level	multi-hop	multi-hop	no	no	full
EEHC-VA[a]	multi-level	multi-hop	multi-hop	no	no	variable

[a]proposed model

although not directly related to this work—include unequal clustering [37, 38], particle swarm/colony based optimization [39, 40], genetic algorithms [41], fuzzy logic approaches [42], and multi-metric optimization [43].

In this thesis, we study the optimal design of multi-hop multi-level hierarchical clusters alongside developing new analytical, computational and experimental frameworks for large-scale networks:

1.2 Optimal multi-level clustering

Sensor networks are limited by their battery reserves. Hence, an energy-efficient design is critical to improving network lifetime. The system architecture has to be tailored to minimize the communication cost, which constitutes a predominant factor in the total energy requirement. Often, a fixed number of levels is assumed and the number of nodes operating at each level is optimized. However, there is no prescriptive guide for the optimal number of levels to be implemented. Further, existing cluster optimization models consider "full aggregation, where a unit of data gathered from all the nodes within a cluster is aggre-

gated at the clusterhead, resulting in a single unit only. This assumption limits the class of applications the cost model can represent.

In Chapter 2, we optimize both variables: 1) The number of levels, and 2) The number of nodes operating at each level within a multi-hop, multi-level hierarchical network of variable size that gathers and aggregates data at each level. We have introduced the EEHC-VA stochastic model which unifies the study of the different classes of applications. By considering variable aggregation at the clusterhead, the aggregated data size can be any number of units that independently vary at each level.

1.3 Optimal inter-level routing

In a majority of clustering schemes the clusterhead communicates directly with the base station and/or other clusterheads. This requires careful assembly of nonhomogeneous devices and risks network connectivity in uneven terrains. Moreover, the long-haul communications create an energy hole and a large interference footprint around the clusterhead. The above drawbacks can be overcome by adopting multi-hop routes for the inter-cluster communications. Multi-hop route design for inter-cluster communication is an uncharted territory in homogeneous sensor networks. A low-delay and energy-balancing inter-level routing scheme needs to be designed for achieving reliable and long-lasting service.

In Chapter 3, we present an analytical framework for visualizing large-scale networks as surfaces as opposed to graphs in optimizing routing paths. The inter-level routes are optimized to reduce the mean end-to-end total time rather than the conventional number of hops, by accounting for the time wasted in unsuccessful attempts for channel access. The systems view of the network results in an AODV-like distributed algorithm that is easy to implement.

1.4 Environment monitoring testbed

A real system is necessary to conduct experiments and validate the assumptions. A deployable testbed for long-term synchronized data collection is yet to be achieved. Existing wireless structural health monitoring platforms lack accurate synchronization of measurements. They have a comparatively reduced lifetime due to higher standby power consumption and do not support operation of the network from a remote server.

In Chapter 4, as a step towards achieving a large-scale testbed, we discuss the the design, development, and deployment of an inexpensive, power-efficient, clustered, and scalable wireless sensor network. The structural health monitoring cluster is test deployed at the Bobby Dodd stadium to collect vibration data remotely during the games. The signals from multiple locations are synchronized with a GPS- and beacon-free algorithm.

Finally, we conclude in Chapter 5 with a short discussion summarizing the scope for future work.

CHAPTER 2

APPLICATION-BASED OPTIMIZATION OF MULTI-LEVEL CLUSTERING

2.1 Introduction

Existing cluster optimization studies such as EEHC [35] and LEACH [27] consider "full aggregation", where a unit of data gathered from all the nodes within a cluster is aggregated at the clusterhead, resulting in a single unit only. The resulting unit is forwarded to the next higher level clusterhead or the processing center. This assumption limits the class of applications the cost model can represent. For instance, in an event detection application, forwarding a single decision bit along the levels of the hierarchy could be sufficient. However, typically, multiple bits are necessary in order to include performance statistics or location information [44]. In applications monitoring spatial-temporal variation of state variables in a multi-sensor environment, the data may accumulate along the hierarchy, the size of which is determined by the signal processing schemes and sensing systems in place [45]. On the other hand, in data mining applications, the forwarded data size reduces at each level of the hierarchy [46, 47]. Therefore, all of these classes of applications need to be unified by incorporating parametric data sizes into the network model. We can then consider "variable aggregation" at the clusterhead, where the aggregated data size can be any number of units that independently vary at each level. This would expand the horizon of applications that energy-efficient clustering algorithms encompass. Furthermore, it is important to understand the impact of forwarded data sizes—in addition to the network size—on the optimality of the multi-level cluster design. However, this has not been previously considered in literature. Motivated by this, we study two multi-level cluster design questions that are critical to achieving energy-efficient algorithms:

1. What probability for choosing clusterheads is optimal at each level in order to mini-

mize the total communication cost?

2. What is the optimal number of levels in the hierarchy for a given size of and other characteristics of the network?

The first question: What is the ideal number of clusters, i.e., the number of clusterheads, at each level? This has been studied, for example, in LEACH [27, 28] where a closed form solution is provided for a single level of hierarchy, albeit in a significantly different network model with fixed data sizes for all transmissions. A comparison of the proposed EEHC-VA model with other energy models serving distributed cluster optimization is shown in Table 1.1. Multi-level network design necessitates further tailoring of the architecture based on the application and aggregation scheme in place. Therefore in this work, we study the formulated communication cost for multiple hierarchies and variable data sizes. Specifically, we show that a unique minimum exists for the cost functional in single- and two-level hierarchies as solutions of polynomial equations that allows for the easy computation of the optimal solution of an otherwise complex minimization problem.

The second question: How many levels are necessary/sufficient? Although a number of multi-level protocols have been proposed for sensor and adhoc networks [48, 34, 49, 50, 51, 52], only a few analytical studies have been persued. Certain protocols are indeed designed to dynamically adjust the number of levels. For example, in the hierarchical protocol for mobile wireless networks [53], the clusters split and merge to minimize the number of levels while simultaneously bounding the cluster size. In scalable ad-hoc routing [50], depth of the hierarchy is dynamically adjusted in response to the changing network topology. An analysis for computing the optimum number of levels in computer networks was pioneered by Kleinrock et. al. [54, 55]. The results show that the optimal solution minimizing the size of the routing database varies as the logarithm of the number of nodes. Another study to this end—pertaining to multi-level wireless sensor networks—is provided with the EEMC algorithm [34]. The authors have shown that the approximated optimal number of levels is $O(\log \log n)$ given n nodes. In this work, we have derived very distinct intervals on the

number of nodes within which only a single level or only two-levels of clustering are sufficient. In contrast to other studies, these intervals are governed by the application and its implementation, which together specify the size of forwarded data at each level. With an intent to provide a reference guide for design engineers, we provide a decision tree guiding the choice amongst single level, two levels and three levels of hierarchy.

Tailoring the system architecture to minimize the communication cost, which constitutes a predominant factor in the total energy requirement, is of our primary interest. Work presented in this chapter builds on the framework of Energy-Efficient Hierarchical Clustering (EEHC) algorithm designed by Bandyopadhyay and Coyle [56, 35]. The communication cost model in EEHC is a fitting choice for the subject matter of this chapter, since it is—unlike other clustered network models—scalable and analytically tractable for multiple levels of hierarchy. The primary contributions of this chapter include:

- Extension of the EEHC data gathering communication model to include independent data sizes up through the levels of hierarchy along with the generalizations of the shape of the deployment area and the location of the processing center.

- Analytical results on the optimal clusterhead election probabilities for multi-level networks. These parameters are critical to distributed clustering algorithms and the results provide a fast and robust alternative to the computationally very expensive numerical optimization methods that are often sensitive to the initial guess.

- Derivation of thresholds on the number of nodes that determine the optimal number of levels in multi-level hierarchical clusters.

- The above results on optimal probabilities for clusterhead selection and the number of levels are parameterized by both the aggregated data sizes that are forwarded and the number of nodes in the network.

- Design considerations for selected classes of data gathering applications.

The importance of such generalizations and analysis within the EEHC framework has been recognized but not performed since it has been considered relatively complex [34]. The focus of this chapter is to establish a new framework for the analysis of *multi-hop, multi-level* hierarchical clusters with possibly different degrees of data aggregation at each level, a scenario not priorly considered (Table 1.1)[1]. The results in this chapter can be used directly within the EEHC distributed clustering algorithm.

The rest of the chapter is organized as follows: Section 2.2 starts with the definitions and assumptions pertaining to our model and the formulation of the cost objective incorporating parameterized data-sizes. In Section 2.3, we derive the conditions for the existence of optimal probabilities of clusterhead selection and their solutions in single- and two-level hierarchies. In Section 2.4, we analyze the desirable number of levels, given the number of nodes and the aggregated data sizes. We corroborate our results using numerical validation and simulation results presented in Section 2.5. Finally, we discuss inferences related to selected application cases in Section 2.6.

2.2 Communication cost in multi-hop multi-level clusters

The architecture of the hierarchically clustered network considered in this chapter is shown in Figure 2.1. It is a multi-hop, multi-level, data gathering network. The illustration shows two levels of clustering before data is sent to the processing/fusion center. Notably, it is a homogeneous ad hoc network where all the nodes, including clusterheads (CHs), have the same fixed range of communication. Consequently, the routes between CHs on consecutive levels is multi-hop via the end (level-0) nodes. Further, the amount of data routed at any level is variable and independent of other levels. To model the total communication cost, we make the following assumptions:

1. The nodes are distributed according to a homogeneous spatial Poisson process with

[1]Table 1.1 shows representative algorithms that optimize different classes of networks. Although comparison of the EEHC-VA model to other algorithms would be desirable, it would be very difficult because of the substantial differences between them.

intensity λ in a 2D space of area $A = ca^2$.

2. The communication cost increases linearly with the data size.

The architecture we have considered has hop-by-hop routes, both within a cluster and between the CHs of any two levels, as demonstrated in Figure 2.1. In this case: (i) The range of communication r is a fixed constant. (ii) The energy required to transmit (ϵ_{TX}) and receive (ϵ_{RX}) a unit of data over one hop—although determined by the the electronics—are also fixed constants. (iii) The true length of the multi-hop shortest route (L_r) can be approximated to the scaled Euclidean distance between the source and destination (L_e). In fact, the scaling factor between their means has been shown to be $4/\pi$ [57]. Approximating the hop length to the range of communication r, the total cost of communicating a unit of data over a route of length L_r is (# hops)*(Energy per hop) = $\frac{\frac{4}{\pi}L_e}{r}(\epsilon_{TX} + \epsilon_{RX})$. By eliminating the scaling factors, minimization of the total communication cost reduces to the minimization of the sum of the Euclidean distances.

When the level-i CHs are chosen independently from level-(i-1) CHs with probability p_i (the "clusterheads" on "level 0" are indeed all the nodes in the network), their locations are governed by the thinned homogeneous spatial Poisson process $\mathbf{PP}1_i$ of intensity $\lambda_{1i} = \lambda \prod_{j=1}^{i} p_j$. The non-CHs of level-i are also governed by a thinned Poisson process $\mathbf{PP}0_i$ of intensity $\lambda_{0i} = \lambda_{1(i-1)} - \lambda_{1i}$. Suppose L_i is the total length of all the segments connecting the points of $\mathbf{PP}0_i$ process to the nearest point of a $\mathbf{PP}1_i$ process, then [58]

$$\mathbb{E}[L_i] = \frac{\lambda_{0i}}{2\lambda_{1i}^{3/2}} = \frac{(1-p_i)}{2p_i\sqrt{\lambda \prod_{j=1}^{i} p_j}} \tag{2.1}$$

Since the expected total number of level-i CHs $\mathbb{E}[TCH_i] = \lambda_{1i}A$, the expected communication cost to gather a unit of data from all the nodes of level $i < h$ at their respective CHs

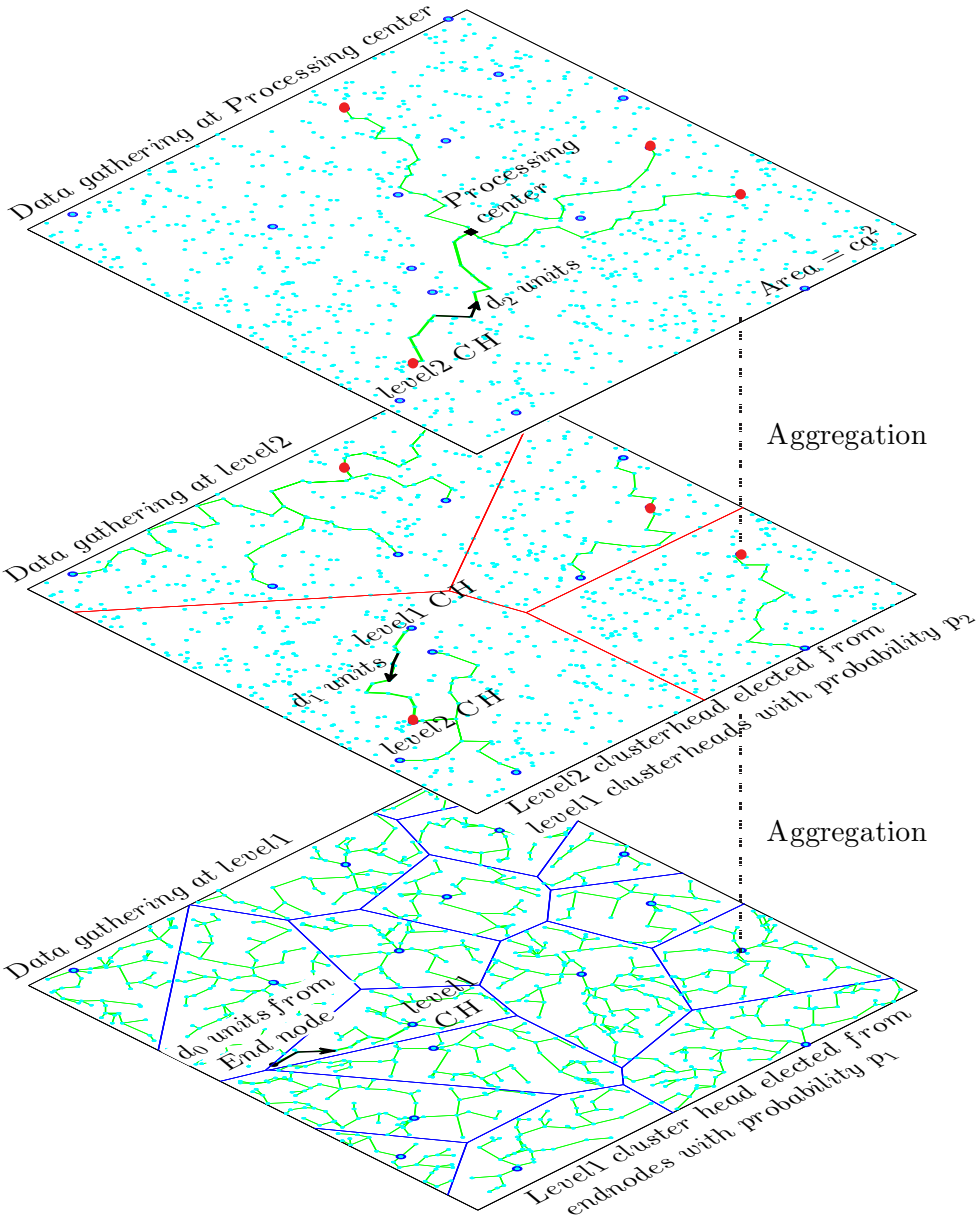

Figure 2.1: Architecture of a multi-hop, two-level data gathering clustered network. The clusterheads (CHs) at level-1 are chosen independently from the end nodes. Similarly, the CHs at level-2 are chosen independently from the level-1 CHs. A level-1 cluster consists of end nodes and their associated level-1 CH. A level-n cluster consists of the level-$(n-1)$ CHs and their associated level-n CH $\forall n > 1$. Association of the respective nodes to their nearest CH results in the Voronoi tessellations shown in both levels. The amount of data generated by the nodes at any level are independent of that at the other levels; i.e., each end-node sends d_0 units to its respective level-1 CH, each level-1 CH sends d_1 units to its respective level-2 CH, which, in turn, sends d_2 units to the processing center.

Table 2.1: Scaling factor ρ for a specified location of the processing center

Deployment region $A = ca^2$	Processing center location	ρ'	$\rho = \frac{2\rho'}{\sqrt{c}}$
Square $2a \times 2a$	Center	0.765	0.765
Square $2a \times 2a$	Corner	1.530	1.530
Rectangle $2a \times 4a$	Center	1.186	0.838
Rectangle $a \times 2a$	Corner	1.186	1.677
Circle radius a	Center	0.666	0.751

in a network with h levels of hierarchy is given by [35]:

$$\mathbb{E}[C_i] \approx \mathbb{E}[L_i]\,\mathbb{E}[TCH_i] = \lambda A(1-p_i)\left[\prod_{j=1}^{i-1} p_j\right]\left[\frac{1}{2\sqrt{\lambda \prod_{j=1}^{i} p_j}}\right] \tag{2.2}$$

The above approximation due to the bounded area over which the nodes are distributed is better as the number of nodes increases. The network simulations provided in Section V.B verify that it accurately models the cost when $\mathbb{E}[TCH_i] \geq 1$.

The expected distance between a node in a region of area $A = ca^2$ and the processing center at the origin is given by

$$\mathbb{E}[D] = \frac{1}{A}\iint_A \sqrt{u^2+v^2}\,du\,dv = \rho' a \tag{2.3}$$

where ρ' for various reference cases are computed in Table 2.1. Therefore, the additional cost of communicating a unit of data from the CHs at level h to the processing center is

$$\mathbb{E}[C_h] = \mathbb{E}[TCH_h]\,\mathbb{E}[D] = \lambda A\left[\rho' a \prod_{i=1}^{h} p_i\right] \tag{2.4}$$

For an absolute aggregation at the CHs, the number of data units transmitted at any level-i, d_i, is same as the number of data units generated by the end nodes, d_0. But, for any partial aggregation scheme, $d_i > d_0 \quad \forall\ i = 1,2,...h$. The aggregated data size is pre-determined and independent of cluster size within a broad class of data fusion algorithms. Assuming a linear scaling of the communication cost with the data size, $\mathbb{E}[C_i]$ is

Table 2.2: Notations and definitions

Notation	Definition
n	Number of nodes
$A = ca^2$	Area of deployment
λ	Density of nodes
h	Number of levels of hierarchy
$\rho' a$	Expected distance from a node to the processing center
C	Total communication cost for gathering data
f	Cost objective function parameterized by n
$\widehat{p_i}$	i^{th} coordinate of the critical point of f
$p_i^\star$	i^{th} coordinate of the unconstrained minimum of f
p_i^{min}	i^{th} coordinate of the constrained minimum of f in $(0, 1)$
d_0	Number of data units generated by the end node
d_i	Number of data units forwarded by the level-i CH
$\alpha_i = \frac{d_i}{d_0}$	Data ratio variable at level-i
α, β, γ	Deterministic values taken by the data ratios α_is

pre-multiplied by d_i. Therefore, the total communication cost of collecting data from all the nodes and forwarding the aggregated data to the processing center follows from Eqn. 2.2 and Eqn. 2.4, given by

$$\mathbb{E}[C] = \sum_{i=1}^{h} \mathbb{E}[C_i] = \lambda A \left[\sum_{i=1}^{h} \frac{d_{i-1}(1-p_i) \prod_{j=1}^{i-1} p_j}{2\sqrt{\lambda \prod_{j=1}^{i} p_j}} + \rho' a d_h \prod_{i=1}^{h} p_i \right] \tag{2.5}$$

The symbols used in the rest of the chapter and their definitions are summarized in Table 2.2. The optimal number of levels and the optimal probabilities of choosing the CHs that minimize $\mathbb{E}[C]$ are studied in relation to the number of nodes n and the data ratios $\alpha_i = d_i/d_0$ within the hierarchy. Note that we are minimizing only the communication cost for successful transmissions in the network. In addition to $\mathbb{E}[C]$, idle energy at the nodes and data retransmissions constitute the total communication cost. However, both of these factors largely depend on the protocols in place for medium access control and hop-by-hop routing. For instance, a synchronized spatially sampled data gathering scheme [59] can

effectively minimize this overhead. However, a system-level reduction in the number of transmissions favorably reduces interference, idle energy and retransmissions as well.

2.3 Optimal probabilitites of electing clusterheads

The goal is to choose the probabilities p_i of electing clusterheads (CHs) at levels $i = 1,2,...h$ that minimize $\mathbb{E}[C]$. This is formulated as a constrained optimization problem:

$$\left(p_1^{min}, p_2^{min}, ..., p_h^{min}\right) = \underset{p_1,p_2,...,p_h}{\arg\min}\, \mathbb{E}[C] \quad s.t. \quad 0 \leq p_1, p_2, ..., p_h \leq 1 \tag{2.6}$$

For a given number of nodes n, we have $\lambda = \frac{n}{A} = \frac{n}{ca^2}$. In this new perspective, the optimal probabilities p_i^{min} are viewed as functions of n, making further analysis tractable.

$$\min_{p_1,p_2,...,p_h} \mathbb{E}[C] = \min_{p_1,p_2,...,p_h} f(p_1, p_2, ..., p_h) \tag{2.7}$$

where the cost objective f parameterized by n is given by

$$f(p_1, p_2, ..., p_h) = \sum_{i=1}^{h} \frac{\alpha_{i-1}(1-p_i)\prod_{j=1}^{i-1} p_j}{\sqrt{\prod_{j=1}^{i} p_j}} + \rho\alpha_h \sqrt{n} \prod_{i=1}^{h} p_i \tag{2.8}$$

Here $\rho = \frac{2\rho'}{\sqrt{c}}$ (Table 2.1) and the "data ratio" $\alpha_i = d_i/d_0$ is the ratio of the number of data units forwarded by each CH on level i to the number of data units generated at each end node ($\alpha_0 = 1$). Suppose that each end node sends 1 unit of data to its level-1 CH. Then, each level-1 CH sends α_1 units of data to its level-2 CH, and each level-2 CH sends α_2 units of data to its level-3 CH, and so on. The level-h CHs at the top all send α_h units of data to the processing center. It is assumed that $\alpha_i \geq 1$; i.e., the size of the aggregated data at the CH at any level d_i is at least the size of data d_0 generated by an end node. However, it is still possible to have $\alpha_{i+1} < \alpha_i$, $\alpha_{i+1} = \alpha_i$ or $\alpha_{i+1} > \alpha_i$. Figure 2.2 demonstrates how

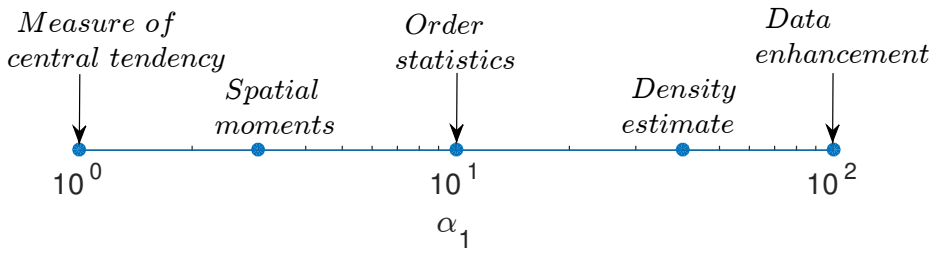

Figure 2.2: An example of the variation of the data ratio with the statistical processing schemes: Consider a unit of data gathered from air-quality monitoring CO_2 sensors in a cluster. The aggregated data can be either the mean/median/mode, first- and second-order geometric moments, the ten highest values, or a histogram with 40 bins. Even supplementary temporal data sensed between successive rounds can be appended at the clusterhead. Further, the data size at the next level clusterhead could be smaller, equal, or larger depending on whether there is a decision, a pooled estimate or enhancement, respectively.

α_is vary with the application requirements.

In this section, we perform an unconstrained optimization of $\mathbb{E}[C]$ for $h = 1$ and $h = 2$ and derive the conditions on α_i for which the critical solution satisfying the derivative test is unique and is a minimum within constraints. Note that in the rest of the chapter p_i^{min} denotes the value of the constrained minimum, whereas $p_i^\star$ denotes the value of the unconstrained minimum.

$$\left(p_1^\star, p_2^\star, ..., p_h^\star\right) = \underset{p_1,p_2,...,p_h}{\arg\min}\ \mathbb{E}[C] = \underset{p_1,p_2,...,p_h}{\arg\min}\ f \tag{2.9}$$

2.3.1 Optimal probability of electing clusterheads in a single-level cluster

In single-level clustering, i.e. $h = 1$, the data collected by the CH from the end nodes within its cluster is aggregated and forwarded to the processing center. From Eqn. 2.5,

$$\mathbb{E}[C] = \lambda A \left[\frac{d_0(1-p_1)}{2\sqrt{\lambda p_1}} + \rho' a d_1 p_1\right] \tag{2.10}$$

Following Eqn. 2.7, for a given number of nodes n we have,

$$\min_{p_1} \mathbb{E}[C] = \min_{p_1} \left[\frac{1-p_1}{\sqrt{p_1}} + \rho\alpha_1 \sqrt{n} p_1 \right] \tag{2.11}$$

$$p_1^\star = \arg\min_{p_1} \mathbb{E}[C] \tag{2.12}$$

Theorem 1. *In a single level hierarchical cluster, there exists a unique $p_1^\star$ that minimizes $\mathbb{E}[C]$. Further, $0 < p_1^\star < 1$ when $\rho\alpha_1 \sqrt{n} > 1$.*

Proof. Defining $d = \rho\sqrt{n}$, the objective function f (Eqn. 2.8) and its derivative are given by,

$$f(p_1) = \frac{1-p_1}{\sqrt{p_1}} + \alpha_1 d p_1 \tag{2.13}$$

$$f'(p_1) = -\frac{1+p_1}{2p_1\sqrt{p_1}} + \alpha_1 d \tag{2.14}$$

Let $\widehat{p}_1$ be the critical solution satisfying the first order criterion. This results in the cubic equation:

$$f'(\widehat{p}_1) = 0 \implies 2\alpha_1 d x^3 - x^2 - 1 = 0 \tag{2.15}$$

where $x = \sqrt{\widehat{p}_1}$. The polynomial $2\alpha_1 d x^3 - x^2 - 1$ has a single real-valued root and the root lies in $(0,1)$ when $\alpha_1 d > 1$ (Appendix A.1). Therefore, $\widehat{p}_1 \in (0,1)$ for $\alpha_1 d > 1$. Further, $\widehat{p}_1$ satisfies the second order criterion, showing that it is indeed a minimum.

$$f''(\widehat{p}_1) = (3+\widehat{p}_1)/(4\widehat{p}_1^2\sqrt{\widehat{p}_1}) > 0 \quad \forall \widehat{p}_1 \in (0,1)$$

$$\implies \widehat{p}_1 \text{ is a minimum}$$

Hence, $p_1^\star = \widehat{p}_1$ and $p_1^\star \in (0,1)$ when $\rho\alpha_1\sqrt{n} > 1$. ∎

Corollary 1. *When $\rho\alpha_1\sqrt{n} > 1$, the optimal probability of clusterhead election in a single level cluster is given by the square of the real-valued solution of $2\alpha_1 d x^3 - x^2 - 1 = 0$ where*

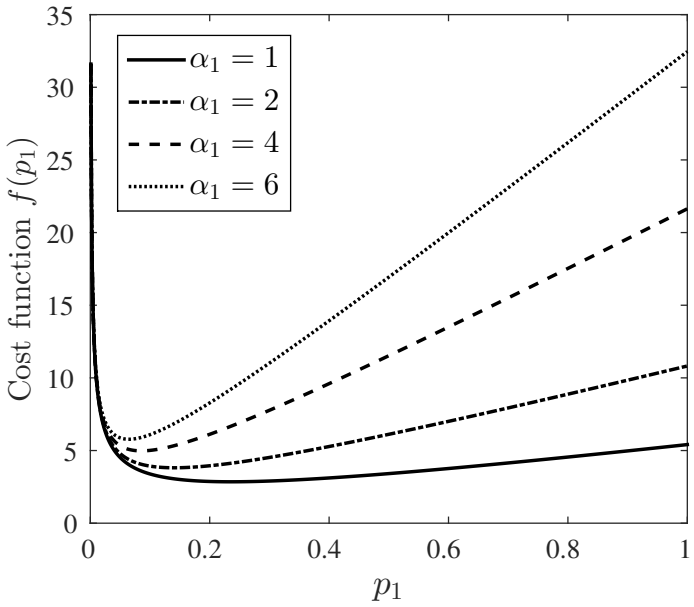

Figure 2.3: Variation of energy objective with the probability of CH election. There are $n = 50$ nodes and $\rho = 0.765$ (processing center located at the center of a square). Note the relatively flat minimum for the data ratio $\alpha_1 = 1$ and the increasing sharpness of it as α_1 increases.

$d = \rho\sqrt{n}$. *Thus,*

$$p_1^{min} = \left[\frac{1}{6\alpha_1 d}\left(1 + \left(1 + 54\alpha_1^2 d^2 + 6\alpha_1 d\sqrt{3(1 + 27\alpha_1^2 d^2)}\right)^{1/3} + \frac{1}{\left(1 + 54\alpha_1^2 d^2 + 6\alpha_1 d\sqrt{3(1 + 27\alpha_1^2 d^2)}\right)^{1/3}}\right)\right]^2 \quad (2.16)$$

Note that the above solution is consistent with Eqn. 11 in [35] when $\alpha_1 = 1$, $\rho = 0.765$ and $n = 4a^2\lambda$. ■

The variation of the objective function f with p_1 (Eqn. 2.13) for different values of α_1 is shown in Figure 2.3. The results indicate that as the aggregated data size decreases, the optimal number of CHs in a network will increase. The reason is that the energy savings from each aggregation is larger. Also, the smaller α_1 is, the less sensitive the energy usage in the network is to variations in the probability of choosing a CH. In other words, because

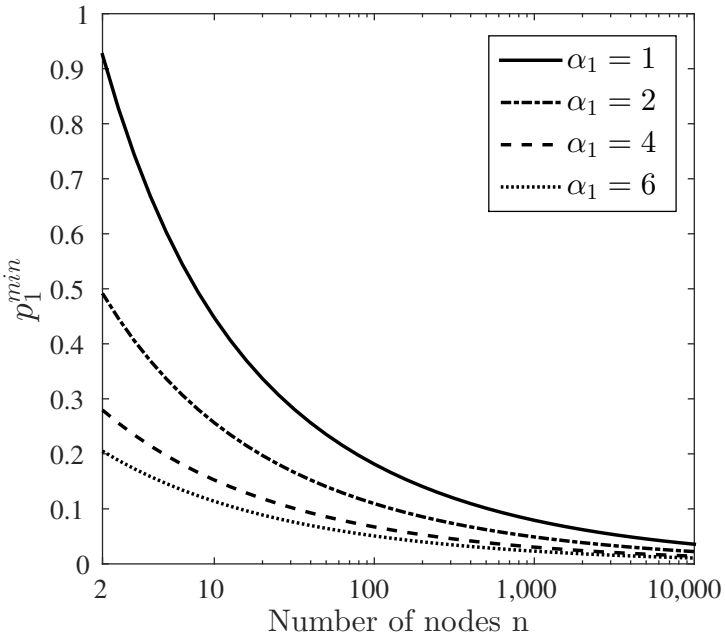

Figure 2.4: The optimal probability of CH election across the different size-scales of a single-level network. Here $\rho = 0.765$ (processing center located at the center of a square).

the minimum is more acute for larger aggregated data sizes, the probability needs to be more accurately implemented within the clustering algorithm. The variation in the cost is more rapid with a variation in the aggregated data size compared to variations due to the number of nodes. Overall, as $\alpha_1 \sqrt{n}$ increases, the minimum communication cost $\mathbb{E}[C]$ increases, the optimal probability of choosing a CH decreases (Figure 2.4), and the network's sensitivity to error in the probability of clusterhead selection increases. Therefore, the reduction in energy with a reduction in the aggregated data size is more pronounced when the size of the network is relatively large.

2.3.2 Optimal probabilities of electing clusterheads in a two-level hierarchical cluster

In two-level clustering, i.e. $h = 2$, the data collected by the level-1 CHs from the end nodes within their clusters is aggregated and forwarded to the level-2 CHs. The level-2 CHs may perform additional aggregation and send the results to the processing center. From Eqn.

2.5,

$$\mathbb{E}[C] = \lambda A\left[\frac{d_0(1-p_1)}{2\sqrt{\lambda p_1}} + \frac{d_1(1-p_2)p_1}{2\sqrt{\lambda p_1 p_2}} + \rho' a d_2 p_1 p_2\right] \tag{2.17}$$

Following Eqn. 2.7, for a given number of nodes n,

$$\min_{p_1,p_2} \mathbb{E}[C] = \min_{p_1,p_2}\left[\frac{1-p_1}{\sqrt{p_1}} + \alpha_1(1-p_2)\sqrt{\frac{p_1}{p_2}} + \rho\alpha_2\sqrt{n}p_1p_2\right] \tag{2.18}$$

$$(p_1^\star, p_2^\star) = \arg\min_{p_1,p_2} \mathbb{E}[C] \tag{2.19}$$

Theorem 2. *In a two-level hierarchical cluster, when* $\rho^2\alpha_2^2 n > \alpha_1^2(2\alpha_1 - 1)$*, there exist unique* $p_1^\star, p_2^\star \in (0,1)$ *that minimize the communication cost* $\mathbb{E}[C]$.

Proof. Defining $d = \rho\sqrt{n}$, the objective function f (Eqn. 2.8) is given by

$$f(p_1,p_2) = \frac{1-p_1}{\sqrt{p_1}} + \alpha_1(1-p_2)\sqrt{\frac{p_1}{p_2}} + \alpha_2 d p_1 p_2 \tag{2.20}$$

A surface plot of f is shown in Figure 2.5. Taking partial derivatives w.r.t. p_1 and p_2, we have

$$\begin{aligned} f_{p_1}(p_1,p_2) &= -\frac{1+p_1}{2p_1\sqrt{p_1}} + \alpha_1\frac{1-p_2}{2\sqrt{p_1p_2}} + \alpha_2 d p_2 \\ f_{p_2}(p_1,p_2) &= -\alpha_1\frac{\sqrt{p_1}(1+p_2)}{2p_2\sqrt{p_2}} + \alpha_2 d p_1 \end{aligned}$$

Let $(\widehat{p_1},\widehat{p_2})$ be the critical solution satisfying the first order criteria $f_{p_1}(\widehat{p_1},\widehat{p_2}) = 0$ and $f_{p_2}(\widehat{p_1},\widehat{p_2}) = 0$. This results in the equations below:

$$y = \frac{\alpha_1(x^2+1)}{2d\alpha_2 x^3} \tag{2.21}$$

$$p(x) = 4\alpha_2^2 d^2 x^7 + \alpha_1^2 x^5 - 2\alpha_1^3 x^4 + 2\alpha_1^2 x^3 - 4\alpha_1^3 x^2 + \alpha_1^2 x - 2\alpha_1^3 = 0 \tag{2.22}$$

where $y = \sqrt{\widehat{p_1}}$ and $x = \sqrt{\widehat{p_2}}$. The above polynomial equation (Eqn. 2.22) has a unique real-valued root in (0,1) for $\alpha_2^2 d^2 > \alpha_1^2(2\alpha_1 - 1)$ (Proof in Appendix A.2). Combined with

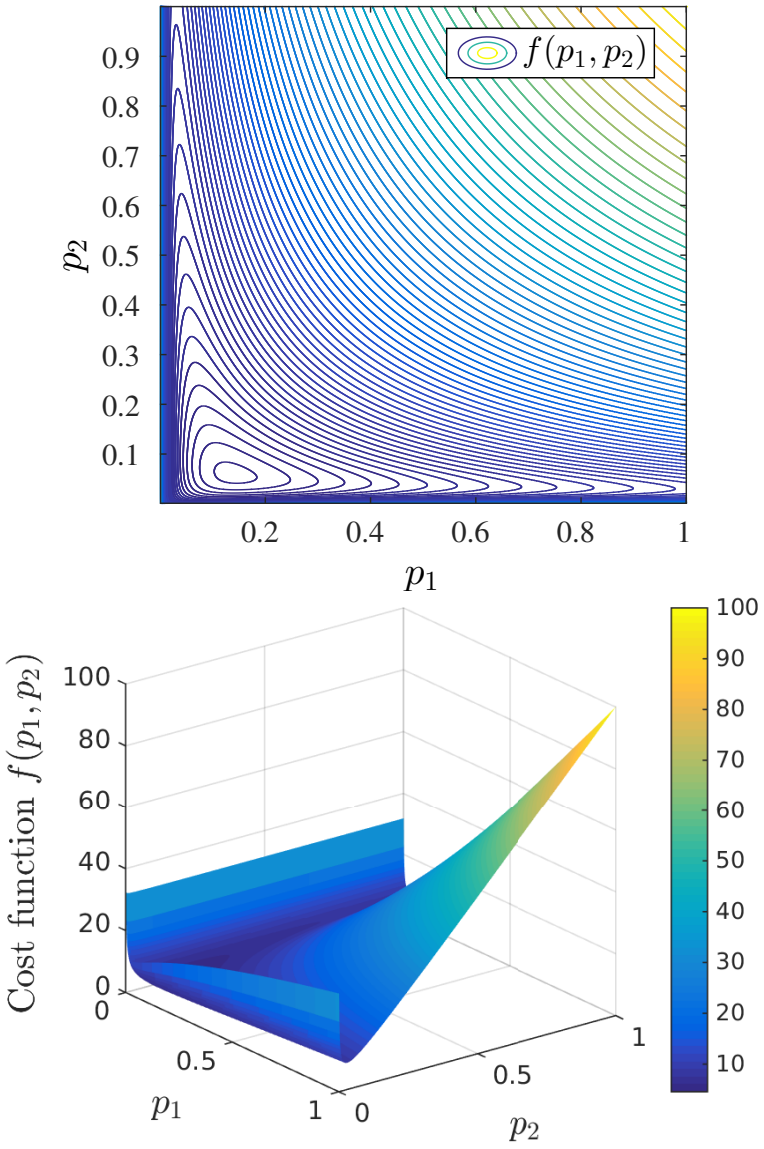

Figure 2.5: The contour and surface plots of a sample objective function $f(p_1, p_2)$ with $d = \rho\sqrt{n} = 100$ and data ratios $\alpha_1 = \alpha_2 = 1$. Note that it is a non-convex surface. The minimum is more acute and gets closer to the origin for higher values of d. Here, the minimum is located at $p_1^\star = 0.138$ and $p_2^\star = 0.059$.

Eqn. 2.21, we have $0 < \widehat{p}_1, \widehat{p}_2 < 1$ (Appendix A.3). We further show that the critical solution satisfies the second order criteria for minimality: $D = f_{p_1p_1} f_{p_2p_2} - f_{p_1p_2}^2 > 0$ and $f_{p_1p_1} > 0$ at $(\widehat{p}_1, \widehat{p}_2)$. Using Eqn. 2.21, D equals

$$\frac{\alpha_2^4 d^4 x^6}{\alpha_1^4 (1+x^2)^4}\left[3\alpha_1 x(3+x^2) + \frac{\alpha_1^3(1+x^2)^2(-4\alpha_1+3x+x^3)}{4\alpha_2^2 d^2 x^6}\right]$$

Since $\alpha_1, \alpha_2, d, x > 0$, in order to show $D(\widehat{p}_1, \widehat{p}_2) > 0$, it is enough to show that the polynomial $g(x) > 0$ where,

$$g(x) = 12\alpha_2^2 d^2 x^9 + (36\alpha_2^2 d^2 + \alpha_1^2)x^7 + 5\alpha_1^2 x^5 - 4\alpha_1^3 x^4 + 7\alpha_1^2 x^3 - 8\alpha_1^3 x^2 + 3\alpha_1^2 x - 4\alpha_1^3$$

Since $g(x) = g(x) - (3x^2+9)p(x)$,

$$g(x) = \alpha_1^2(-2x^7 + 6\alpha_1 x^6 - 10x^5 + 26\alpha_1 x^4 - 14x^3 + 34\alpha_1 x^2 - 6x + 14\alpha)$$

Since $x \in (0,1)$, $x^{n+1} < x^n \ \forall n \in \mathbb{N}$. Therefore, $g(x) > 0 \ \forall \alpha_1 \geq 1$ *i.e.*, $D(\widehat{p}_1, \widehat{p}_2) > 0 \ \forall \alpha_1 \geq 1$. Further,

$$f_{p_1p_1}(p_1, p_2) = \frac{1}{4p_1^2\sqrt{p_1}}\left[3 + p_1 + \alpha_1\sqrt{p_1}(p_2 - 1)\sqrt{\frac{p_1}{p_2}}\right]$$

$$\begin{aligned} f_{p_1p_1}(\widehat{p}_1, \widehat{p}_2) \quad = \quad & \frac{2\alpha_2^3 d^3 x^8}{\alpha_1^5(1+x^2)^5}\Big[12\alpha_2^2 d^2 x^7 + \alpha_1^3 x^6 + \alpha_1^2 x^5 \\ & + \alpha_1^3 x^4 + 2\alpha_1^2 x^3 - \alpha_1^3 x^2 + \alpha_1^2 x - \alpha_1^3\Big] \end{aligned}$$

Since $\alpha_1, \alpha_2, d, x > 0$, in order to show $f_{p_1p_1}(\widehat{p}_1, \widehat{p}_2) > 0$, it is enough to show that the polynomial $h(x) > 0$ where,

$$h(x) = 12\alpha_2^2 d^2 x^7 + \alpha_1^3 x^6 + \alpha_1^2 x^5 + \alpha_1^3 x^4 + 2\alpha_1^2 x^3 - \alpha_1^3 x^2 + \alpha_1^2 x - \alpha_1^3$$

Since $h(x) = h(x) - 3p(x)$,

$$h(x) = \alpha_1^2(\alpha_1 x^6 - 2x^5 + 7\alpha_1 x^4 - 4x^3 + 11\alpha_1 x^2 - 2x + 5\alpha_1)$$

Since $x \in (0,1)$, $x^{n+1} < x^n \ \forall n \in \mathbb{N}$. Therefore, $h(x) > 0 \ \forall \alpha_1 \geq 1$ *i.e.*, $f_{p_1 p_1}(\widehat{p}_1, \widehat{p}_2) > 0 \ \forall \alpha_1 \geq 1$.

Thus, $(\widehat{p}_1, \widehat{p}_2)$ satisfies the second order conditions for minimality, showing that it in fact minimizes $\mathbb{E}[C]$. Therefore, $(p_1^\star, p_2^\star) = (\widehat{p}_1, \widehat{p}_2)$ and $p_1^\star, p_2^\star \in (0,1)$ when $\rho^2 \alpha_2^2 n > \alpha_1^2(2\alpha_1 - 1)$. ■

Corollary 2. *When $\rho^2 \alpha_2^2 n > \alpha_1^2(2\alpha_1 - 1)$ in a two-level hierarchical cluster, the optimal probability of level-2 clusterhead election is given by the square of the real-valued solution x^* of $4\alpha_2^2 d^2 x^7 + \alpha_1^2 x^5 - 2\alpha_1^3 x^4 + 2\alpha_1^2 x^3 - 4\alpha_1^3 x^2 + \alpha_1^2 x - 2\alpha_1^3 = 0$ and the optimal probability of level-1 clusterhead election is given by $\frac{\alpha_1^2 (x^{*2}+1)^2}{4\rho^2 \alpha_2^2 n x^{*6}}$* ■

The behavior of the optimal probabilities (p_1^{min}, p_2^{min}) w.r.t n, α_1 and α_2 is presented in Figure 2.6 and Figure 2.7. At level-1, the optimal number of CHs increases as the data size at either level decreases. However at level-2, the optimal number of CHs increases as the data size at level-1 increases or the data size at level-2 decreases. This shows that it is beneficial to have more first-level CHs in order to exploit the energy savings from reduced-size aggregations not only at that level, but also at higher levels. Likewise, it is beneficial to have more second-level CHs not only when they produce smaller data sizes but also when the size of the data coming from the CHs at the lower level is large.

2.3.3 Optimal probability of electing clusterheads in a h-level hierarchical cluster

In a general h-level hierarchical network, the optimal probabilities of CH election at each level is obtained by minimizing the communication cost $\mathbb{E}[C]$ in Eqn. 2.5. Specifically, for a given number of nodes n, we need to minimize the cost objective f in Eqn. 2.8. By equating the partial derivatives of f w.r.t $p_1, p_2, ..., p_h$ to zero, we obtain the following

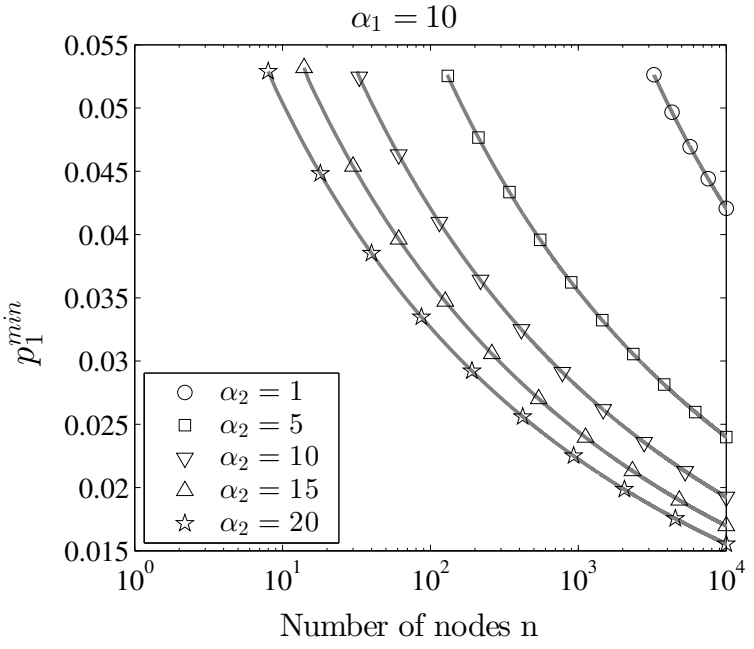

(a)

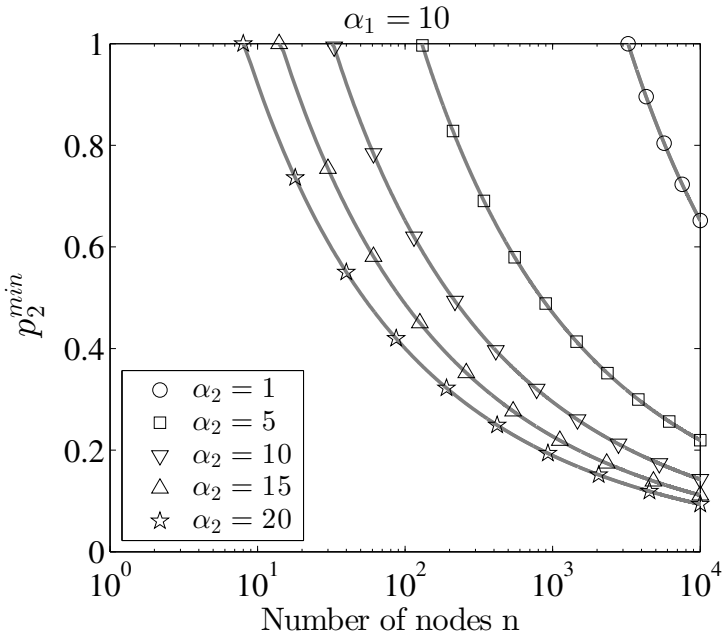

(b)

Figure 2.6: Variation of the optimal probabilities p_1^{min} and p_2^{min} with the number of nodes n, within the region of interest $\rho^2\alpha_2^2 n > \alpha_1^2(2\alpha_1 - 1)$. The plots (a) and (b) depict the variation of optimal probabilities with the data ratio at level-2 $\alpha_2 = d_2/d_0$ for a constant data ratio at level-1 $\alpha_1 = d_1/d_0$.$\rho = 0.765$, corresponding to the processing center located at the center of a square.

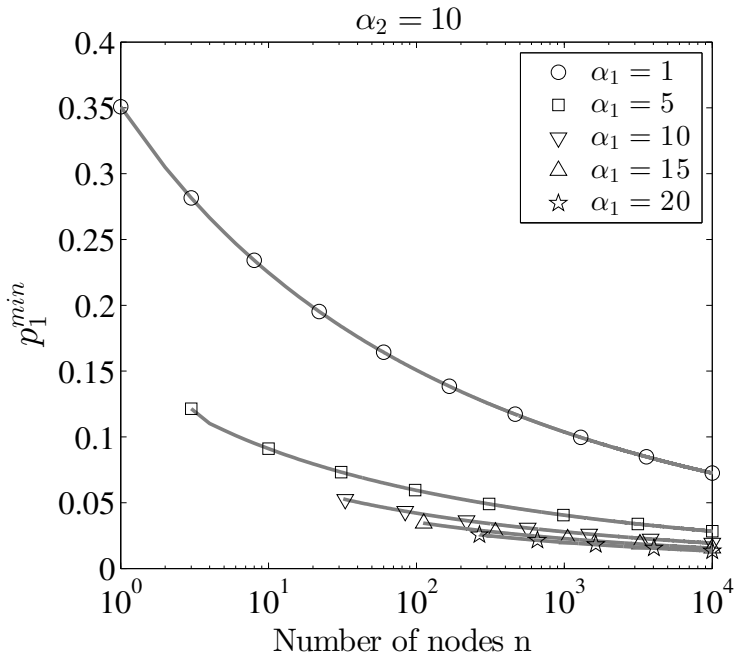

(a)

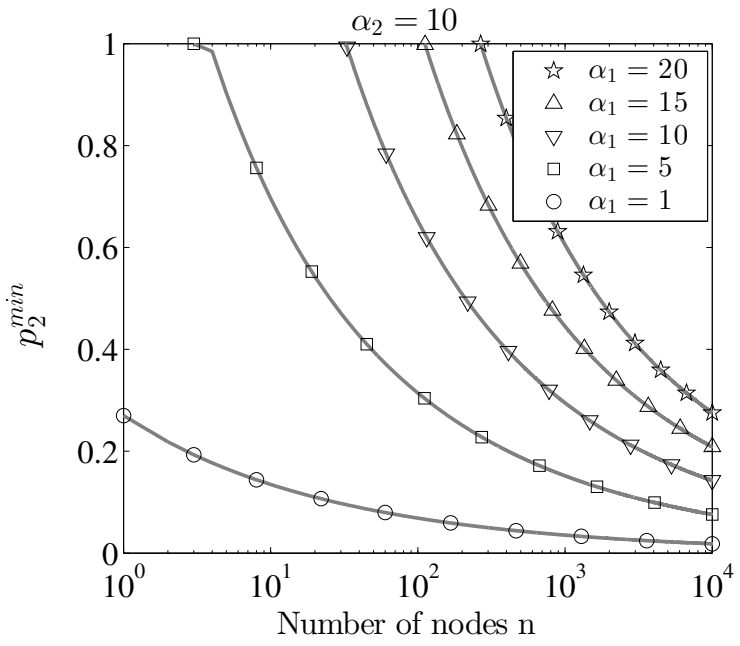

(b)

Figure 2.7: Variation of the optimal probabilities p_1^{min} and p_2^{min} with the number of nodes n, within the region of interest $\rho^2\alpha_2^2 n > \alpha_1^2(2\alpha_1 - 1)$. The plots (a) and (b) depict the variation of the optimal probabilities with the data ratio at level-1 $\alpha_1 = d_1/d_0$ for a constant data ratio at level-2 $\alpha_2 = d_2/d_0$. $\rho = 0.765$, corresponding to the processing center located at the center of a square.

system of h simultaneous equations indexed by $k = 1,2,...,h$:

$$\alpha_{k-1}\left[\prod_{j=0}^{k-1} x_j\right]\left(1+x_k^2\right) = \sum_{i=(k+1)\leq h}^{h} \alpha_{i-1}\frac{1-x_i^2}{x_i}x_k\prod_{j=0}^{i-1}x_j + 2\rho\sqrt{n}\alpha_h x_k\prod_{j=0}^{h}x_j^2$$

where $\alpha_0 = 1$, $p_0 = 1$ and $x_i = \sqrt{p_i} \quad \forall i = 1,2,...,h$. The solution ($p_1 = p_1^\star, p_2 = p_2^\star, ..., p_h = p_h^\star$) satisfying Eqns. 2.23 provides the unconstrained minimum. It warrants a case-by-case analysis to determine the conditions that bound $p_i^\star$ to (0,1).

When the above system of equations for hierarchy h is expressed in the matrix form $X(h)\mathbf{1} = Y(h)$, where $\mathbf{1}$ is vector of all ones and $X(h)$ is a $h \times h$ upper-triangular matrix, then the system for hierarchy $(h+1)$ can be expressed as

$$\left[\left[\begin{array}{c|c} 0 & X(h)C \\ \hline 0 & 0 \end{array}\right] + D\right]\mathbf{1} = \left[\begin{array}{c} Y(h) \\ \hline y_{h+1} \end{array}\right] \tag{2.23}$$

where C is a $(h \times h)$ diagonal matrix and D is a $(h+1 \times h+1)$ diagonal matrix. $C(i,i) = 1 \quad \forall i = 1,2,...,h-1$ and $C(h,h) = \frac{\alpha_{h+1}}{\alpha_h}x_{h+1}^2$; $D(i,i) = \alpha_h\frac{1-x_{h+1}^2}{x_{h+1}}x_i\prod_{j=0}^{h}x_j \quad \forall i = 1,2,...,h$ and $D(h+1,h+1) = 2\rho\sqrt{n}\alpha_{h+1}x_{h+1}\prod_{j=0}^{h+1}x_j^2$; $y_{h+1} = \alpha_h\prod_{j=0}^{h}x_j(1+x_{h+1}^2)$. Thus, interestingly, the system of equations for any hierarchy can be inductively obtained starting with $X(1) = 2\rho\sqrt{n}\alpha_1 x_1^3$ and $Y(1) = 1 + x_1^2$.

2.4 Optimum number of levels in the hierarchy

2.4.1 Decision threshold between single-level and two-level hierarchies

It follows from Theorem 2 that in a two-level hierarchy with a data ratio $1 : \alpha : \beta$, the optimal probabilities $p_1^\star$ and $p_2^\star$ minimizing the communication cost $\mathbb{E}[C]$ specified in Eqn. 2.17 are within the bounds (0,1) when $\rho^2\beta^2 n > \alpha^2(2\alpha - 1)$. Further for $\rho^2\beta^2 n < \alpha^2(2\alpha - 1)$, we numerically validate the existence of a unique real-valued root for the polynomial $p(x)$ in Eqn. 2.22 using Sturm's theorem in Lemma 3 over a wide range of n, α and β.

Accordingly, $\mathbb{E}[C]$ has a single minimum even in this case, although $p_2^\star$ is greater than 1 and therefore outside the bounds [0,1] as shown along the dotted lines of Figure 2.8. Due to the fact that $\mathbb{E}[C]$ has a single unconstrained minimum, the constrained minimum lies on the boundary of the respective constraint. Hence $p_2^{min} = 1$ when $\rho^2\beta^2 n < \alpha^2(2\alpha - 1)$.

When $p_2^{min} = 1$, every level-1 CH is elected to be a level-2 CH. In practice, this means that a network with two levels of clusters is reduced to one with a single level of clustering. A two-level cluster sending d_1 units of data at level-1 and d_2 units of data at level-2 reduces to a single-level cluster sending d_2 units of data from its CHs. This is made clear by substituting $p_2 = 1$ in Eqn. 2.17 for a data ratio $1 : \alpha : \beta$, whereby it reduces to Eqn. 2.10 with a data ratio $1 : \beta$. Thus, p_1^{min} for $h = 2$ is equivalently obtained by the minimization of the communication cost $\mathbb{E}[C]$ with $h = 1$. Therefore, there exists a threshold on the number of nodes below which a single level of clustering is sufficient for optimality. The threshold is given by

$$th_{12}(\alpha, \beta) = \frac{\alpha^2(2\alpha - 1)}{\rho^2\beta^2} \tag{2.24}$$

The threshold effect is illustrated in Figure 2.8. When $n < th_{12}$, $p_2^{min} = 1$ and p_1^{min} for the two-level hierarchical cluster (with $\alpha_1 = \alpha$ and $\alpha_2 = \beta$) coincides with the p_1^{min} for the single-level cluster (with $\alpha_1 = \beta$).

Since th_{12} is a function of the data ratios α and β, the number of levels required within a hierarchy depends on the network application; in particular, on the aggregated data size at each level. Note that the threshold increases as the cube of α, whereas it decreases as the square of β. Figure 2.9 provides a quick guide to check if one level of clustering is sufficient or if an additional level can be more efficient in terms of energy usage. For a particular α and β specified by the application, it is beneficial to employ more than one level when the number of nodes is greater than the threshold indexed on the contour. In other words, for a given number of nodes indexed on the contour, and the data ratio of a single-level cluster being β, the data ratio at an additional lower level needs to be smaller than the respective α read from the graph to be effective in reducing the total communication cost.

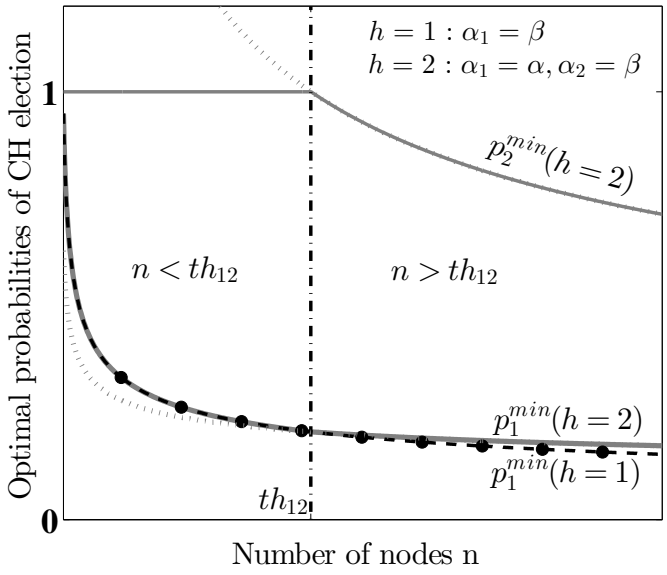

Figure 2.8: An illustration of the threshold effect on the number of nodes below which a single-level of clustering is sufficient. When $n < th_{12}$, an optimal two-level cluster with a data ratio of $1 : \alpha : \beta$ reduces to an optimal single-level cluster with a data ratio of $1 : \beta$. The dotted lines in the region below the threshold represent the unconstrained minimum of the formulated communication cost $\mathbb{E}[C]$ when $h = 2$.

2.4.2 Decision threshold between two-level and three-level hierarchies

In order to find the thresholds on the number of nodes demarcating two and three levels of hierarchy, we continue with the assumption of a single minimum/critical point for $\mathbb{E}[C]$ when $h = 3$ and numerically verify the ensuing results. Along the lines of the argument presented in the previous section, we are interested in finding the thresholds at which p_2^{min} and p_3^{min} saturate in an optimized three-level cluster. For $h = 3$ we have from Eqn. 2.5,

$$\begin{aligned} \mathbb{E}[C] &= \lambda A \Bigg[\frac{d_0(1-p_1)}{2\sqrt{\lambda p_1}} + \frac{d_1(1-p_2)p_1}{2\sqrt{\lambda p_1 p_2}} \\ &\quad + \frac{d_2(1-p_3)p_1p_2}{2\sqrt{\lambda p_1 p_2 p_3}} + \rho' a d_3 p_1 p_2 p_3 \Bigg] \end{aligned} \tag{2.25}$$

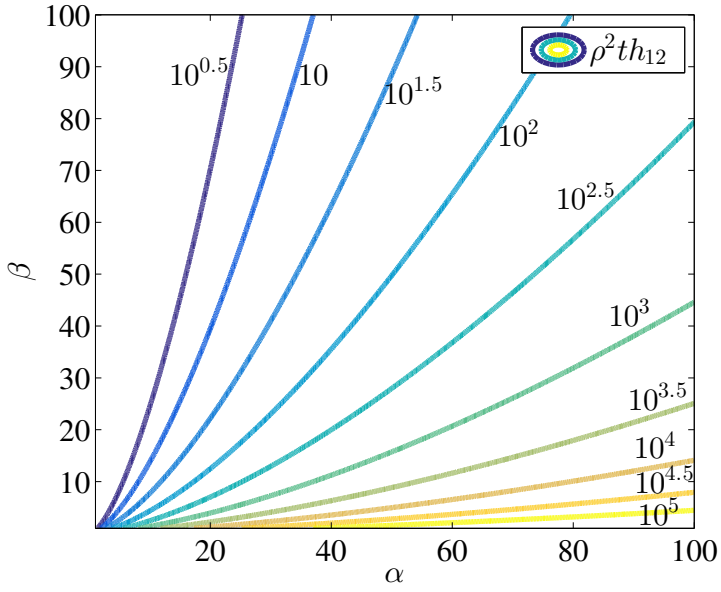

Figure 2.9: A contour plot of the scaled threshold $\rho^2 th_{12}$ as a function of the data ratios α and β. A two-level cluster forwarding data at each level in a ratio of $1 : \alpha : \beta$ is more energy efficient than a single-level cluster with a data ratio $1 : \beta$ under optimal conditions iff the number of nodes times ρ^2 is more than the threshold value on the contour. Also, for a given number of nodes n, processing center location (ρ), and data size at the highest level β, adding a lower level can be beneficial only if the aggregated data ratio at the new level is less than the corresponding α on the contour $\rho^2 n$.

Let $(p_1^\star, p_2^\star, p_3^\star) = \arg\min_{p_1,p_2,p_3} \mathbb{E}[C]$. We have, $\min_{p_1,p_2,p_3} \mathbb{E}[C] = \min_{p_1,p_2,p_3} f(p_1, p_2, p_3)$ where, $d = \rho\sqrt{n}$.

$$\begin{aligned} f(p_1,p_2,p_3) &= \frac{1-p_1}{\sqrt{p_1}} + \alpha_1(1-p_2)\sqrt{\frac{p_1}{p_2}} \\ &\quad + \alpha_2(1-p_3)\sqrt{\frac{p_1p_2}{p_3}} + \alpha_3 d p_1 p_2 p_3 \end{aligned} \tag{2.26}$$

Setting the partial derivatives to zero at the critical solution $(p_1^\star, p_2^\star, p_3^\star)$ results in the system of equations below, where $z = \sqrt{p_1^\star}$, $y = \sqrt{p_2^\star}$ and $x = \sqrt{p_3^\star}$.

$$x = \frac{2\alpha_2 y^2}{\alpha_1(1+y^2)} \tag{2.27}$$

$$z = \frac{\alpha_1(\alpha_1^2 + 4\alpha_2^2)y^6 + \alpha_1(3\alpha_1^2 + 4\alpha_2^2)y^4 + 3\alpha_1^3 y^2 + \alpha_1^3}{16\alpha_2^2\alpha_3 d y^7} \tag{2.28}$$

$$\begin{aligned} q(y) &= (y - 2\alpha_1)\Big(\alpha_1^3(1+y^2)^3 + 4\alpha_1\alpha_2^2 y^4(1+y^2)^2 \\ &\quad + 256\alpha_2^4\alpha_3^2 d^2 y^{15}\Big) = 0 \end{aligned} \tag{2.29}$$

Consider a three-level hierarchical cluster with data ratios $\alpha_1 = \alpha$, $\alpha_2 = \beta$ and $\alpha_3 = \gamma$. The threshold of saturation for the constrained optimal probability p_3^{min} is found by setting $x = 1$ i.e., $y = \sqrt{\frac{\alpha}{2\beta-\alpha}}$ (Eqn. 2.27) and solving for the corresponding n in Eqn. 2.29.

$$th_{23}\{p_3\} = \frac{\beta^2(2\beta-\alpha)\left[2\alpha\sqrt{\frac{2\beta-\alpha}{\alpha}} - 1\right]}{\rho^2\alpha\gamma^2} \tag{2.30}$$

Similarly, the threshold of saturation for p_2^{min} is found by setting $y = 1$ in Eqn. 2.29

and solving for the corresponding n.

$$th_{23}\{p_2\} = \frac{\alpha^2 (2\alpha - 1) \left(\alpha^2 + \beta^2\right)^2}{4\rho^2 \beta^4 \gamma^2} \tag{2.31}$$

Note that the 3-level hierarchy reduces to a 2-level hierarchy when

$$n < max\ \{th_{23}\{p_2\}, th_{23}\{p_3\}\}.$$

The threshold on the number of nodes below which only two-levels are sufficient for optimality is therefore given by

$$th_{23} = max\ \{th_{23}\{p_2\}, th_{23}\{p_3\}\} \tag{2.32}$$

However the data ratios of the reduced network differs between the two cases depending on which threshold is indeed the higher one. It can shown that (Lemma 6 in Appendix A.3),

$$\alpha < \beta \implies th_{23}\{p_2\} < th_{23}\{p_3\}$$
$$\alpha > \beta \implies th_{23}\{p_2\} > th_{23}\{p_3\}$$

Hence, $th_{23} = th_{23}\{p_3\}$ when $\alpha < \beta$ and $th_{23} = th_{23}\{p_2\}$ otherwise, as illustrated in Figure 2.10.

When $\alpha < \beta$ and $n < th_{23}\{p_3\}$ in a three-level network with data ratio $1 : \alpha : \beta : \gamma$, $p_3^{min} = 1$ while p_1^{min} and p_2^{min} coincide with that of a two-level cluster with a data ratio of $1 : \alpha : \gamma$. In practice, this means, every level-2 CH is elected as a level-3 CH and a network forwarding d_1 units of data at level-1, d_2 units of data at level-2 and d_3 units of data at level-3 reduces to two levels forwarding d_1 units of data at the fist level and d_3 units of data at the second level. This is also evident on substituting $p_3 = 1$ in Eqn. 2.5 for the communication cost $\mathbb{E}[C]$ with $h = 3$.

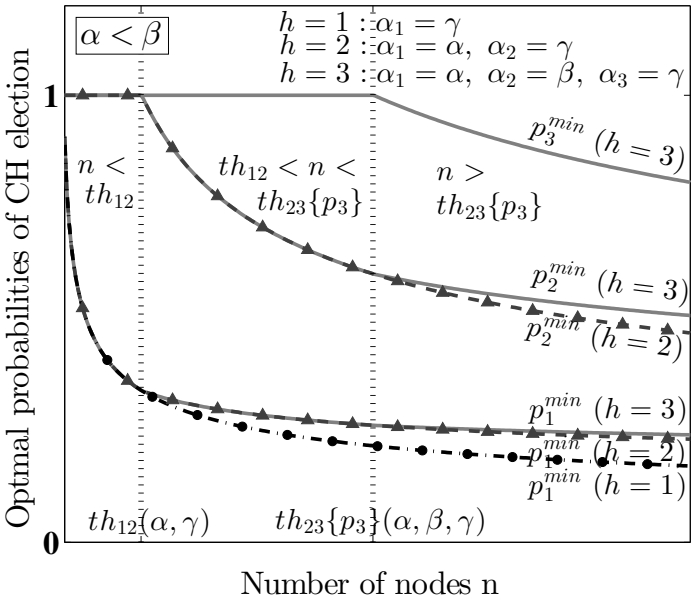

(a)

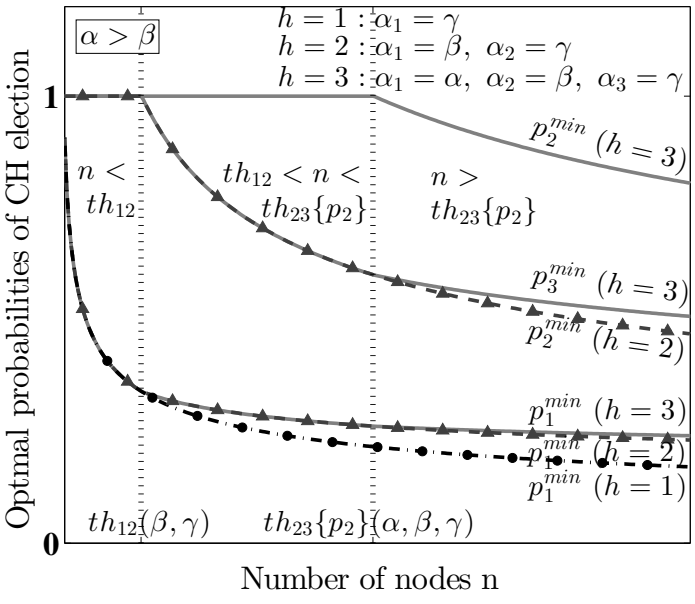

(b)

Figure 2.10: (a) An illustration of the threshold effect on the number of nodes below which two-levels of clustering is sufficient when $\alpha < \beta$. When $n < th_{23}\{p_3\}$, an optimal three-level cluster with a data ratio of $1 : \alpha : \beta : \gamma$ reduces to an optimal two-level cluster with a data ratio of $1 : \alpha : \gamma$. (b) An illustration of the threshold effect on the number of nodes below which two-levels of clustering is sufficient when $\alpha > \beta$. When $n < th_{23}\{p_2\}$, an optimal three-level cluster with a data ratio of $1 : \alpha : \beta : \gamma$ reduces to an optimal two-level cluster with a data ratio of $1 : \beta : \gamma$.

Analogously, when $\alpha > \beta$ and $n < th_{23}\{p_2\}$ in a three-level network with data ratio $1 : \alpha : \beta : \gamma$, $p_2^{min} = 1$ while (p_1^{min}, p_3^{min}) coincide respectively with (p_1^{min}, p_2^{min}) of a two-level cluster with a data ratio of $1 : \beta : \gamma$. In practice, this means, every level-1 CH is elected as a level-2 CH and a network forwarding d_1 units of data at level-1, d_2 units of data at level-2 and d_3 units of data at level-3 reduces to two levels forwarding d_2 units of data at the fist level and d_3 units of data at the second level. This is also evident on substituting $p_2 = 1$ in Eqn. 2.5 for the communication cost $\mathbb{E}[C]$ with $h = 3$.

It is noteworthy that below the threshold th_{23}, there is a natural selection of the intermediate layer with a lower data ratio; i.e., when $n < th_{23}$, a $1 : \alpha : \beta : \gamma$ cluster reduces to a $1 : min(\alpha, \beta) : \gamma$ cluster when optimum. Note that the threshold increases as the cube of $max(\alpha, \beta)$, whereas it decreases as the square of γ. Based on the data ratios defined by the application, Figure 2.11 provides a quick guide to check if two levels are sufficient or a third level is necessary.

2.4.3 Choosing the optimal number of levels in a hierarchical cluster

In the previous section we derived the thresholds on the number of nodes below which single-level and/or two-level clusterings are sufficient and an additional level becomes redundant in conserving the communication cost. Within the intervals above the thresholds, higher the number of levels more energy efficient is the network as illustrated in Figure 2.12. Although, the gain is marginal for hierarchies beyond three. It can be verified along the lines of Lemma 6 that $th_{12}(min(\alpha, \beta), \gamma) < th_{23}(\alpha, \beta, \gamma)\ \forall \alpha \neq \beta$.

In view of this, we propose the decision tree presented in Figure 2.13 for choosing the number of levels of clustering. We start with a three-level cluster and application specific data ratios (α, β, γ) as our candidate. Based on the aggregation schemes that can be employed, α, β and γ are the feasible ratios at any level. The actual number of nodes in the network n is compared with the thresholds th_{12} and th_{23} to determine the number of levels. Further, the ordering of the data ratios in the hierarchy determines which ones propagate

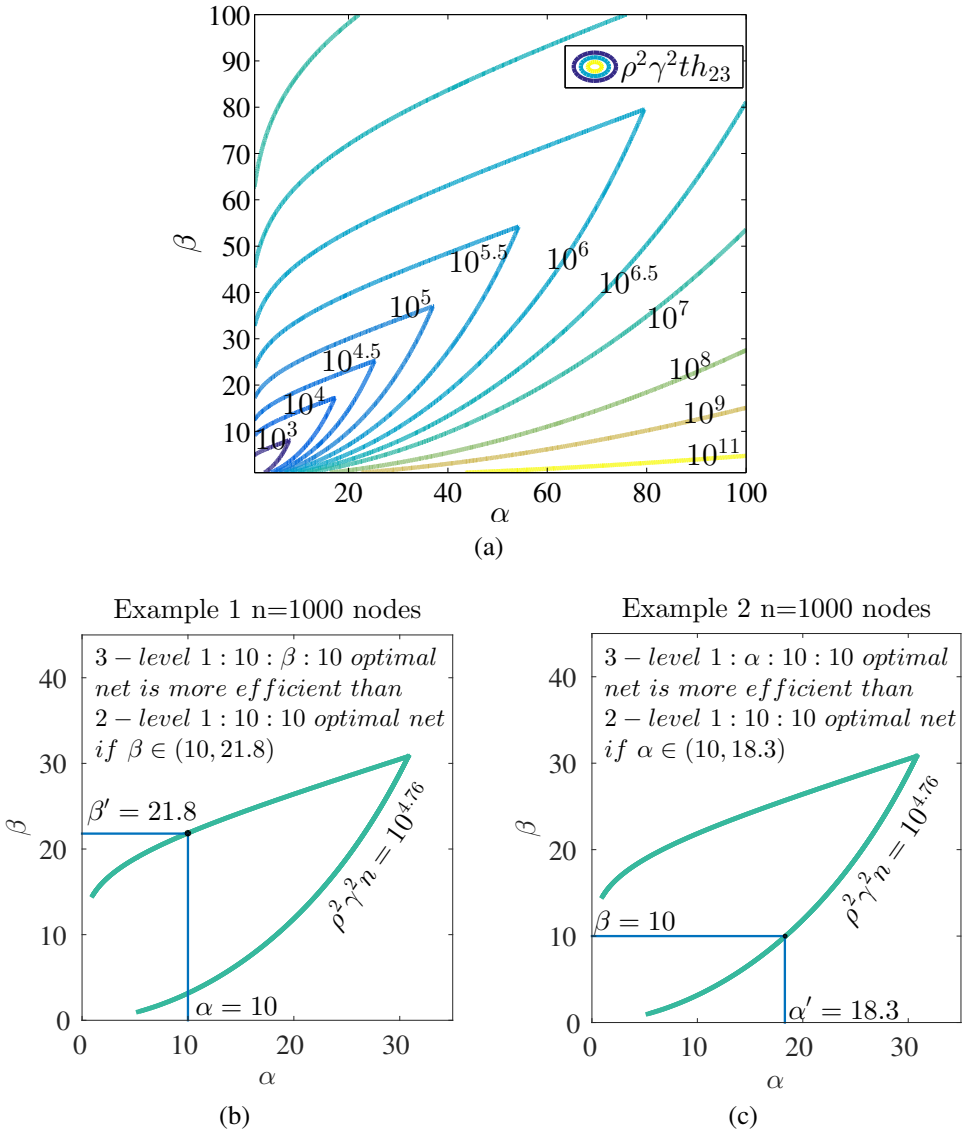

Figure 2.11: A contour plot of the scaled threshold $\rho^2\gamma^2 th_{23}$ as a function of the data ratios α and β. A three-level cluster forwarding data at each level in a ratio of $1:\alpha:\beta:\gamma$ is more energy efficient than a two-level cluster with a data ratio $1:min\{\alpha,\beta\}:\gamma$ under optimal conditions iff the number of nodes is larger than the threshold value along the contour scaled down by $\rho^2\gamma^2$. To check if adding a level above the first level of a two level cluster with n nodes and data ratio $1:\alpha:\gamma$ makes it more efficient, read the intersect $\beta' > \alpha$ corresponding to α on the contour indexed by $\rho^2\gamma^2 n$. Adding this level is beneficial if the aggregated data ratio at the new level $\beta \in (\alpha, \beta')$ (Example 1). Similarly, the network can be more efficient on adding another level below the first level of a cluster with ratio $1:\beta:\gamma$ when the aggregated data ratio at the new level $\alpha \in (\beta, \alpha')$ where $\alpha' > \beta$ is read from the intersect of β on the corresponding contour (Example 2). When the data ratio at level-1 of a two-level cluster does not intersect the contour $\rho^2\gamma^2 n$, a third level of clustering is unnecessary.

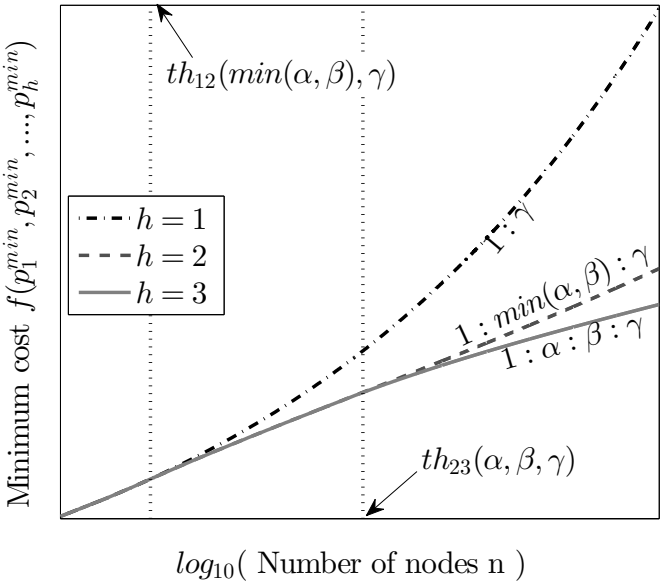

Figure 2.12: An illustration showing the variation of the cost functional across the level thresholds under optimal conditions. On retaining appropriate data ratios, the communication cost within a clustered network lower-bounds that with fewer levels of clustering.

into the reduced network.

2.5 Verification and Validation

We have used large-scale parallel computing to verify the results using numerical optimization as well as to validate the approximations in our analysis using network simulations. Note that the numerical search for the minimum is computationally very expensive in addition to being sensitive to the initial guess. Simulation of large-scale networks with a routing framework is even more expensive, making parametric studies infeasible within a reasonable amount of time. This highlights the importance of the theoretical analysis in this chapter.

2.5.1 Numerical Verification

We have numerically validated all our analytical results using a bounded nonlinear optimization program *fminsearchbnd* [60]. The algorithm applies transformation methods to

```
Candidate ← (1 : α : β : γ) (h=3)
if α < β then
    if n < th12(α, γ) then
        Candidate ← (1 : γ) (h=1)
    else if n < th23{p3} then
        Candidate ← (1 : α : γ) (h=2)
    end
else
    if n < th12(β, γ) then
        Candidate ← (1 : γ) (h=1)
    else if n < th23{p2} then
        Candidate ← (1 : β : γ) (h=2)
    end
end
```

Figure 2.13: Algorithm to chose the number of levels and data ratios at each level starting with a potential three-level hierarchy.

convert the constrained problem into an unconstrained one and then uses the simplex search algorithm of Lagarias et.al. [61] to find the minimum. We have validated the results for a wide range of parameters with high resolution and the combinations thereof. In this section, without loss of generality, we have assumed $\rho = 0.765$, corresponding to the location of the processing center at the center of a square region. The tolerance for convergence is 1.e-4 and hence the results are validated up to three decimal places.

Single level hierarchy (h = 1)

The theoretical calculation of p_1^{min} (Corollary 1) is consistent with the numerical results on the minimization problem stated in in Eqn. 2.6 for $h = 1$. We have verified the results for α_1 ranging 1-100 in steps of size 0.5 and n ranging 2-10000 in steps of size 1 for each choice of α_1.

Two level hierarchy (h = 2)

We have numerically validated the following results for the two-level clustering with α and β ranging 1-100 in steps of size 0.5 and n ranging 2-10000 in steps of size 1 and the

combinations thereof:

1. There exists exactly one real-valued root in $(0, \infty)$ for the polynomial in Eqn. 2.22 $\forall\ \alpha_1 = \alpha,\ \alpha_2 = \beta$ in compliance with the Sturm's theorem (quoted in Lemma 3). Hence there exists a unique global minimum for $\mathbb{E}[C]$.

2. For $n < th_{12}(\alpha, \beta)$ (Eqn. 2.24), $p_2^{min} = 1$.

3. For $n > th_{12}(\alpha, \beta)$,

   (a) p_1^{min} and p_2^{min} computed from Corollary 2 are consistent with the numerical results on the minimization problem stated in Eqn. 2.6. Here, $h = 2$, $\alpha_1 = \alpha$ and $\alpha_2 = \beta$.

   (b) $f(p_1^{min}, p_2^{min} \mid h = 2, \alpha_1 = \alpha, \alpha_2 = \beta) < f(p_1^{min}) | (h = 1, \alpha_1 = \beta)$. Hence the communication cost $\mathbb{E}[C]$ of an optimal $1 : \alpha : \beta$ two level cluster is less than that of an optimal $1 : \beta$ single level cluster.

Three level hierarchy (h = 3)

We have numerically validated the following results for the three-level clustering with α, β and γ ranging 1-100 in steps of size 1 and n ranging 2-10000 in steps of size 10 and the combinations thereof:

1. For $\alpha < \beta$,

   (a) For $n < th_{23}\{p_3\}(\alpha, \beta, \gamma)$ (Eqn. 2.30), $p_3^{min} = 1$.

   (b) For $n > th_{23}\{p_3\}(\alpha, \beta, \gamma)$,
   $f(p_1^{min}, p_2^{min}, p_3^{min} \mid h = 3, \alpha_1 = \alpha, \alpha_2 = \beta, \alpha_3 = \gamma) < f(p_1^{min}, p_2^{min} \mid h = 2, \alpha_1 = \alpha, \alpha_2 = \gamma)$. Hence the communication cost $\mathbb{E}[C]$ of an optimal $1 : \alpha : \beta : \gamma$ three level cluster is lesser than that of an optimal $1 : \alpha : \gamma$ two level cluster.

2. For $\alpha > \beta$,

(a) For $n < th_{23}\{p_2\}(\alpha, \beta, \gamma)$ (Eqn. 2.31), $p_2^{min} = 1$.

(b) For $n > th_{23}\{p_2\}(\alpha, \beta, \gamma)$,
$f(p_1^{min}, p_2^{min}, p_3^{min} \mid h = 3, \alpha_1 = \alpha, \alpha_2 = \beta, \alpha_3 = \gamma) < f(p_1^{min}, p_2^{min} \mid h = 2, \alpha_1 = \beta, \alpha_2 = \gamma)$. Hence the communication cost $\mathbb{E}[C]$ of an optimal $1 : \alpha : \beta : \gamma$ three level cluster is less than that of an optimal $1 : \beta : \gamma$ two level cluster.

In summary, we have corroborated the formulations of optimal probabilities and hierarchy thresholds, and the assertions on relative energy efficiencies between different levels, using numerical optimization.

2.5.2 Simulation Studies

We have used the tools within MATLAB to simulate networks of one, two and three levels with varying number of nodes, clusterhead election probabilities, and data-size ratios. The purpose of these simulations is to validate the following approximations in the analytical model: 1) Hop-length is approximated by the range of communication. 2) Route-length is approximated by the scaled Euclidean distance 3) Distances in unbounded Voronoi tessellations are used to approximate equivalent distances in bounded clustered networks, such as the sum of distances from Poisson points in a Voronoi cell to its center (Eqn. 2.1).

Representative results are shown in Figure 2.14, Figure 2.15 and Figure 2.16. Here, 1000 nodes are uniformly distributed in a square region, the area of which is chosen to ensure network connectivity w.h.p. [62]. The election of clusterheads and cluster formations are as demonstrated in Figure 2.1. A unit of data from all the end nodes is gathered at the processing center located at the center of the square area. At each level, the data is routed via the shortest path in a greedy fashion. While the size of the data at level-i is specified by α_i, we have counted one unit of energy every hop for each unit of data. For a first-order radio model in [28], a unit of energy is equivalent to 0.35 $\mu J/bit$ when the range is 50 m. In the event that no CHs are elected at level-i, the α_i units are directly forwarded to the processing center. We have simulated 1000 instances of clusters for each of the probability

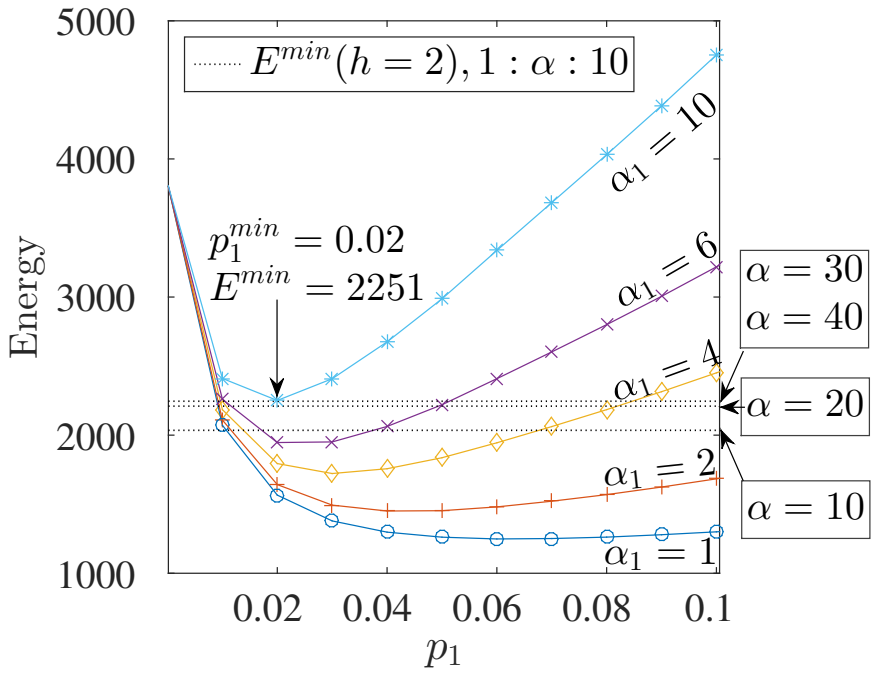

Figure 2.14: Simulation results for a network of 1000 nodes with specified data ratios. Single-level clustered networks with data ratio α_1. The energy is computed for different clusterhead election probabilities p_1. Note that the optimal values p_1^{min} are in accordance with Eqn. 2.16 (Figure 2.3, Figure 2.4). Further, a comparison of the minimum energies E^{min} in the $1:10$ network and the $1:\alpha:10$ two-level networks with different values of α shows that the additional level is effective in reducing the cost only when $\alpha < 30$, as predicted by Eqn. 2.24 (Figure 2.9).

values and used the average energy consumption to plot the graphs.

We observe that the results on Voronoi tessellation [58] are applicable to bounded area/finite networks having at least one CH at each level. Accordingly, within our region of interest $\mathbb{E}[TCH_h] = n\prod_{i=1}^{h} p_i \geq 1$, we have validated that the results from simulations are in very good agreement with the theoretical predictions. Further, the results are found to be applicable even when the nodes are placed on a regular grid.

2.6 Application cases

In the network model presented, the data ratios α_i determine the optimal number of levels and the number of clusters at each level in a hierarchical network. Figure 2.2 demonstrates an example of how α_1 varies with the application requirements. Below, we further consider

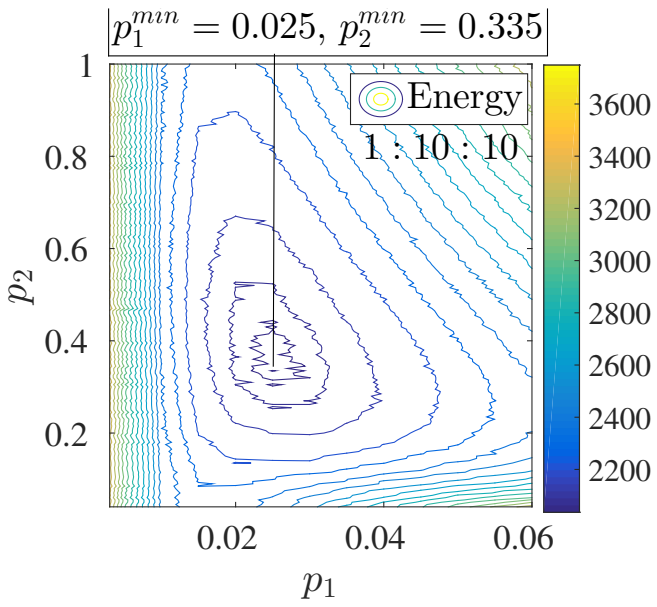

Figure 2.15: Simulation results for a network of 1000 nodes with specified data ratios. Two-level clustered networks with data ratios $\alpha_1 = 10$ and $\alpha_2 = 10$. The contour plot is generated by computing the energy for different clusterhead election probabilities p_1 and p_2. Note that the optimal probabilities p_1^{min} and p_2^{min} are in accordance with Corollary 2 (Figure 2.6, Figure 2.7). The minimum energy is computed to be 2035, which sets a lower limit on the achievable minimum in certain three-level networks considered in Figure 2.16.

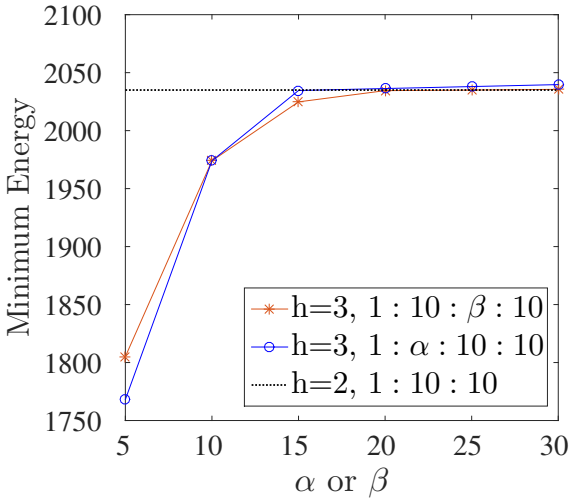

Figure 2.16: Simulation results for a network of 1000 nodes with specified data ratios. Three-level clustered networks considered in the Examples of Figure 2.11. The computed minimum energy saturates close to 2035 when $\beta > 20$ (Example 1) and when $\alpha > 15$ (Example 2). These results are in very good agreement with the theoretical predictions given by Eqn. 2.30 and Eqn. 2.31, respectively. Indeed, it can be generalized that these three-level networks are more efficient iff $\beta < 20$ or $\alpha < 15$.

different application cases categorized by the interrelation of α_is. It is evident that the optimality of an ad-hoc wireless network largely depends on the underlying application and the data processing schemes in place.

When $\alpha_1 = \alpha_2 = ... = \alpha_h = 1$, the number of data units forwarded at each level is same as the number of data units generated by the end node. Consider an event detection application, wherein each end node sends a decision bit to its clusterhead (CH). Depending on the reliability test adopted, the CH forwards a decision bit further. Any logical operation performed at the CH retains the size of the data unit, qualifying as an example. In this case, $th_{12} = th_{23} = 1/\rho^2$. The thresholds have a very small magnitude and hence, for any network of substantial size, it is desirable to have three levels of hierarchy.

When $\alpha_1 = \alpha_2 = ... = \alpha_h = k$, the number of data units forwarded at each level is k times the number of data units generated by the end node. For example, in the event detection application stated in the previous case the CH could forward the local detection error probability along with the decision bit. Likewise, a CH could compute and append such statistics as the mean, variance, maximum etc. of the data generated by the end nodes. In this scenario, $th_{12} = th_{23} = (2k - 1)/\rho^2$. Hence, the threshold is proportional to the data size k. When k is significantly large, a single or three level hierarchy is employed depending on the number of nodes.

When $\alpha_1 < \alpha_2 < ... < \alpha_h$, the number of data units forwarded increases up the hierarchy. This occurs in environment monitoring applications using multiple sensors, which includes the study of spatio-temporal variation of state variables such as temperature, pressure, sound, vibrations, video etc. Low cost variables can be locally monitored within a cluster and only the statistics/decision computed at the CH may be forwarded. More complex sensing can be performed at the higher levels to cover larger areas with lower spatial intensity. When the data ratios increase rapidly up through the hierarchy, threshold th_{12} is then small, and an optimal network will require at least two-levels. Three levels are favored when the number of nodes is greater than $th_{23}\{p_3\}$. In contrast, when the increments in α_is

are small—depending on their magnitude—a single level might be sufficient for a small network.

When $\alpha_1 > \alpha_2 > ... > \alpha_h$, the number of data units forwarded decreases up the hierarchy. This can be expected in data mining applications in an ad-hoc network. Parameter/density estimation in a three tier network is an example where the data generated by the end nodes undergo temporal/spatial sampling at the level-1 CH and the estimation is performed at level-2 using the aggregated samples. When the decrease in data ratio up the hierarchy is of a high degree, threshold th_{12} is fairly high, and a single level would be sufficient. However, when the decrements in α_is are small, their magnitude mainly determines the optimum number of levels. Three levels are favorable when the number of nodes is greater than $th_{23}\{p_2\}$.

Overall, for large values of data ratios α_is, the thresholds are less sensitive to variations in their magnitudes, whereas for small values, they are highly sensitive.

CHAPTER 3

DELAY-EFFICIENT ROUTING ACROSS HIGH-THROUGHPUT CLUSTERS

3.1 Introduction

Large-scale wireless networks are intrinsic to the concept of the Internet of Things (IoT). Recent advances in processing and communication technologies have resulted in small battery powered sensing devices with wireless modules embedded in them. This has further enabled the deployment of thousands of nodes without prior knowledge of the network configuration. Performance of the adhoc network that would emerge depends on certain distinctive aspects like management of the available energy, scalability of the installed algorithms, and reliability of the communication environment [7].

Routing algorithms designed for wireless sensor networks are primarily classified into two groups, i.e., planar and hierarchical [18]. Hierarchical clusters are scalable and energy-efficient, befitting large-scale network operation [16]. However, in a majority of clustering schemes, such as LEACH, PEGASIS, TEEN, HEED, EEMC and their variations, the clusterhead communicates directly with the base station and/or other clusterheads. This requires careful assembly of nonhomogeneous devices and risks network connectivity in uneven terrains. Moreover, the long-haul communications create an energy hole and a large interference footprint around the clusterhead [20]. The above drawbacks can be overcome by adopting multi-hop routes [63, 64] for the inter-cluster communications. This motivates the question: What is the best inter-cluster multi-hop route?

Characteristics that must be considered in the design of an inter-cluster routing scheme are: Firstly, the energy-usage distribution in a clustered network is uneven. In order to achieve a global energy balance and improve the network lifetime, the nodes subject to less traffic need to be utilized. Secondly, packets sent by the clusterheads often hold time-

sensitive information for detection, synchronization and streaming applications. In these cases, delivery of the aggregated data to the sink requires a QoS protocol with guaranteed end-to-end latency [65]. Thirdly, in contrast to the sensed data that hold local and limited information with redundancies, the aggregated data at the clusterheads hold essential high-cost information pertaining to larger spatial areas. Therefore, a reliable service that keeps packet loss in check becomes critical. Indeed, all the above characteristics are closely associated with each other in high-throughput clusters.

Motivated by these considerations, we study the properties of route delays in navigating a packet across a data gathering cluster. The primary contributions include:

- Introduction of a new analytical framework for visualizing large-scale networks as surfaces as opposed to graphs when optimizing routing paths.
- Computation of the spatial per-hop delay cost function and the associated end-to-end delay minimizing paths.
- An energy-aware, low-delay, distributed algorithm devoid of location information that can be readily integrated into existing clustering schemes with minimal overhead.
- An ns-3 based clustered wireless network simulator that enables a parametric study of the routes in a large-scale latticed network.

Multi-hop route design for inter-cluster communication is an uncharted territory in homogeneous sensor networks. The conventional distributed algorithms for adhoc networks include proactive routing, reactive routing and geographic routing. In proactive routing protocols like OLSR [66], the link states are exchanged to create the network topology at every node and the shortest route is computed. In reactive routing protocols like AODV [67], the routes are created on demand by flooding the network with a request and thereby building a backtracking tree. In local geographic routing [68], the location information

of the next-hop neighbors is used to greedily select the relay node. The above protocols essentially try to achieve the shortest path.

A more recent approach called opportunistic routing [69] selects relays dynamically at each hop depending on the MAC layer properties. The idea is to reduce the mean end-to-end total time rather than the number of hops, by further accounting for the time wasted in unsuccessful attempts for channel access. We use the same underlying principles in our approach; however, a systems view of the network is developed, resulting in an AODV-like algorithm which overcomes the technical difficulties in the implementation of opportunistic routing [70].

Starting with the problem formulation, its analysis for a model functional is presented in Section 3.2. The spatial delay distribution in a CSMA cluster is modeled for computing the delay minimizing paths in Section 3.3. A distributed algorithm for inter-cluster edge routing is proposed in Section 3.4, followed by its simulation results in Section 3.5. Application of edge routing for inter-level routing in optimally clustered Voronoi tessellated network is discussed in Section 3.6, followed by characterization of its length distribution in Section 3.7.

3.2 Motivation: Model Problem

Consider all continuously differentiable curves $y = y(x) \geq 0 \; \forall x$ which pass through two given points (x_1, y_1) and (x_2, y_2). The length along one particular curve between the given points is obtained by integrating the element of arc length $ds = \sqrt{1 + \left(\frac{dy}{dx}\right)^2}$. For a spatial cost function $F(x, y)$, the total cost accumulated along this curve is therefore given by

$$I = \int_{x_1}^{x_2} F(x, y) \sqrt{1 + \left(\frac{dy}{dx}\right)^2} \, dx. \tag{3.1}$$

In polar coordinates, where $r = r(\theta)$ is the path with end points (r_1, θ_1) and (r_2, θ_2), Eqn. 3.1 becomes

$$I = \int_{\theta_1}^{\theta_2} F(r,\theta) \sqrt{r^2 + \left(\frac{dr}{d\theta}\right)^2}\, d\theta. \tag{3.2}$$

Let the spatial distribution of the per-hop delay in a multi-hop clustered network be defined by F. Now, the end-to-end delay incurred by a test packet routed along the chosen path $y = y(x)$ is given by I. Optimal inter-cluster route design involves finding the path y that minimizes the total delay I.

Since the hop-delay increases/decreases as the channel load increases/decreases, F radially decreases from the center in a data gathering cluster. Therefore, to gain an analytical insight to path design, let us first consider a model problem where F is a general two-dimensional circularly symmetric Gaussian function $F(x,y) = b\, e^{-\left(\frac{x^2+y^2}{2c^2}\right)}$ or equivalently $F(r,\theta) = b\, e^{-\left(\frac{r^2}{2c^2}\right)}$ with the height parameter b and the width parameter c, and study the two extreme cases of interest: (I) Routing along the shortest path via a straight line. (II) Routing around the edges of the cluster via a circular path.

3.2.1 Euclidean route vs. circular route: diametric end points

Consider routing a test packet from a starting point $(x_1, y_1) = (-a, 0)$ to an end point $(x_2, y_2) = (a, 0)$ across a single cluster centered at the origin. In case I, $y(x) = 0$. From Eqn. 3.1, the total cost is given by

$$I_1 = 2\int_0^a b\, e^{-\frac{x^2}{2c^2}} dx = \sqrt{2\pi}\, bc\ \mathrm{erf}\left(\frac{a}{\sqrt{2}c}\right) \tag{3.3}$$

In case II, $r(\theta) = a$. From Eqn. 3.2, the total cost is given by

$$I_2 = \int_0^{\pi} b\, e^{-\frac{a^2}{2c^2}} a d\theta = \pi a b e^{-\frac{a^2}{2c^2}} \tag{3.4}$$

Figure 3.1 shows the variation of I_1 and I_2 with respect to a. We can see that the total

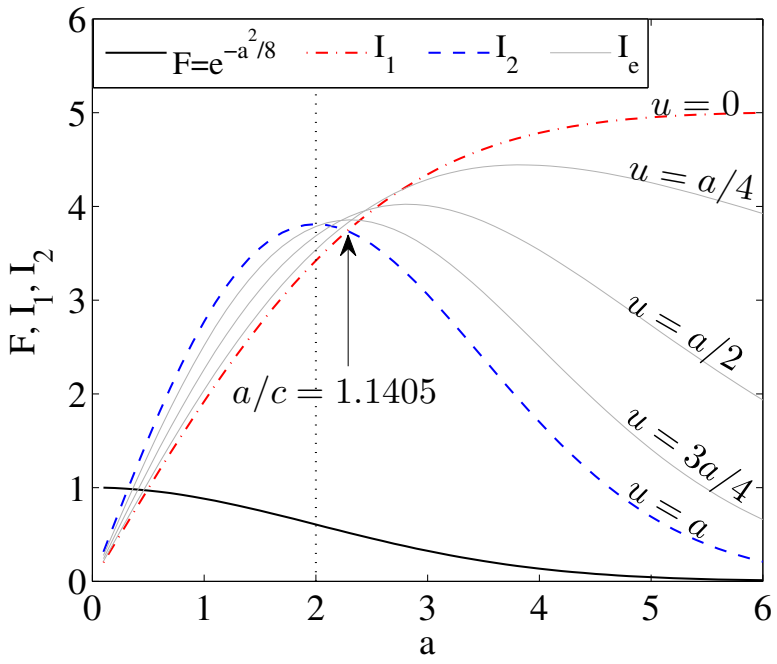

Figure 3.1: Variation of the Euclidean and circular cost integrals I_1 and I_2 respectively w.r.t the distance of the end points $-x_1 = x_2 = a$. The plot illustrates a Gaussian function F with the height parameter $b = 1$ and the width parameter $c = 2$. It further shows I_1 and I_2 as limiting functions of the elliptical path integrals $I_e(u)$. Note that I_e is lower bounded by $min(I_1, I_2)$.

route delay for the euclidean path is an increasing function that saturates to a maximum value as the distance between the end points increases. However, the total route delay for the circular path reaches a maximum when the distance between the end points $2a$ equals the width parameter $2c$, and decreases thereafter. The point of intersection between the two curves is found by setting $a = qc$ and equating Eqn. 3.3 and Eqn. 3.4. Solving the non-linear equation

$$qe^{\frac{-q^2}{2}} = \sqrt{\frac{2}{\pi}}\,\mathrm{erf}\left(\frac{q}{\sqrt{2}}\right) \tag{3.5}$$

results in $q = 1.1405$. Hence, in terms of end-to-end delay of a packet to be navigated across a cluster, although routing through the cluster via the shortest path is more optimal when the distance between the end points is less than $1.1405c$, routing around the edges of the cluster is more optimal otherwise. This demonstrates that the shortest path routing is

not always optimal for inter-cluster routing and alternative paths need to be explored .

To generalize the above statement, let us consider routing between $(-a,0)$ and $(a,0)$ via an elliptical path described by $\frac{x^2}{a^2} + \frac{y^2}{u^2} = 1$, i.e. $y(x) = \frac{u}{a}\sqrt{a^2 - x^2}$ for $u \in (0,a)$. The total cost would then be given by

$$I_e(u) = \frac{b}{a} e^{-\frac{u^2}{2c^2}} \int_{-a}^{a} e^{-\frac{(a^2-u^2)x^2}{2a^2c^2}} \sqrt{\frac{a^4 + (u^2 - a^2)x^2}{a^2 - x^2}} dx \tag{3.6}$$

Figure 3.1 further shows the plots for the cost integral I_e parameterized by the elliptical height u. Notably, the set of functions I_e w.r.t a are lower bounded by $min(I_1, I_2)$, where I_1 and I_2 are the limiting cases with $u = 0$ and $u = a$ respectively. Therefore, among all possible elliptical paths, there are only two minima: the euclidean path for $a < 1.1405c$, and the circular path for $a > 1.1405c$.

3.2.2 Euclidean route vs. circular route: chordal end points

Consider routing a test packet from any starting point $(-a < x_1 < a, y_1 = \sqrt{a^2 - x_1^2})$ to an end point $(x_2, y_2) = (a,0)$ partly crossing a single cluster centered at the origin. Let $\theta_{max} \in (0,\pi)$ be the central angle subtended by the chord connecting these end points as illustrated in Figure 3.2. Note that Section 3.2.1 addressed the special case where $\theta_{max} = \pi$. In case I, the equation of the chord is $y(x) = \cot\left(\frac{\theta_{max}}{2}\right)(a - x)$. From Eqn. 3.1, the simplified total cost is given by

$$I_1 = \int_{a\cos\theta_{max}}^{a} b\, e^{-\frac{x^2 + \cot^2\left(\frac{\theta_{max}}{2}\right)(a-x)^2}{2c^2}} \sqrt{1 + \cot^2\left(\frac{\theta_{max}}{2}\right)} dx \tag{3.7}$$

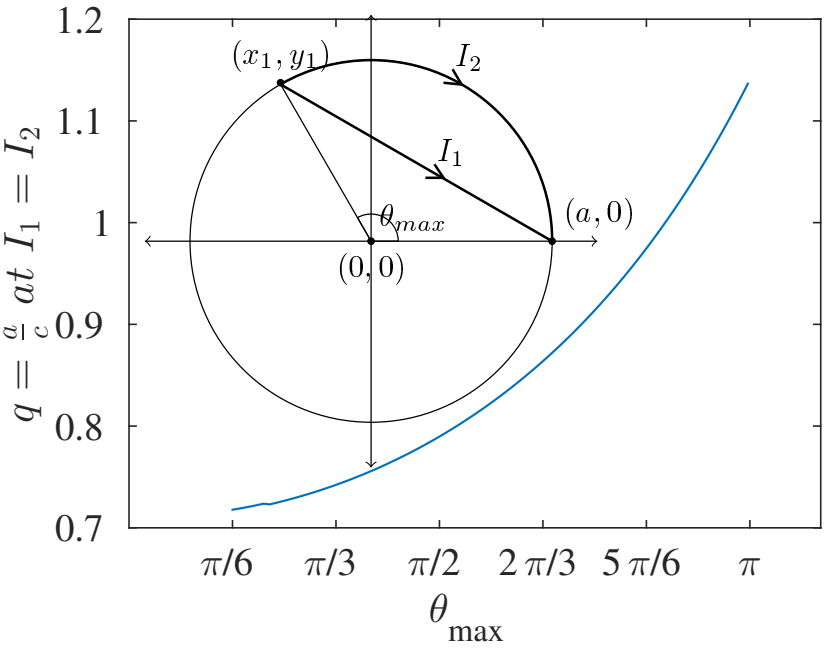

Figure 3.2: The inset geometric illustration shows the chordal endpoints w.r.t cluster layout as considered in Section 3.2.2. The graph depicts the ratio of the radial distance a to the delay function width parameter c at the point of intersection of the curves I_1 and I_2 as a function of the central angle θ_{max} subtended by the corresponding chord.

Suppose $M = b\ \sqrt{1 + \cot^2\left(\frac{\theta_{max}}{2}\right)} e^{-\frac{a^2}{2c^2}\cot^2\frac{\theta_{max}}{2}}$, then

$$
\begin{aligned}
I_1 &= M \int_{a\cos\theta_{max}}^{a} e^{-\frac{1}{2c^2}\left[\left(1+\cot^2\frac{\theta_{max}}{2}\right)x^2 - 2a\cot^2\left(\frac{\theta_{max}}{2}\right)x\right]} dx \\
&= M \int_{a\cos\theta_{max}}^{a} e^{-\frac{1+\cot^2\frac{\theta_{max}}{2}}{2c^2}\left(x - a\cos^2\frac{\theta_{max}}{2}\right)^2 + \frac{a^2\cot^4\frac{\theta_{max}}{2}}{2c^2\left(1+\cot^2\frac{\theta_{max}}{2}\right)}} dx \\
&= \sqrt{2\pi}\ bc\ e^{-\frac{a^2}{2c^2}\cos^2\frac{\theta_{max}}{2}}\ \mathrm{erf}\left(\frac{a}{\sqrt{2}c}\sin\frac{\theta_{max}}{2}\right)
\end{aligned}
\tag{3.8}
$$

In case II, $r(\theta) = a$. From Eqn. 3.2, the total cost is given by

$$
I_2 = \int_0^{\theta_{max}} b\ e^{-\frac{a^2}{2c^2}} a d\theta = \theta_{max} a b e^{-\frac{a^2}{2c^2}} \tag{3.9}
$$

I_1 and I_2 still have trends similar to those illustrated in Figure 3.1, but with different

points of intersection. Setting $a = qc$ and equating Eqn. 3.8 and Eqn. 3.9 results in the following non-linear equation.

$$q\theta_{max}e^{-\frac{q^2}{2}} = \sqrt{2\pi}e^{-\frac{q^2}{2}\cos^2\frac{\theta_{max}}{2}}\,\mathrm{erf}\left(\frac{q}{\sqrt{2}}\sin\frac{\theta_{max}}{2}\right) \tag{3.10}$$

Figure 3.2 shows the behavior of the solution q of the above equation w.r.t the central angle θ_{max}. It is evident that q increases with θ_{max} and reaches the maximum value $q = 1.1405$ when $\theta_{max} = \pi$. This is very important to route design.

Consider routing a packet between any two points in a network of clusters, each of radius a. The euclidean path between these two end points intersects the encountered intermediate clusters. The intersecting segment within each cluster is analogous to a chord in a circle. When the size of these clusters relative to the width[1] of the delay distribution function is large enough ($a > 1.1405c$), it is indeed more optimal to route the packet around the edges of all the clusters than to route via the shortest path.

3.3 Minimum delay inter-cluster route

In the previous section we formulated the optimal paths using the analytically feasible Gaussian function for the delay distribution in a multi-hop cluster. In this section, we study the spatial delay distribution within a CSMA wireless cluster, and numerically solve for the resulting minimum delay path.

3.3.1 Spatial distribution of the hop delay in a multi-hop cluster

A sensor node with communication range R is physically i hops away from the center of a multi-hop cluster if the Euclidean distance between the node and the clusterhead is in $[(i-1)R, iR]$. The cluster can thus be divided into concentric rings, each of depth R. In a data-collecting cluster with K rings, the sensed data from individual nodes in ring K are

[1] Here, width refers to the value of the independent variable r at which the dependent variable F is equal to $e^{-\frac{1}{2}}$ of its maximum value.

forwarded to the nodes in ring $(K-1)$. The nodes in ring $(K-1)$ further forward the data to the nodes in ring $(K-2)$, along with the data they generate. Sensor data from all the nodes in the cluster are finally gathered at the clusterhead.

In such a cluster with K rings, the mean number of nodes will be $\pi K^2 R^2 \lambda$, where λ is the spatial node density. Suppose the packet length is $\frac{1}{\lambda_p}$ and the channel throughput at the clusterhead where channel load is maximum is η, the packet generation rate at each node can be expressed as

$$g = \frac{\eta \lambda_p}{\pi K^2 R^2 \lambda} \tag{3.11}$$

Contribution to the total channel load by a node in ring i, including both the generated and the forwarded data, will be on an average

$$g_i = \frac{K^2 - (i-1)^2}{i^2 - (i-1)^2} g \tag{3.12}$$

Consider a node at a radial distance r from the clusterhead. The corresponding ring number is $i = \lceil r/R \rceil$. The rate at which new packets arrive to the channel as seen by this node in its communication range is $G = [A_{i-1} g_{i-1} + A_i g_i + A_{i+1} g_{i+1}]\lambda$, where A_i is the area of intersection of ring i with the disc of radius R centered at r. For appropriate boundary conditions, $g_{K+1} = g_K$ and $A_0 = 0$.

Now, we need to find the hop-delay associated with the packet arrival rate G in the carrier sense multiple access (CSMA) wireless protocol. To this end, previous works [71][72] present a continuous time Markov chain (CTMC) model that characterizes these networks by a matrix whose dimensions are independent of the number of users and provides a closed form expression for the expected delay. For simplicity, let us consider the infinite population case with a constant load retransmission policy. Operating the channel within the stable region, the retransmission rate is chosen to be $\gamma = L_{max} - G$, where L_{max} is the total channel load at highest maximum throughput, as shown in Figure 3.3. It can be observed that, as the input rate increases, the retransmission rate and its feasible interval decreases

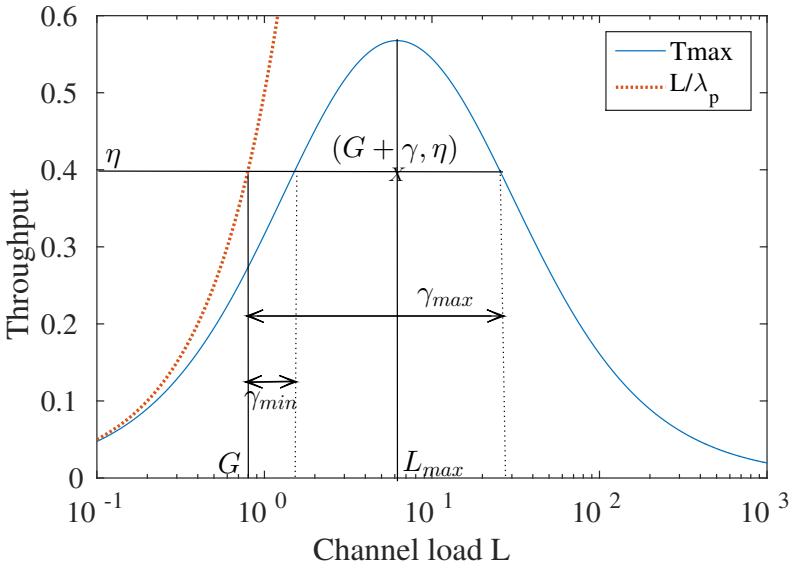

Figure 3.3: A plot of the maximum throughput vs channel load curve following [71, Eqn. 65] for the CSMA protocol showing the operating point. Here, the conflict truncation time is equal to packet length ($\lambda_c = \lambda_p = 2$) emulating collision avoidance and the transmission detection time is set to be $\frac{1}{\lambda_d} = \frac{0.1}{\lambda_p}$.

and thereby, the hop-delay increases.

The expected hop-delay can be calculated using Little's result, which requires computing the stationary probabilities of the CTMC. Further details on the resulting matrix equations is provided in Appendix B. Accordingly, we can calculate the hop-delay encountered by a test packet in different rings of the clustered network. Figure 3.4 shows the variation of the resulting expected hop-delay in a cluster in terms of packet length and fits a Gaussian model of the form $\{be^{-\frac{a^2}{2c^2}} + d\}$ for different throughput cases. The additive constant is close to the asymptotic value; i.e., $d \approx 1$. Consider $\eta = 0.5$ for example, the parametric values of the corresponding fit are $b = 3.421$, $c = 1.052$ and $d = 1.165$. Note that Eqn. 3.5 can be updated accordingly to obtain a more accurate demarcation. Furthermore, we proceed to find the optimal path that minimizes the end-to-end delay by employing the derived Gaussian fit as the spatial hop-delay distribution function.

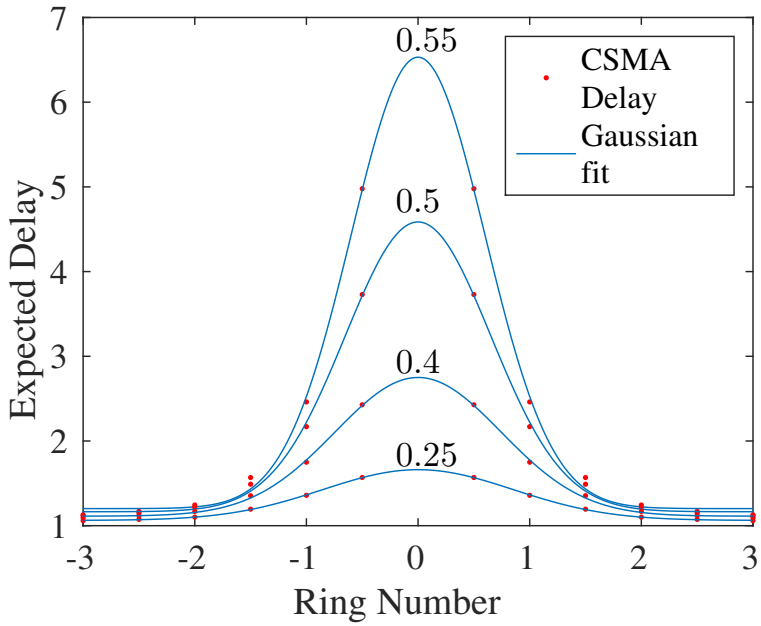

Figure 3.4: Plot of the expected hop-delay within the different rings of a 3-hop cluster fitted with the (constant+Gaussian) function. Delay for the given load G is computed using a CTMC model of the CSMA channel. The plots are indexed by the channel throughput η of the innermost ring.

3.3.2 Minimization of the end-to-end delay functional

In order to find the optimal path between two points $(-a,0)$ and $(a,0)$, we must minimize the functional I of Eqn. 3.1 subject to boundary conditions $y(-a) = 0$ and $y(a) = 0$. Using the principles of variational calculus [73], we find the gradient of the functional defined on the infinite-dimensional function space. The critical function satisfies the first order condition

$$\frac{d}{d\epsilon} I(y + \epsilon z)\Big|_{\epsilon=0} = 0, \tag{3.13}$$

resulting in the equation below.

$$\int_{-a}^{a} \left[\frac{F(x,y)}{\sqrt{1 + \left(\frac{dy}{dx}\right)^2}} \frac{dy}{dx}\frac{dz}{dx} + z\frac{\partial}{\partial y} F(x,y) \sqrt{1 + \left(\frac{dy}{dx}\right)^2} \right] dx = 0$$

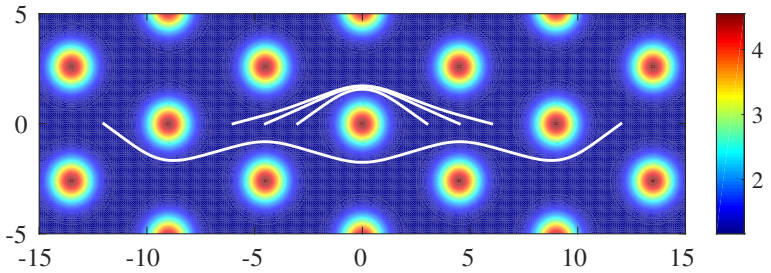

Figure 3.5: Contour map of the hop-delay F in a hexagonal lattice of 3-hop clusters where $\eta = 0.5$. The curves, being solutions of Eqn. 3.14 to within 1e-6 accuracy of convergence, represent the minimum delay routes between their end points.

Applying the method of integration by parts to the first term and reducing the boundary terms to zero due to the boundary conditions, we have

$$\int_{-a}^{a} z \left[\frac{\partial}{\partial y} F(x,y) \sqrt{1 + \left(\frac{dy}{dx}\right)^2} - \frac{d}{dx} \left(\frac{F(x,y)}{\sqrt{1 + \left(\frac{dy}{dx}\right)^2}} \frac{dy}{dx} \right) \right] dx = 0$$

From the fundamental lemma of the calculus of variations, the term within square brackets is zero, leading to the following simplified differential equation.

$$F(x,y)\frac{d^2y}{dx^2} = \frac{\partial F(x,y)}{\partial y} \left(1 + \left(\frac{dy}{dx}\right)^2\right) \tag{3.14}$$

Solving the above equation numerically using second order accurate central finite differences, we obtain the minimum delay routing paths shown in Figure 3.5. Here, F is composed of the mean delay spatial function recurrent within a hexagonal lattice, representing the clustered network. Suppose $m, n \in \mathbb{N}$,

$$F(x,y) = d + b \sum_{i=-n}^{n} \sum_{j=-m}^{m} e^{-\frac{(1.5ai+x)^2 + (0.5\sqrt{3}ai + \sqrt{3}aj + y)^2}{2c^2}} \tag{3.15}$$

The figure demonstrates how an optimal inter-cluster route would navigate a packet so that it avoids the inner rings of clusters.

3.4 Distributed algorithm for Edge Routing

From the above analysis, we have gained an insight into the delay minimizing paths in a clustered network. Accordingly, it could be more optimal to route the inter-cluster packets via the nodes located on the periphery of the clusters—we call this 'edge routing'—rather than routing them via the shortest path. Presented in this section is a distributed algorithm that can achieve edge routing. One of the main aspects of the proposed algorithm is that it does not require any location information to identify the nodes that belong to the outer-most rings in the cluster. Classification of such edge nodes is instead integrated into the clustering algorithm.

3.4.1 Clusters

Consider a distributed multi-hop clustering algorithm along the lines of [35]. The clusterhead broadcasts a Route-REQuest (RREQ) packet to initiate the clustering process. On receiving a RREQ packet, the node associates with the corresponding clusterhead. The RREQ is then forwarded if the hop count is within the specified upper bound. Since it is desirable to cluster the nodes with the nearest clusterhead, a node here is re-assigned whenever it receives a RREQ with hop count fewer than its preceding assignment. A pseudo-code to setup the intra-cluster routes and to identify the edge nodes within this framework is presented in Section 3.4.4.

3.4.2 Intra-cluster routes

Routes for communicating to and from the clusterhead are established in close association with the clusterhead assignment. During each assignment of a node, the routing table entry for the clusterhead which originated the RREQ is updated. These backward routes to the clusterhead have the immediate RREQ source node as the next hop. Likewise, forward routes to the nodes from the clusterhead are established with a Route-REPly (RREP)

packet. The nodes unicast the RREP to their clusterhead after waiting an initial time period for the reassignments to complete. In order to achieve a more uniform cluster size and routing tree structure, we can re-assign the nodes and/or update the routes with a certain probability whenever a RREQ with hop count equal to the preceding assignment is received.

3.4.3 Inter-cluster routes

Classification of the edge nodes is based on the hop count information in the RREQ packet. The edge nodes consist of: 1) The nodes which are equal number of hops away from their two nearest (in terms of hop count) clusterheads. 2) The nodes with hop counts from their two nearest clusterheads differing by one. 3) The nodes that remain unassigned to a clusterhead, if any. The nodes so identified can be used for inter-cluster routing between any two designated edge nodes. The route request is initiated by the origin and the rest of the protocol is similar to AODV [67]. However, the broadcast and forwarding of the RREQ packet is restricted to only the edge nodes here. Like before, the routing table entries for the origin are recorded and updated to establish the backward route with fewest hops via the edge network. Further, the destination node replies with a RREP packet to establish the forward route.

3.4.4 Psedo-code: Distributed Clustering, Classification and Routing

The ClusterHead (CH) component

$ch\_assigned$ = TRUE; my_class = CH; $my\_chId = my\_id$; ch_hops = 0;
Broadcast < $RREQ$, my_chId, my_id, $hop = 1$ >
if < RREP, $origin$, $dest == my\_id$, src > *message received* **then**
  Add Route < Dest: $origin$, Next hop: src >

The End-Device (ED) component

K = maximum number of hops
T_{wait} = Reply wait time
T = Cluster setup time
T_{lag} = Random lag time windiw for stability

▷ Initialization
$ch\_assigned$ = FALSE; my_class = ED; my_chId = inf; ch_hops = inf;
while $clock < current\_time + T$ **do**
    Listen for messages
    if < RREQ, $chId$, $srcId$, hop > *message received* **then**
        $EDtoEG\_now$ = FALSE;
        if $| ch\_hops - hop | \leq 1$ **and** $chId! = my\_chId$ **then**
            ▷Edge-node classification
            my_class = EG; $EDtoEG\_now$ = TRUE;
        if $ch\_assigned \neq$ TRUE **or** $hop < ch\_hops$ **then**
            $ch\_assigned$ = TRUE; $my\_chId = chId$; $ch\_hops = hop$;
            if EDtoEG_now = FALSE **then**
                ▷Re-classification of re-assigned nodes
                my_class = ED;
            ▷Forward Route to CH
            Add Route < Dest: my_chId, Next hop: $srcId$ >
            if $reply\_scheduled = FALSE$ **then**
                Start timer $T_B = T_{wait}$ + Uniform(0,T_{lag})
                $reply\_scheduled$ = TRUE;
            if $hop <$ K **then**
                $hop = hop + 1$;
                Broadcast < RREQ, my_chId, my_id, hop >
    if < RREP, $origin$, $dest$, src > *message received* **then**
        ▷Backward routes to connected nodes
        Add Route < Dest: $origin$, Next hop: src >
        Unicast < RREP, $origin$, $dest$, my_id >
if $ch\_assigned \neq$ TRUE **then**
    ▷ Forced edge-node
    my_class = EG;

Reply-Timer T_B **expire event** ()
$origin\_id = my\_id$; $dest\_id = my\_chId$; $reply\_scheduled$ = FALSE;
Unicast < RREP, $origin\_id$, $dest\_id$, my_id >

3.5 Simulation studies: AODV vs. Edge routing

In this section, we perform simulations with common networking protocols in place to study the characteristics of the edge route and the shortest path route across a single cluster. To this end, we have implemented the described distributed clustering and routing algorithm within the framework of the ns-3 simulator [74][75]. We have used large-scale parallel computing to perform the following expensive simulations, comprising large-scale networks of more than a thousand nodes.

3.5.1 NS-3 simulation: Network setup

The nodes are uniformly randomly distributed with a spatial density λ in a square region. A network of n nodes has a high probability of connectedness, if each node is connected to more than $1.5\ log_e\ n$ neighbors [76]. We approximate λ using the above guideline. Further, we consider a hexagonal lattice of clusters by appropriately specifying the locations of the clusterheads. Thereby, communications in the cluster of interest are also subject to interference from communications in the clusters that surround it. The algorithm described in the previous section is implemented to: set-up the clusters, classify edge nodes and establish the intra- and inter-cluster routes, as shown in Figure 3.6. The resulting edge route is compared with the AODV route, on further selecting the one with the fewest number of hops. The routes of interest are compared with the following protocol stack in place.

Application: The nodes generate $ECHO$ packets with a payload of 64 bytes bound to their clusterhead at a specified rate. Each packet is sent at a time instant uniformly randomly chosen within the corresponding data interval ranging between 50 ms and 1 s. On receiving an ECHO packet from a node, the clusterhead responds with an $ECHO\_REPLY$. The test packets between inter-cluster source and destination are however generated at a lower rate, i.e., within time intervals of 1 s. *MAC and Physical*: 802.11a 6 Mbps OFDM with RTS/CTS, availed from the NS3 wifi models: 'AdhocWifiMac', 'YansWifiChannel' and

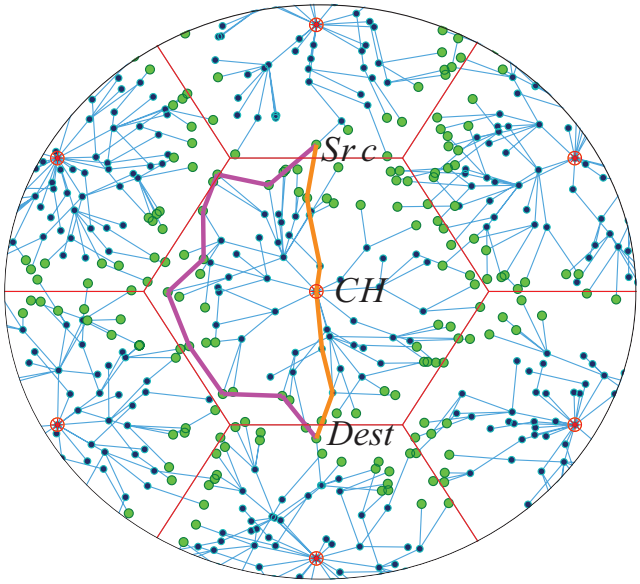

Figure 3.6: A visualized instance of the clusters, and the intra- and the inter-cluster routes generated by the proposed distributed algorithm. As seen, the classified edge-nodes highlighted in green lie along the edges of the tessellation created by the clusterheads (CH). The test packets are routed between the origin (src) and the destination (dest) located on either side of a 3-hop cluster via the routes shown for edge-routing and AODV shortest path routing.

'YansWifiPhy'. Channel errors are discounted to make the simulations more robust, while maintaining focus on the routing schemes.

3.5.2 Results

Simulation results for a 3-hop network, where adjacent clusters share the outermost rings are presented in Figure 3.7 and Figure 3.8. Each data point is computed by taking the mean over 2500 network simulations. This includes 50 instances of clusters corresponding to different seeds of the random number generator, followed by 50 test packet simulations for each instance. While the delay performances are comparable in a lightly loaded network, shortest path routing has a significantly higher delay in high throughput clusters. Lower backoff delays coupled with smaller queue sizes along an edge route renders it immune to the fluctuations in cluster throughput. Further, packets on an edge route do not suffer loss, even when the clustered network is critically congested, thereby achieving a robust

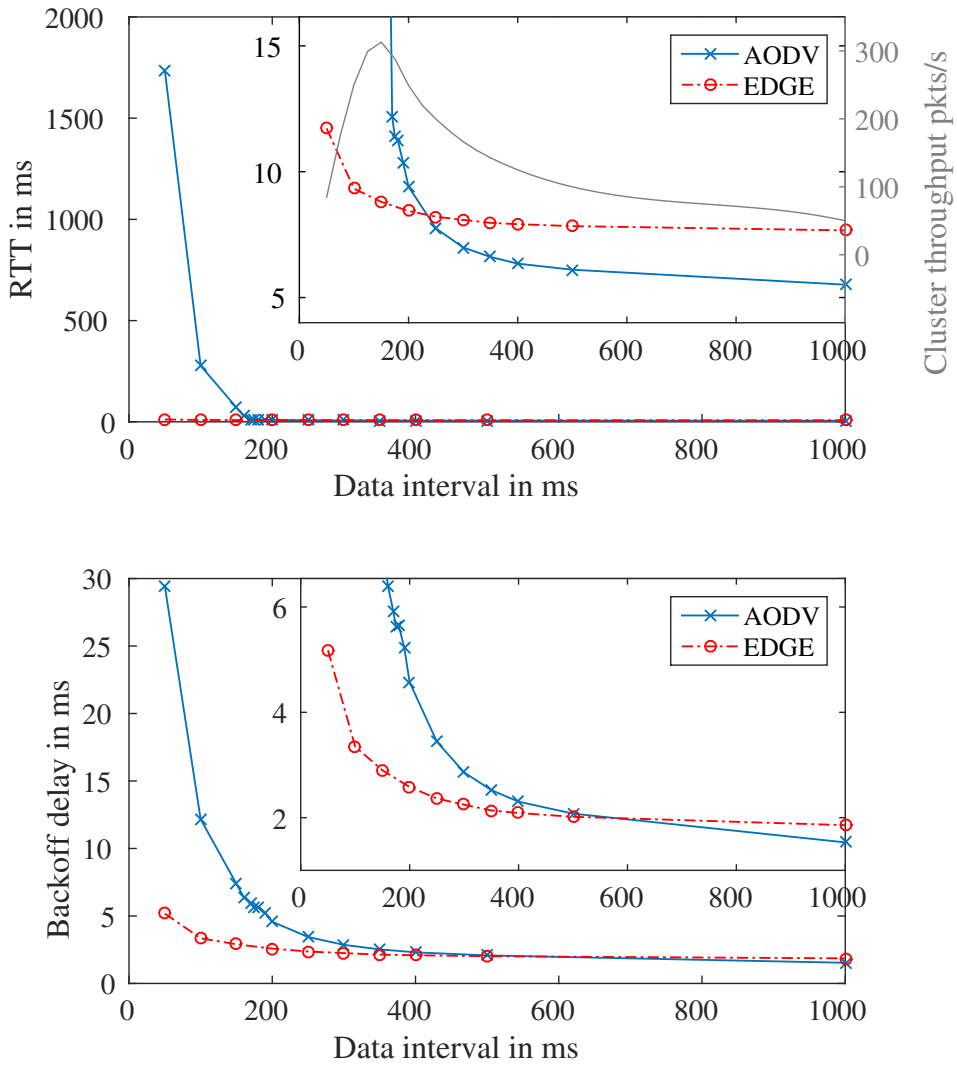

Figure 3.7: Simulation of the shortest AODV and the edge routing protocols at different data generation rates within clusters of radial size 2.5 hops. In this case, the expected number of hops in the AODV and edge routes are 5.37 and 8.26 respectively. The x-axis represents the interval/time-window within which a data packet is uniformly randomly generated by a node. The y-axes represent the expected end-to-end Round Trip Time (RTT) of the inter-cluster test packets, and the expected sum total time between channel access request and successful transmission of the test packet at the route nodes. While the plots show the behavior of a congested network, the insets are zoomed to show the behavior for different degrees of throughput in the data gathering cluster.

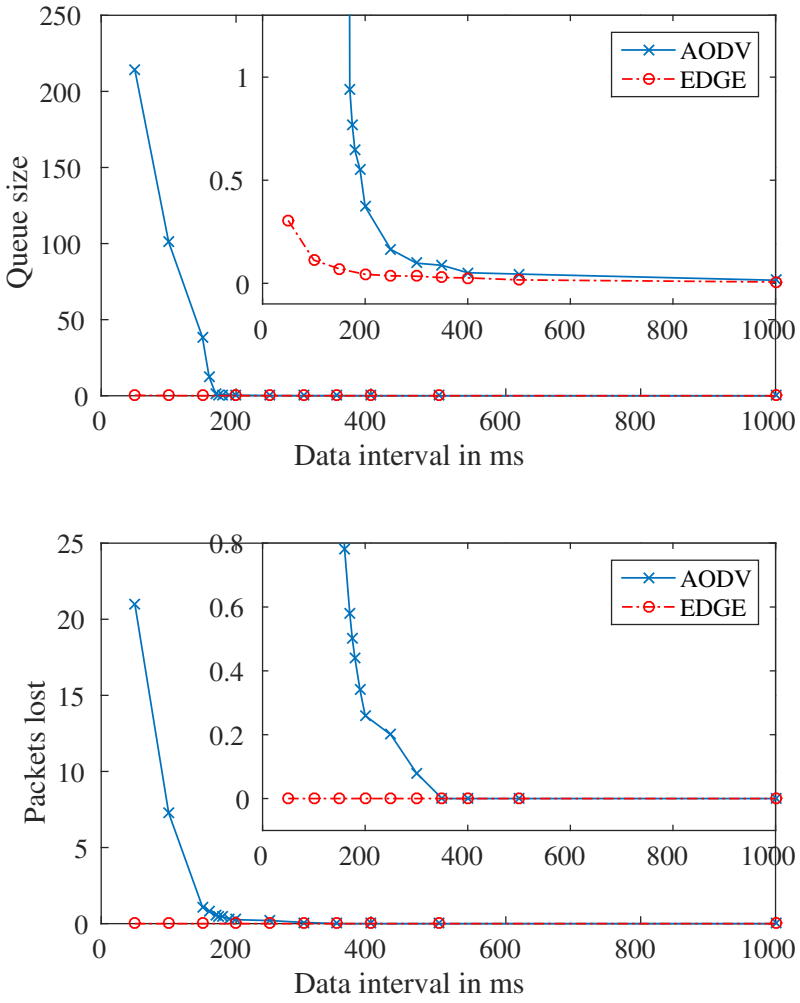

Figure 3.8: Simulation of the shortest AODV and the edge routing protocols at different data generation rates within clusters of radial size 2.5 hops. In this case, the expected number of hops in the AODV and edge routes are 5.37 and 8.26 respectively. The x-axis represents the interval/time-window within which a data packet is uniformly randomly generated by a node. The y-axes represent the expected sum total queue size encountered by the test packet at the intermediate nodes, and the expected number of packets lost of the 50 test packets launched. While the plots show the behavior of a congested network, the insets are zoomed to show the behavior for different degrees of throughput in the data gathering cluster.

and reliable service. Note that the performance of edge route can be significantly higher if an optimally designed channel access protocol is used [70].

Figure 3.9 presents the route characteristics as a function of the size of the traversed cluster. It shows that even though edge routes take many more hops than AODV shortest routes, their mean round trip time is smaller by an order of magnitude under maximum throughput cluster conditions. Furthermore, the variance of the end-to-end round trip time in AODV shortest route is approximately 10^5 $(\text{ms})^2$, whereas that of the edge route is only 1 $(\text{ms})^2$, offering a tightly bound delay guarantee. The difference in performances is utmost in 2-3 hop clusters, which constitute a majority of the energy-efficient clusters in large-scale adhoc networks [64].

3.5.3 Remark

Comparing the two routes with plots analogous to Figure 3.1 upon using the established (constant+Gaussian) fit for the distribution function shows that the circular route outperforms euclidean route when $\eta > 0.4$ for $a = K = 2.5$. Substituting the parameters: $R = 160$, $\lambda = 0.00018$, and $\lambda_p = 2500/2$ in Eqn. 3.11, we have $g = 5.5$ pkts/s. Equivalently, the data interval is 182 ms, lower-bounding the crossing point from simulations shown in Figure 3.7. Taking queue delay into account, η would be lower resulting in a more accurate match.

3.6 Application case: Inter-level routing in a Voronoi Tessellated network

In this section, we discuss the application of the edge routes for communicating between the different levels of an optimally clustered multi-level hierarchical network. The required modifications for routing along the edges of a Voronoi tessellated network are discussed, followed by the characterization of the inter-level routes that emerge.

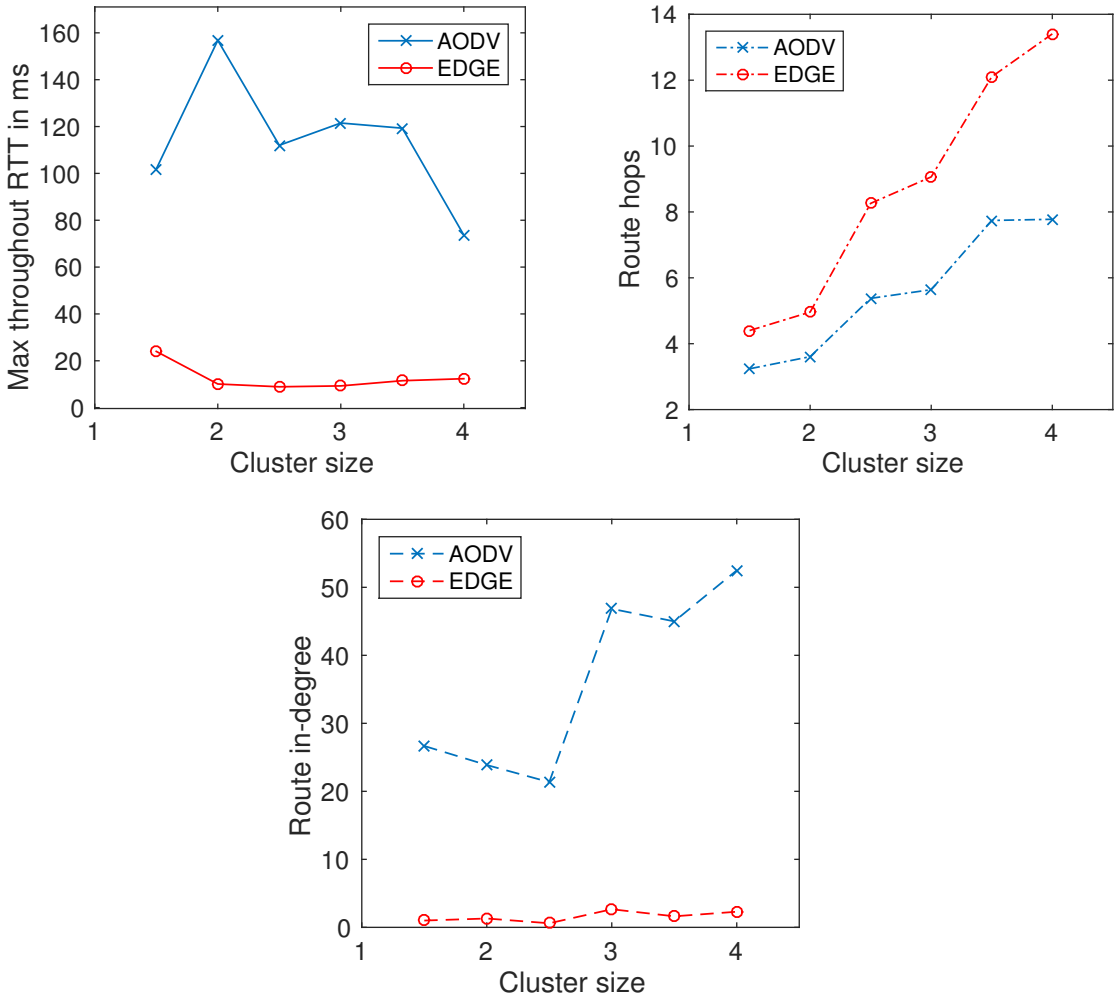

Figure 3.9: Simulation of the shortest AODV and the Edge routing protocols for different sized clusters. The x-axis represents the radial size in terms of hops. The y-axes represent the end-to-end Round Trip Time (RTT) of the inter-cluster test packets at maximum throughput conditions of the data gathering cluster, the number of hops in the route, and the expected sum total of children nodes to the route nodes, within the cluster.

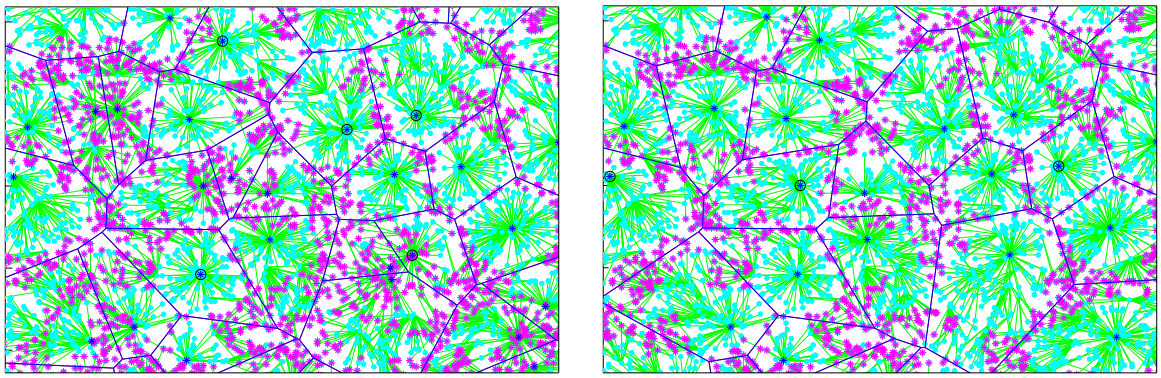

(a) Original tessellation (b) Merging of the CHs within a hop of each other

Figure 3.10: Effect of CH merging on the identification of edge nodes in a Poisson Voronoi tessellated network.

3.6.1 Regularizing the clusters

The edge node identification scheme is critical in determining the performance of the edge routing protocol as well as the connectivity of the network. In Figure 3.10a, the nodes equal number of hops away from at-least two nearest clusterheads are visualized. We see that the nodes identified as edges are not always restricted along the tessellation. One main reason is that, when two CHs are within a hop of each other, most of the nodes in proximity are at equal number of hops from both of them and are hence classified as edge-nodes. A solution to this would be to randomly elect only one CH of the pair and reset the other as a common node. It is apparent in Figure 3.10b that such a merging of close-by CHs also improves the regularity of the tessellation to a great extent.

In the implementation of the clustering algorithm, the clusterheads broadcast the route request RREQ message at an instant uniformly randomly chosen within a time window T_{REQ}. Any CH receiving RREQ from another CH within its range R is reset as a common node. When the CH location is originally described by the process $Poisson(\lambda_1)$, this sort of dependent thinning of the Poisson process maintaining a minimum distance between the points results in what is known as a *hard core process*. The thinned CH intensity λ_{th} can

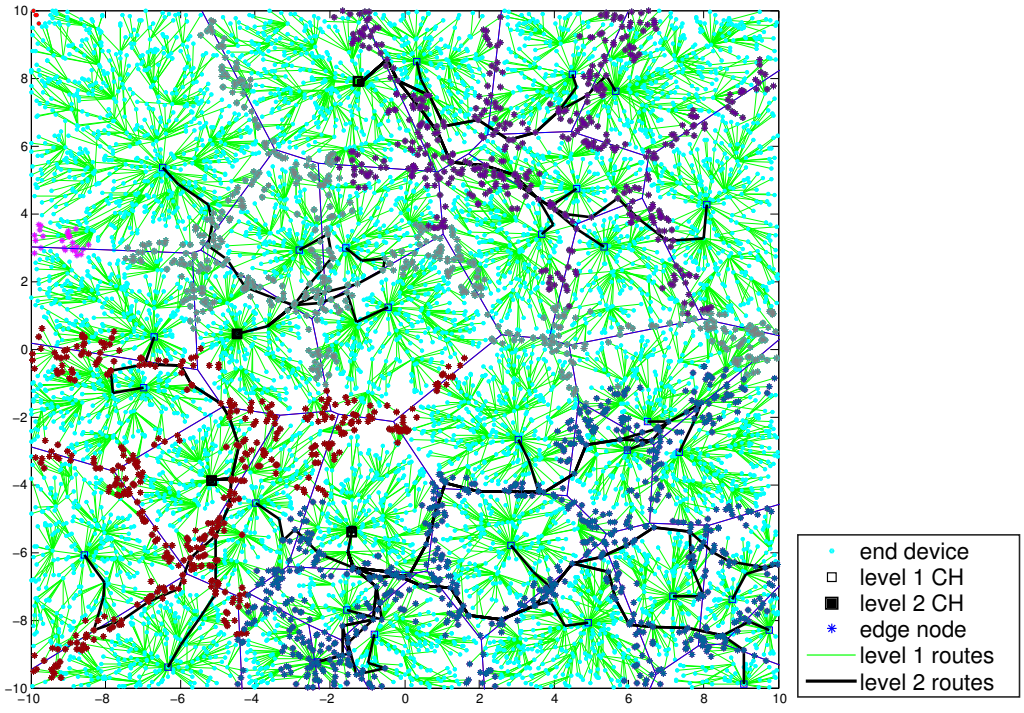

Figure 3.11: Inter-cluster edge routing in a multi-level hierarchically clustered network.

be approximated[2] by the *Matern's model II* [77] [78],

$$\lambda_{th} = \frac{1 - e^{-\lambda_1 \pi R^2}}{\pi R^2} \quad and \quad \lambda_{th} \to \frac{1}{\pi R^2} \quad as \quad \lambda_1 \to \infty$$

The original optimal probability of clusterhead election p_{opt} [56][64] can thereby be adjusted to a higher value using a prefactor. If λ is the node density,

$$p_{opt}^{new} = \frac{\lambda_1}{\lambda_{th}} p_{opt} = \frac{\pi R^2 p_{opt}^2 \lambda}{1 - e^{-p_{opt}\lambda\pi R^2}} \tag{3.16}$$

Further, consider two uniform random variables $X, Y \sim U(0,T)$. The probability distribution of their absolute difference can be computed as

$$\mathbb{P}(|X - Y| \leq \Delta) = \frac{\Delta(2T - \Delta)}{T^2} \tag{3.17}$$

[2]In *Matern's model II*, a point is retained in the secondary process if there is no other point within a radius R in the *primary process* that has a lower mark. Whereas, in our case, a point is retained if there is no other point of the *secondary process* with a smaller mark (broadcast time). This is in fact the third model suggested by Matern, that hasn't been studied so far.

We need $|X - Y|$ greater than the propagation delay T_p to merge the CHs.

$$\mathbb{P}(|X - Y| > T_p) = \frac{(T - T_p)^2}{T^2} \geq \tau \implies T \geq \frac{T_p}{1 - \sqrt{\tau}} \tag{3.18}$$

Therefore, in order to achieve CH merging with probability greater than τ, the time-window T_{REQ} has to be at-least $\frac{T_p}{1-\sqrt{\tau}}$.

3.6.2 Inter-level routing

Consider a two level hierarchical network. Level-1 clusterheads are independently elected from the end-devices and level-2 clusterheads are independently elected from level-1 clusterheads with probabilities that achieve energy-efficiency [56][64]. Upon merging clusterheads located within a hop of each other, the level-1 clusters and intra-cluster routes are setup as described earlier in Section 3.4. For routing between the clusterheads at different levels, the packets are relayed via the 'edge-CH', the edge-node that is closest to the clusterhead as demonstrated in Figure 3.11. The level-2 edge-CHs broadcast the L2RREQ packet to initiate setup of the edge network. On receiving the L2RREQ, an edge node associates with the corresponding edge-CH and updates the routing table for backward routes. A node is reassigned whenever it receives a request with fewer hop counts. After waiting for the reassignmnets to complete, an L2RREP packet is sent to its level-2 edge-CH for establishing the forward routes. A pseudo-code for the distributed clustering, classification and routing algorithms along with the structure of the control packets is provided in Appendix C.

3.7 Further discussion: Characterization of the inter-level routes

For a node intensity λ, the level-1 CH intensity is $\lambda_1 = p_1\lambda$, level-2 CH intensity is $\lambda_2 = p_1p_2\lambda$ and the PVT intensity is $\gamma = 2\sqrt{\lambda}_1$ [79]. The route between a level-1 CH and a level-2 CH consists of three components: (1) R_1: The first segment to exit a cluster, i.e., the

route between the CH and the nearest edge-node (level-1 edge-CH) (2) C^*: The shortest edge-path along the tessellation (3) R_2: The last segment to enter the level-2 cluster, i.e., the route between the level-2 CH and it's nearest edge-node (level-2 edge-CH). R_1 and R_2 are the in-radii of a typical Voronoi cell. Hence, $R_1, R_2 \sim Rayleigh(\frac{1}{2\sqrt{2\pi p_1 \lambda}})$ [58].

Spatial stochastic model for network components and underlying infrastructure in a telecommunication network with two hierarchy levels considered in [80] provides a framework for the analysis of edge routes. Analogously, level-1 edge-CHs serve as the Low Level Components (LLC) and level-2 edge-CHs serve as High Level Components (HLC). The underlying infrastructure modeled as a random geometric graph is the Poisson Voronoi tessellation created by the level-1 CHs. The components of the stochastic model can be defined as follows: (1) T_γ : Poisson Voronoi Tessellation with intensity γ, induced by level-1 CHs . (2) $T_\gamma^{(1)}$: Edge set of T_γ. (3) X_L : Cox process describing locations of level-1 edge-CHs with linear intensity λ_1^l and spatial intensity $\lambda_1 = \lambda_1^l \gamma$. (4) X_H : Cox process describing locations of level-2 edge-CHs with linear intensity λ_2^l and spatial intensity $\lambda_2 = \lambda_2^l \gamma$. (5) $(X_{L,n}, C_n)$: Marked point process of each point $X_{L,n}$ of X_L marked with the shortest path along the edges of T_γ to the nearest point of X_H. (6) C^* : Typical shortest path along edge route from level-1 edge-CH to level-2 edge-CH.

The distribution of C^* is the Palm mark distribution $P^0_{X_{L,C}}$. The main properties of the length of shortest route between the exit and entry points of the clusters are [80]:

- C^* is fully specified by T, γ, λ_1^l and λ_2^l but does not depend on λ_1^l. If the quotient $\kappa = \gamma/\lambda_2^l$ is constant, then the underlying structure is fixed.
- For $\kappa \to 0$ with λ_2^l fixed, i.e, an unboundedly sparse edge set $T_\gamma^{(1)}$, C^* converges weakly to an exponential distribution $Z \sim Exp(2\lambda_2^l)$ (Figure 3.12a).
- For $\kappa \to \infty$ with $\gamma\lambda_2^l$ fixed, i.e, an unboundedly dense edge set $T_\gamma^{(1)}$, C^* converges weakly to a Weibull distribution $1.145\ Z$ where $Z \sim Wei(\lambda_2\pi, 2)$ (Figure 3.12b).

As the network gets larger, the optimal probabilities of CH election decrease. There-

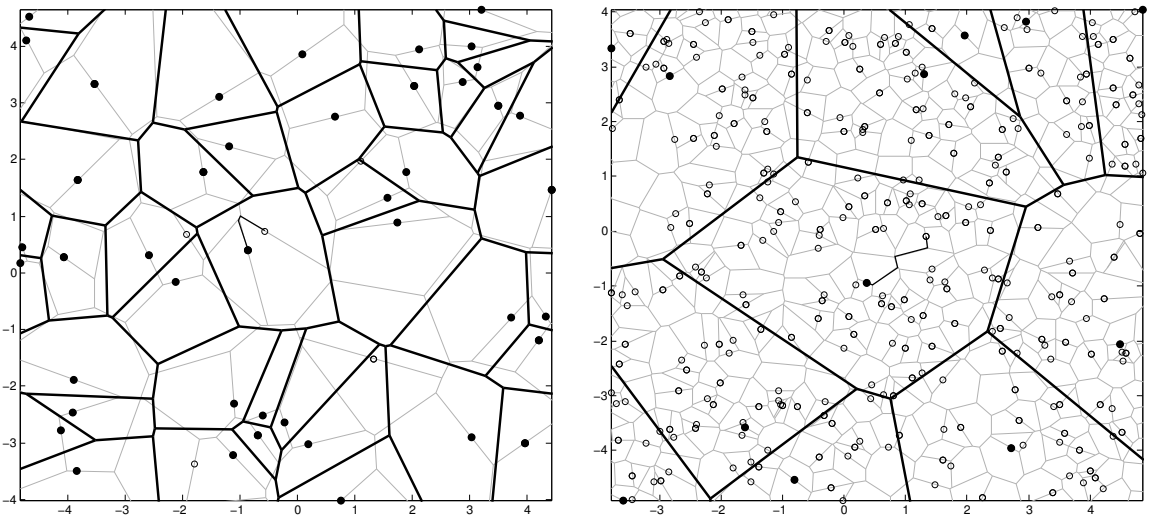

(a) $\gamma \to 0$, λ_2^l fixed, $C^*(\gamma, \lambda_2^l) \xrightarrow{D} Exp(2\lambda_2^l)$ (b) $\gamma \to \infty, \lambda_2^l \to 0, C^*(\gamma, \lambda_2^l) \xrightarrow{D} Wei(\frac{\lambda_2 \pi}{1.145^2}, 2)$

Figure 3.12: Scaling limits for the length of shortest path as $\kappa \to 0$ and $\kappa \to \infty$.

fore, the distribution of C^* gets closer to the Weibull, larger the scale of the network. The distribution of route length can be obtained by fitting a parametric family which contains the exponential and Weibull as the limiting cases, further satisfying the condition $f_{C^*}(0) = 2\lambda_2^l$ [81]. A suitable candidate is the truncated Weibull distribution with density [81]

$$f_{C^*}(x; \alpha, \beta) = C\left(x + \left(\frac{2}{\alpha\beta\kappa}\right)^{\frac{1}{\beta-1}}\right)^{\beta-1} e^{-\alpha\left(x+\left(\frac{2}{\alpha\beta\kappa}\right)^{\frac{1}{\beta-1}}\right)^{\beta}} \tag{3.19}$$

where $C = \alpha\beta \exp\left((\alpha^{-1}(2/(\beta\kappa))^{\beta})^{\frac{1}{\beta-1}}\right)$. The above distributions are useful for studying the route delay and the network connectivity.

For comparison of the mean lengths, The expected Euclidean distance between level-1 and level-2 CHs is given by [58]

$$\mathbb{E}[L_{euclid}] = \frac{1}{2\sqrt{p_1 p_2 \lambda}}. \tag{3.20}$$

The expected length of the center-to-center route via clusterheads is given by [57]

$$\mathbb{E}[L_{CtoC}] = \frac{4}{\pi}\mathbb{E}[L_{euclid}] = \frac{2}{\pi\sqrt{p_1 p_2 \lambda}}. \tag{3.21}$$

The expected total length of edge route has limits [3]

$$\mathbb{E}[L_{edge}] = \frac{1}{2\sqrt{p_1\lambda}} + \frac{1}{p_2\sqrt{p_1\lambda}} \quad as\ \kappa \to 0 \tag{3.22}$$

$$\mathbb{E}[L_{edge}] = \frac{1}{2\sqrt{p_1\lambda}} + \frac{1.145}{2\sqrt{p_1 p_2\lambda}} \quad as\ \kappa \to \infty \tag{3.23}$$

Numerical evaluations indicate that the euclidean distance is scaled by a factor of 1.19 in moderately sized clusters.

[3] $Wei(\alpha,\beta)$ has the pdf $f_X(\alpha,\beta) = \alpha\beta x^{\beta-1}e^{-\alpha x^\beta}\mathbb{1}_{[0,\infty)}(x)$, the cdf $F_X(\alpha,\beta) = 1 - e^{-\alpha x^\beta}$, and the mean $\mu_X = \alpha^{-\frac{1}{\beta}}\Gamma\left(1+\frac{1}{\beta}\right)$. $Rayleigh(\sigma)$ has the pdf $f_X(\sigma) = \frac{c}{\sigma^2}e^{-\frac{x^2}{2\sigma^2}}\mathbb{1}_{[0,\infty)}(x)$, the cdf $F_X(\sigma) = 1 - e^{-\frac{x^2}{2\sigma^2}}$, and the mean $\sigma\sqrt{\frac{\pi}{2}}$.

CHAPTER 4

IN PRACTICE: A SYNCHRONIZED TESTBED FOR MONITORING THE STRUCTURAL HEALTH

4.1 Introduction

We have developed a WSN testbed as part of the eStadium project of the Vertically Integrated Projects (VIP) Program [82] at Georgia Tech. The goals of the project include: enhancing the game-day experience and safety of football fans. This is accomplished by serving innovative infotainment and venue-related information to their mobile devices. Driven by these goals, we have developed a low-power WSN and deployed it in Bobby Dodd stadium. It facilitates unique applications that support crowd-tailored in-stadium content, interaction among fans, crowd safety and security, etc. Potential applications include measuring the popularity of a play by the level of cheering and booing that follows it, estimating waiting times for concessions and detecting bio-chemical hazards. In particular, we have developed a vibration sensing application for the Structural Health Monitoring (SHM) of the stands.

SHM systems have been widely explored for measuring the response of large-scale civil

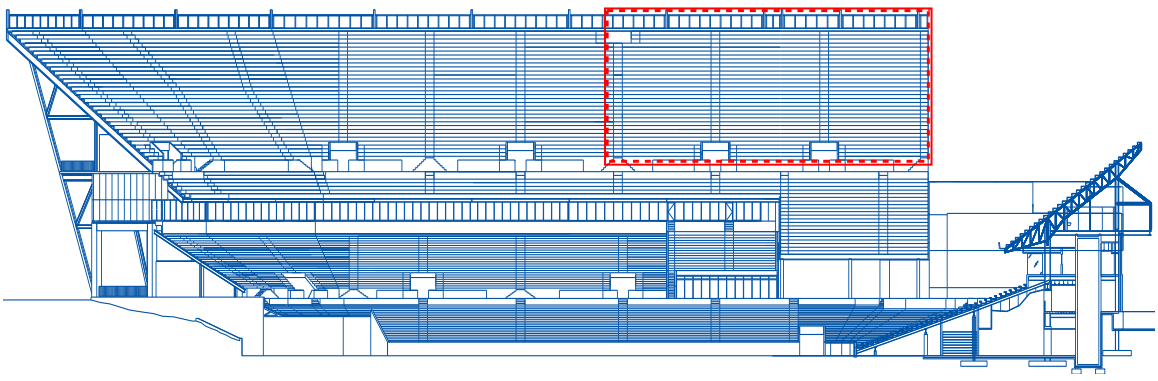

Figure 4.1: North stands of Bobby Dodd Stadium at Georgia Tech. Location of the sensor network currently deployed is marked in red on top-right.

structures. Various types of sensors, such as accelerometers, strain gauges, displacement and velocity transducers can be used for monitoring structural behavior. In order to overcome the high costs associated with cable installation, wireless monitoring systems have been developed. To date, a number of prototypes have been proposed and tested in the field. For example, Lynch et al. validated the performance of a prototype wireless sensor on the Alamosa Canyon Bridge in southern New Mexico [83]. The wireless SHM platform designed by Wang [84] has been validated on a number of bridge structures. In general, these efforts cannot detect twisting in a structure because of the lack of accurate synchronization of measurements. They have a comparatively reduced lifetime due to higher standby power consumption. Also, they do not support operation of the network from a remote server. Some recent work has also been carried out to determine the structural response of stadiums to crowd behavior [85] [86]. These latter efforts are typically based on measurements from one position in the stands or unsynchronized measurements at different positions in the stands over a short period of time. The primary purposes of such endeavors is to determine if the dynamic behavior of the stands exceeds thresholds at which people become uncomfortable or to determine the spectral content of the vibrations at individual positions in the stands.

In this work, we are interested in studying the structural behavior of the North stands of Bobby Dodd Stadium at Georgia Tech. The stands are cantilevered over a plaza, as seen in Figure 4.1. The physical response of the stands is particularly interesting when fans jump to their feet during an exciting play, bounce with music during cheers, and when they all start moving at half-time. The stands' physical responses of interest is therefore correlated with major events in the game. These events may excite resonant modes of the stands in the .5 to 5 Hz range that result in twisting of the concrete deck. Detection of these potentially damaging modes requires highly synchronized measurements of acceleration at many points in the stands. These measurements are collected at a 100 Hz sampling rate over a wireless network and forwarded to our server for analysis. The vibration sensing

SHM application discussed here demonstrates the design and functionality of the WSN tesbed. The pure embedded systems approach devoid of abstraction layers in our design allows for a better definition of the applications compared to the existing embedded OS platforms [87] [88] [89].

Our main results: (1) A WSN designed to operate over a long period of time; i.e, for one or two football seasons. It is well-suited for rare, high user-density events since the network can be remotely operated. (2) A reliable GPS- and beacon-free synchronization algorithm that yields synchronization to within 300 μsec. (3) Wireless backhaul of the data from the stadium via a TV whitespace link. (4) Deployment of the first cluster of the testbed in the stadium. These results are achieved while maintaining the underlying simplicity of the low-cost infrastructure.

The remaining part of this chapter is organized as follows. In Section 4.2, we describe the overall network architecture and detail the hardware and software components of the sensor network testbed. In Section 4.3, we summarize our deployment efforts at Bobby Dodd Stadium. In Section 4.4, we explain the synchronization mechanism developed and in Section 4.5, we present the sleep cycle employed and estimate the power consumption and network lifetime.

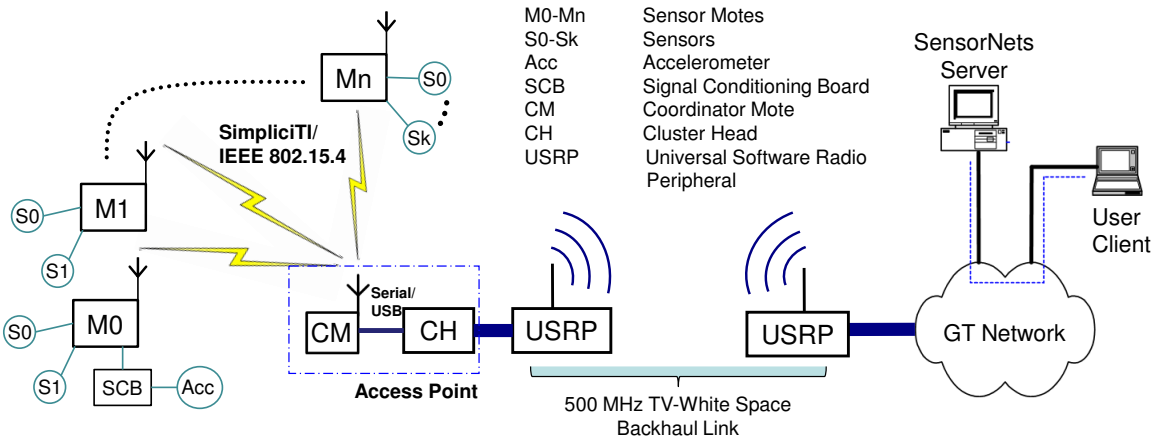

Figure 4.2: The WSN architecture. Note the communication path from the sensors of a single-hop cluster to the server.

4.2 Architecture

End Device (ED)	Sensor network node consisting of a sensor, processing unit and transceiver. Alternatively called a sensor node or sensor mote.
Coordinator Mote (CM)	Master node governing a cluster and responsible for collecting data from the nodes in its cluster.
Cluster-Head (CH)	Computational unit to aggregate and process the information gathered by the coordinator.
Access Point (AP)	CM and CH coupled as one unit.
Backhaul	Communication link between the access point and the remote server.

The WSN is designed to have a clustered, hierarchical architecture. The general layout of the single-hop two-level WSN that we have developed and deployed is shown in Figure 4.2. This can be easily extended to include additional clusters and levels, thus making it scalable. Each cluster of the WSN consists of eight to ten battery-powered end devices that are wirelessly connected to one access point. The access points are connected via the wireless backhaul to the remote server that acts as the sink.

The sensor nodes gather data from local digital and analog sensors for various applica-

tions. The sensed data is packetized and sent wirelessly to the coordinator using the SimpliciTI [90] protocol. The coordinator node then appends a custom header to the packets and forwards them over Universal Asynchronous Receiver/Transmitter (UART) and USB to the cluster-head (CH). The CH aggregates data within the cluster when applicable and generates appropriate queries to the sink. The CH also controls the behavior of the cluster by issuing command packets downstream. Command packets transmitted by the CH are either initiated by the CH or forwarded on behalf of the eStadium SensorNets server. Example scenarios where command packets are applicable include triggering data collection, setting sensor reporting time, and specifying sleep duration. The coordinator and cluster-head together form the access point, which is the gateway to the backhaul network. The CH communicates with the remote server through a TCP/IP connection. A cognitive-radio-enabled TV whitespace bi-directional link is used wherever a wired connection is not available. All of the data collected by the sensor network is stored in a MYSQL database on the server for analysis and for end-user applications. The server also acts as the level-2 cluster-head, thus issuing commands to control functionality of the level-1 cluster-heads. The hardware and software components used to build this network are listed in Table 4.1.

4.2.1 Clustered sensor network

End device

Each sensor mote is a power-efficient system consisting of the MSP-EXP430F5438 microcontroller and a CC2520 (IEEE 802.15.4) radio from Texas Instruments (TI). In addition to several onboard sensors, it has I/O port extensions that allow for interfacing with external sensors. In order to achieve high-resolution acceleration measurement in the vibration sensing project, a low-cost integrated accelerometer package has been developed [91]. The package consists of a MEMS accelerometer (LIS344ALH by STMicroelectronics) and a signal conditioner capable of providing triaxial measurements.The range of the accelerometer can be selected as ±2 g or ±6 g. The noise density of the measurement is 25 $\mu g/\sqrt{Hz}$

Table 4.1: Network Components

Network unit	Hardware	Software
Accelerometer	LT microelectronics LIS344ALH	-
Sensor mote	TI MSP430F5438A Experimenter board	SimliciTI-CCS-1.1.1.exe (Rev. A)
Cluster Communication	TI CC2520EM	SimpliciTI RF protocol
Co-ordinator mote	TI MSP430F5438A Experimenter board	SimliciTI-CCS-1.1.1.exe (Rev. A)
Cluster-head	Advantech PCM-9363D 3.5" Single Board Computer	ch-embedded OS and MYSQL client
SDR	USRP B100 with an Intel NUC PC	GNURadio and gr-mac
Backhaul link	500 MHz Yagi Antennas	-
eStadium SensorNets Server	Dell 2950, 2 Xeon quad core processors	RHEL 6.6 OS with MYSQL Database

along the x and y axes, and 50 $\mu g/\sqrt{Hz}$ along the z axis. The cut-off frequency and gain can be programmed on the fly through an I^2C interface. The power consumption of the integrated accelerometer board is about 12 mA under working conditions and 1 μA while asleep.

Vibration data is acquired during games, concerts, and major weather events for structural health monitoring. For such applications, time-domain vibration data is important. Therefore, sensed vibration data is sent as raw data to the CH and then to the server. The vibration signals of interest have frequencies between 0 and 25 Hz. Hence, a sampling rate of 100 Hz is adequate. Since the vibration measurements of structures as large as a stadium stands are usually in the order of mm/sec^2, small fluctuations in amplitude are of significance to the measurements. To capture such small variations during sampling, a precision of 12 bits/sample is used. The interaction between different modules for an automated processing of the data on the ED is shown in Figure 4.3. The processed data is packetized and transmitted to the coordinator, as explained in the next section. The ED enters a low power

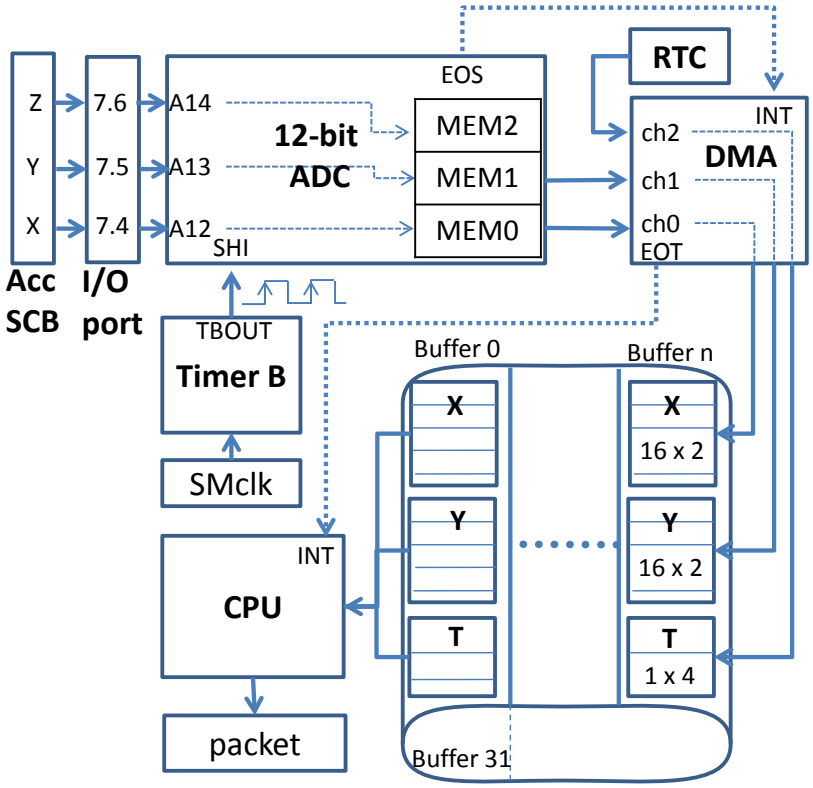

Figure 4.3: Automated vibration sampling and parallel data processing on an ED. The ADC operates in repeat-sequence-of-channels mode, DMA channels 0 and 1 in single transfer mode, and channel 2 in block transfer mode. The sampling is controlled by a pulse-width modulated signal generated by the timer. Once a new sample is ready in the internal memory register, the ADC triggers the Direct Memory Access (DMA) module. The CPU is notified by the DMA module only after the data set for one packet is ready in the data buffer. Multiple data buffers are managed in a round-robin fashion for uninterrupted processing.

mode sleep state and links to the CM at set intervals. The CM controls the sleep cycle of each ED depending on the game time known at the server. The current consumption by the ED is 37 mA in the active state and 20 μA in the sleep state. Hence, the total estimated energy used to collect data during games of one football season is approximately 2 Ahr.

Communication protocol

Each sensor node has a radio module that consists of a CC2520EM daughter board and an antenna. The radio module is interfaced with the MSP430 micro-controller using a Serial Peripheral Interface (SPI) for bi-directional communication of data and radio commands. The CC2520 is a 2.4 GHz transceiver that is compliant with IEEE 802.15.4, which is the standard protocol intended for low-power, low-rate Personal Area Networks (PAN). The IEEE 802.15.4 protocol supports only single-hop networks and comprises only two layers: a physical and a Medium Access Control (MAC) layer. Most IEEE 802.15.4 PANs are configured in a star topology where the central node acts as a coordinator for the rest nodes (i.e., similar to configuration of the network in Figure 4.2). SimpliciTI [90] builds on the IEEE 802.15.4/Zigbee protocol and defines two more layers, the network and application layers. This allows for more advanced features to be implemented in the network, such as multi-hop communication and advanced network management. SimplicTI code runs on the main microcontroller while IEEE 802.15.4 lower layers are implemented in the radio module. The SimpliciTI stack includes an intermediate sub-layer called the Minimal Radio Frequency Interface that conceals the hardware differences.

The vibration data is inserted into the application payload of SimpliciTI packets and sent to the CM at 250 kbps on channel 26 of 802.15.4. The wireless channel uses the CSMA/CA random access with a uniform random backoff scheme. Packing the redundant zero bits in the data results in a further 25% reduction of the wireless traffic and the associated power. The ED also appends a header with both an ID to identify the application and timestamps required for synchronization. On reception of the packet from the ED, the

application on the CM extracts the required information from the headers of lower layers. This is appended as the CM header to the payload and passed to the CH over the serial connection at a baud rate of 230400. The structure of the packet delivered to the CH is shown in Figure 4.4.

Access point

The coordinator mote has the same hardware configuration as that of the sensor mote. It is also an MSP-EXP430F5438 experimenter board equipped with a CC2520 radio module. The coordinator constantly monitors the SimpliciTI channels for packets and passes them to the attached CH in application specific formats.

The Clusterhead (CH) is comprised of an Advantech PCM-6363D 3.5" single board computer (SBC) equipped with an Intel Atom D2525 Dual Core 1.8 GHz processor, Gigabit ethernet, and up to 4 GB of RAM. The role of the CH is to gather the sensor information from the Coordinator over USB, parse it, and update the appropriate MYSQL database via the backhaul network. It is designed to be lightweight, reliable, and efficient. Therefore, a custom minimal but highly efficient Linux distribution, *ch-embedded*, is developed for the CH. The entire distribution is 30 MB. It consists of the Linux kernel and few selected programs required for operation, as shown in Table 4.2. The kernel was extracted from Ubuntu 11.04. There is no persistent file system, only an initial ramdisk (initrd) image is used. The disadvantage of this read-only system is the lack of local writable storage. However, boot time is reduced and the system is more robust against sudden power cycles.

The software architecture of the multi-threaded user-space program that reads data sent over the USB/Serial connection and performs action based on the application type is shown in Figure 4.5. Frame synchronization is performed on the serial data stream in the main thread by using invariant header bits. Once this is achieved, the payload is extracted and the *application id* field is read. Each id is mapped to a thread via a configuration file. Multiple ids may map to a single thread. The main thread passes the payload data to

Field	RSSI	Source Address	Sequence number	CM Received TS	Length	Application ID	First sample TS	Previous sent TS	Data
bytes	1	4	1	4	1	1	4	4	64
Partition	CM header					ED header			ED Payload

Figure 4.4: Structure of the packet passed to the CH from the CM. The payload has 16 vibration samples from the two axes of measurement.

Table 4.2: Clusterhead Software Components

Software	Version	Purpose
Linux Kernel	2.6.38	Operating System
Busybox	1.21.9 (Stable)	Basic Linux Utilities
Dropbear	2013.59	SSH Server
ntp	4.2.6p5	Timing Synchronization
mysql	6.0.2-linux-x64-64	MYSQL Client Library

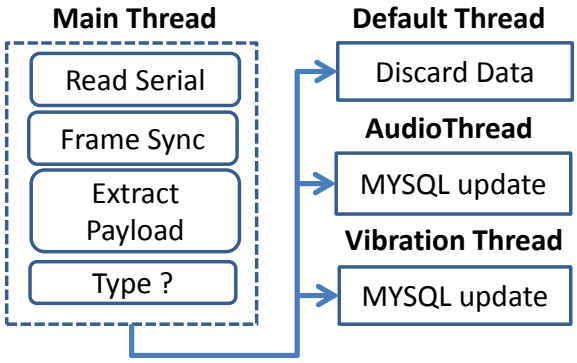

Figure 4.5: Serial Monitor Platform to hand the applications off to right threads.

the processing thread, which performs application-specific processing. For example, the audio and vibration data is uploaded to a MYSQL server. Such an architecture provides abstraction, extensibility, and robustness against failures.

4.2.2 Cognitive radio backhaul

Whitespace software-defined radio

If a wired network is unavailable, a software-defined radio (SDR) can bridge the CHs deployed in the football stadium and the main server infrastructure. Each node consists of an Intel Next Unit of Computing (NUC) Ivy Bridge general purpose computer and an Ettus Research B100 USRP RF digitizer with WBX RF Daughterboard. These SDRs operate in the TV whitespace spectrum (470-690 MHz). The particular operating channel is dictated by the FCC allocation database.

Each NUC uses Ubuntu 14.04 as an operating system and GNURadio [92] for the software radio processing platform. John Malsbury's gr-mac [93] module for GNURadio is

Table 4.3: Data rate and Network capacity

Network	Source	Data Rate (kbps)	Capacity (kbps)
SimpliciTI channel	ED	$4.34 \times p$	250
Whitespace backhaul	CH	$4.58 \times m \times p$	250

used for the PHY/MAC layer implementation but with a modification to use the tap/tun interface. With this change, the bridge between networks is transparent and can be used by multiple clients on each side without any issue. The default modulation scheme in the gr-mac module is Gaussian Minimum Shift Key (GMSK) with a sample rate of 1 Megasample per second and four samples per symbol. The normalized filter bandwidth, $BT = 0.35$ is set as the default.

4.2.3 Network load vs capacity

The bit rates of data generated from the EDs and CHs on the sensor network with m clusters and p nodes per cluster are given in Table 4.3. This includes the sensor generated data and the overhead due to the SimpliciTI, ED, CM and CH headers. For the target deployment of 50 nodes ($m = 5, p = 10$), the load on the SimpliciTI channel is 44 kbps in a cluster and the load on the backhaul network is 229 kbps. Raw data delivered to the server database in a four hour game is 64.4 Mb per node, for a total of 48.3 MB per node in a 6-home-game season.

4.3 Deployment and game data

A sample of the data we have collected is shown in Figure 4.6. It is evident from the plot that crowd behavior and other major events have an influence on the structural excitation. A crowd stomping in unison could excite a resonance in 0.5 - 5 Hz range. The vibration measurements at the intersections of the supporting beams are collected on game days to study the dynamics of the loaded stands. A modal analysis of the structure would reveal the occurrence of harmful modes of resonance and further aid in timely maintenance. Detecting

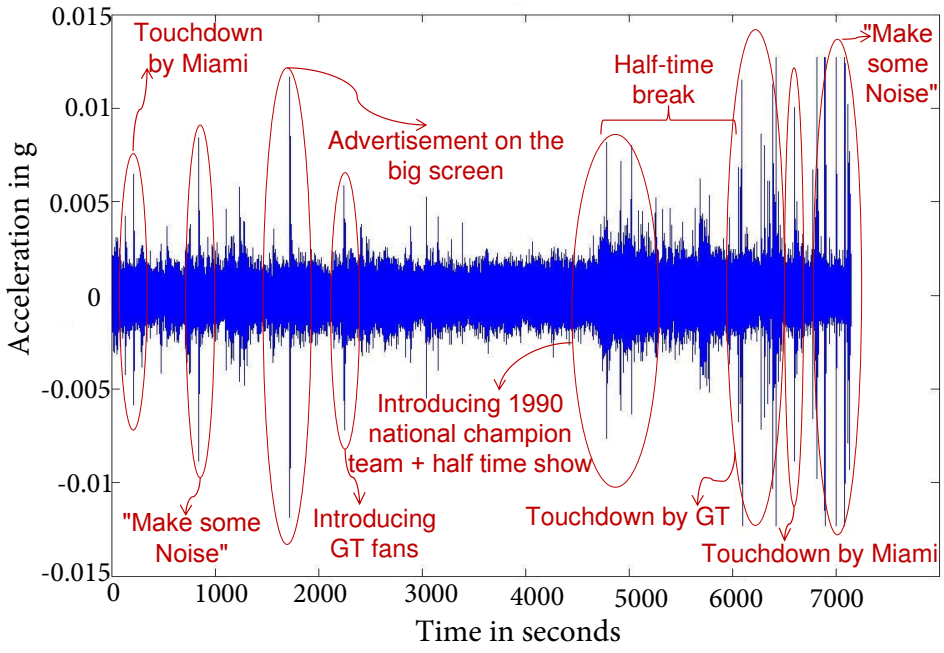

Figure 4.6: Structural vibrations indicating events during a football game.

Figure 4.7: Infrastructure of the sensor network deployed at Bobby Dodd Stadium. (A) Picture of section 119, north stands showing the locations and orientation of sensor nodes. (B) An enclosed node and sensor harnessed on the girder. (C) A node consisting of MSP430, CC2520, and battery packs. (D) Access point consisting of MSP430, CC2520, and clusterhead PCM-9363. (E) Software defined radio showing NUC and USRP.

torsional modes is important as they can result in spalling. Our objective is thus to deploy 40-50 nodes and 5-10 CHs to cover the North stands of Bobby Dodd Stadium. Currently, the first cluster is test deployed as pictured in Figure 4.7. The motes secured to the girders are housed in weather-proof enclosures and sensors are mounted on the junctions with magnets. The synchronized data collected from ED2 and ED3 are uploaded to the eStadium Sensornets website [94] and can be made available on request.

4.4 Synchronization

Along with the frequency of resonance, we require the phase difference of the resonant frequencies between different locations in the stands to determine the modes of vibration. Only the phase lag between the signals at different sample points in a 2D plane can distinguish between in-phase tandem motions and out-of-phase twisting motions. Therefore, in order to differentiate the modes of resonance, we require the end-devices at different locations to be synchronized. We have developed a light-weight, simple time-stamping mechanism to synchronize the devices in a cluster within the desired accuracy.

Due to energy constraints and the lack of good GPS signals in the stands' confined environment, we are using a GPS-free and beacon-free scheme that achieves a synchronization accuracy of 200 to 300 μs with 95% confidence. The simplicity and robustness of this scheme achieves synchronization in disadvantaged networks having minimal processing capabilities. Since wireless sensor networks are characterized by their inexpensive low-power devices, their clocks are subject to drift and skew. The message construction delay at the transmitter, random access backoff delays in accessing the channel, the propagation delay and the message process delay at the receiver introduce additional randomness into the timestamps. These factors pose a challenge in predicting the true-time from the observed local clock timestamps. The commonly used 802.11 protocol is not suitable for high drift rates and results in increased packet loss due to intermittent reverse broadcasts in an otherwise unidirectional network. It will be evident from the section below that our

algorithm, called Untethered Time Transmission Mapping (UTTM), is simple yet robust and not susceptible to the factors above.

According to the survey and classification scheme for synchronization protocols for ad-hoc networks in [95], our UTTM algorithm has the following features: master-slave, untethered clocks, probabilistic, and sender-to-receiver synchronization. It is unique in applying the traditional Time Transmission Protocol (TTP) to wireless sensor networks. The overhead of synchronization messages in TTP is overcome by piggybacking the timestamps into the data packets, which isn't usual for sent timestamps. This works well in continuous environment monitoring such as our vibration sensing application.

A local timestamp on the ED is taken after a packet is successfully sent and later inserted into the subsequent packet. This eliminates both the message processing and the random access delay from the time-critical path. With a fast enough serial out-link on the CM, we eliminate the packet queue in the receiver and thus the associated data processing delay when recording the received timestamp. Hence, the only randomness involved in estimating the ED clocks relative to the CM clock is reduced to the propagation delay. The interpolation technique used here accounts for all offsets, clock drift and constant delays through the communication stack as opposed to continuous offset estimation and correction in TTP. The ED and CM clocks run untethered; i.e, we build a table relating the ED clocks to the CM clock without clock correction, thereby maintaining an uniform accuracy.

4.4.1 Time-stamping mechanism

Synchronization of vibration samples involves the following three TimeStamps (TS) of the Real Time Clock (RTC) as shown in Figure 4.8.

1) *Sample TS*: When the Analog to Digital Converter (ADC) produces the first sample of every packet, accurate timestamp from the RTC is recorded on buffer. DMA is used to automate the immediate recording of the clock on ADC interrupt (Figure 4.3). The TS is sent to CM as part of the application header of the corresponding packet.

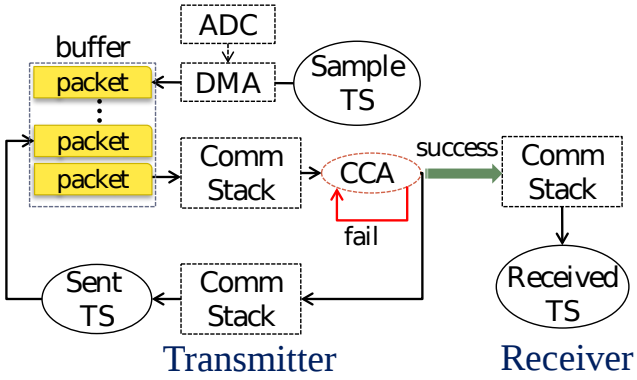

Figure 4.8: Overview of timestamping mechanism.

2) *Sent TS*: Once a packet is successfully sent, the RTC is recorded by the CPU on the ED. The TS is sent to the CM as part of the application header of the next packet.

3) *Received TS*: Once a packet is received, the RTC is recorded by the CPU on the CM. This is forwarded to the CH as a header along with the rest of the packet.

In summary, for each packet on the CH we have the ED clock when the first sample was taken, ED clock when the previous packet was sent, and the CM clock when the current packet was received.

4.4.2 Synchronization of vibration samples

The sent and received TSs are used to construct an estimator for the ED clock in terms of the CM clock. Further, the sample TSs from all the EDs in a cluster are mapped to a common CM clock, thus synchronizing the vibration samples. The data point pairs mapping the CM received TS and ED sent TS of each packet are populated on the CH. This is followed by a two-step process:

1) *Eliminate packet-loss introduced error*: Since the sent TS is received along with the next packet, any packet loss results in erroneous TS pairs. The packet loss is detected from the sequence number and source ID of the packet and these invalid pairs are exempted from further analysis.

2) *Map sample TS to common clock*: Between every two sent TSs there is the sample TS.

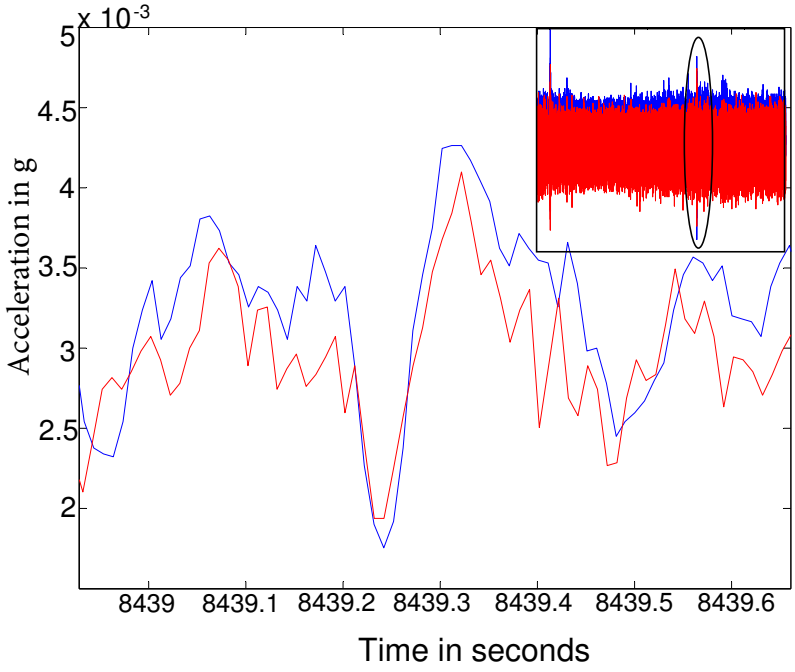

Figure 4.9: Synchronized signals from two EDs hosted on parallel girders.

Hence a cubic interpolation provides a very good map of the sample TS to the CM clock. This requires populating only a few points at any time. Since each packet has a fixed number of samples in it, we can further interpolate at evenly spaced intervals to obtain the CM clock for every sample.

4.4.3 Performance evaluation

Although the observed phenomenon has a low frequency of 0-20 Hz, the achieved accuracy of synchronization is well within a millisecond, surpassing the requirements of modal analysis. The performance mainly depends on the accuracy of the timestamps on the ED and CM. Significant improvements in the performance are possible using a higher clock frequency and time-stamping at the physical layer on Start of Frame Delimiter Tx/Rx, if feasible. This requires cross-layer information exchange at the receiving end to distinguish data packets from handshake packets.

The current implementation uses a 16-bit RTC running at a low frequency of 32kHz. Each packet has 16 samples along the two axes of measurement. Hence each timestamp is

Table 4.4: Statistics and confidence intervals of error residuals

Sync	**Mean**(s)	**Variance**(s^2)	$\tau(\mu s)$**95C**	$\tau(\mu s)$**99C**
ED1-CM	-3.1911e-7	5.4545e-8	212	310
ED2-CM	1.2200e-6	1.5928e-7	255	390
ED1-ED2	8.0280e-7	2.2164e-7	386	660

recorded approximately every 160ms. The data collected from two end-devices hosted on parallel girders after synchronization is shown in Figure 4.9. The peak, when zoomed-in shows an overall correlation between the signals on the two devices. However, the sample correlation coefficient between the two signals after synchronization, computed over an interval around the peak shown in the window, is 0.2356.

The performance of the algorithm is evaluated using a running window linear least mean square estimator. Let N be the total number of packets after loss correction and $(2n + 1)$ be the window size. We use a window of size 16s with $n = 50$ over which the clock is modeled to be linear. Given a packet seq number i ranging between $1 + n$ and $N - n$, CM received TS X_i and ED sent TS Y_i, the estimated true ED clock $\hat{Y}_i = \alpha + \beta X_i$ where

$$\alpha = \bar{Y} - \beta\bar{X}, \quad \beta = \frac{\sum_{j=i-n}^{i+n}(X_i - \bar{X})(Y_i - \bar{Y})}{\sum_{j=i-n}^{i+n}(X_i - \bar{X})^2},$$
$$\bar{X} = \sum_{j=i-n}^{i+n} \frac{X_j}{2n+1} \quad \text{and} \quad \bar{Y} = \sum_{j=i-n}^{i+n} \frac{Y_j}{2n+1}$$

The mean and variance of the error residual $\epsilon_i = Y_i - \hat{Y}_i$ are the performance metrics of synchronization between the ED and CM. The error statistics computed on sample data collected at the stadium is given in Table 4.4. At a confidence level C, the accuracy τ satisfies

$$C = \frac{\sum_{i=n+1}^{N-n} I_{\{|\epsilon_i|<\tau\}}}{N-2n} \quad \text{with} \quad I_A(x) = \begin{cases} 1 \text{ if } x \in A \\ 0 \text{ if } x \notin A \end{cases}$$

i.e, 95% of $|\ \epsilon\ |$ for ED1 is within $212\mu s$. 100% of $|\ \epsilon\ |$ on both the EDs is within 8 ms. The packet loss is 0.0375% for ED1 and 0.0946% for ED2 with $N = 25000$. To estimate

App payload field	Command	parameter
Value (bytes)	SS/ST/SL (2)	hrs:mins (2)
Default	SL	1:0

Figure 4.10: Control packet from the CM to an ED.

the synchronization between the two end devices, the residual samples closer together are added and the statistics are recomputed.

4.5 Sleep cycle and energy usage

A mechanism to determine when a network should be active or when it should go to sleep and save energy is a primary requirement for any sensor network. It could be either a distributed control, where the decision is made on the sensing device or a centralized one, where the cluster-head specifies how the network has to behave. The former is preferable in detection problems and the latter in environment monitoring applications. We explain below a centralized approach to control the sleep cycle within a cluster. The CM controls the state of each linked ED individually. The ED has the flexibility to override the command in detection applications, in which case the data will still be collected at the cluster-head. The sleep cycle can also be synchronized when required since the CH is aware of each ED's clock relative to its own.

In our example, the game-time known at the server determines when to start collecting data. By default, the ED is in low-power (LPM3) sleep mode with all the peripheral modules and radio turned off and it links to the CM once every hour. When the ED links to the CM, the CM replies with a control packet shown in Figure 4.10. This determines whether the ED starts sampling (SS) or goes to sleep (SL). It also specifies the time duration for which these states are to be maintained. The CM can also ask the ED to stop sampling and go to sleep with the stop (ST) command. The flow chart for the sleep-cycle mechanism on the ED is shown in Figure 4.11. The timer is configured in calendar mode to support any sleep duration. The cycle is iterated using system reset; hence, the time duration from the

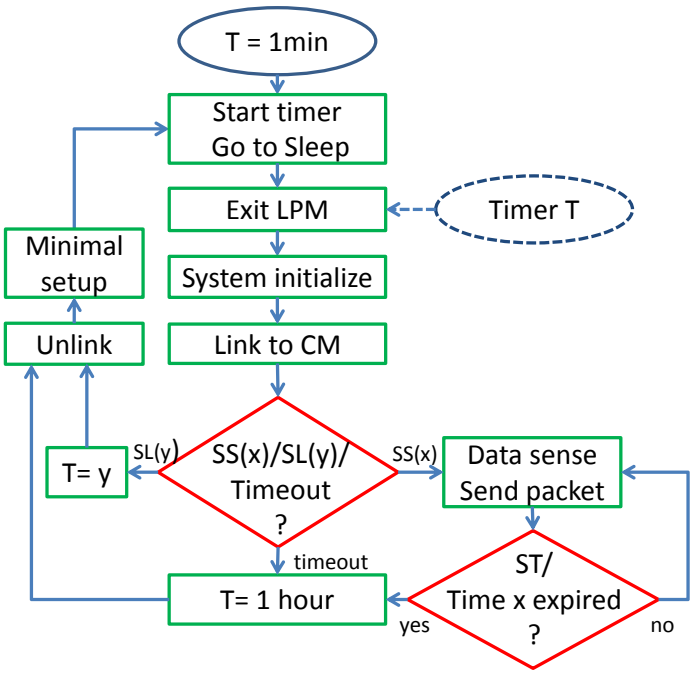

Figure 4.11: Sleep cycle control on an ED.

control packet is maintained in flash memory.

The measured current consumption by the ED is 37 mA in the active state and 20 μA in the sleep state. Hence, the total estimated energy used to collect data during games of one football season is approximately 2 Ahr, which is easily within the capability of 2 AA Lithium batteries. 12-bit ADC samples are stored as a word resulting in 4 redundant zero bits for every sample. Packing the data by removing these redundant bits before sending the packet results in a 25% reduction of the wireless traffic and the associated power usage.

CHAPTER 5
CONCLUSIONS

In this thesis we have addressed three aspects important to the design of wireless sensor and adhoc networks.

In Chapter 2, we have used a stochastic geometry based ad hoc network communication model to study the optimality conditions within a data gathering hierarchical network. The study shows how the application and aggregation dependent data sizes across the levels of hierarchy influence the optimal number of levels and the optimal number of clusters at each level. We have formulated cut-offs on the number of nodes for which single and two levels of hierarchy are sufficient. These results are useful for application-specific tailoring of both the architecture as well as the clustering algorithms in the design of sensor and ad hoc networks of varied sizes.

The problem studied is an example of the bounded minimization of a multi-dimensional objective function typically requiring the solution of a system of non-linear (polynomial) equations. The techniques used here to derive analytical insight from the high-degree polynomial equations could be applied to other bounded optimization problems. Extending the cost model to study the optimality of networks where the data size forwarded by the clusterhead depends on the size of its cluster is a worthwhile topic for future research.

In Chapter 3, we have presented a novel analytical/computational framework for finding the cost minimizing routing paths in a network. Considering a clustered wireless network, we have demonstrated that its well-defined spatial structure can be exploited to optimize the overlying routes. The results show that the shortest path is not always delay-efficient for inter-cluster routing. Instead, a path that traverses along the edges of the clusters has lower delay, especially under high throughput conditions, besides being more robust and reliable. The proposed edge routing is further useful for creating an energy balance, when

applied for routing between levels of optimally clustered large-scale hierarchical adhoc and sensor networks.

The framework for optimizing routes can be applied for any cost function. Spatial properties of the optimal route can be found using tools from calculus to analyze the formulated differential equation. As part of future research, we can characterize the network connectivity and the global energy balance.

In Chapter 4, we have designed and deployed a scalable wireless sensor network tesbed for long-term data collection. We have demonstrated a vibration-sensing structural health monitoring application to collect real-time game data over an entire football season. It has a simple and practical hierarchical architecture with a cognitive radio backhaul. All the network components are custom designed. Further, the network is both synchronized and supports sleep cycles, the two major requirements in a wireless sensor network.

Solar powered nodes with over-the-air programming facility will yield a self-sustainable sensor network. In the big picture, vibration sensing network interfaced with audio and spectrum sensing networks, and web applications developed by the Vertically Integrated Projects Stadium-IoPT team would be the realization of an 'Internet of People and Things' testbed within the high user density, and rich signal space environment of a football game.

Overall, the major outcomes from this thesis include: (1) A scalable, synchronized and deployable sensor network. (2) An NS3-based large-scale sensor network simulator with novel clustering and routing algorithms. (3) Innovative stochastic models for the analysis of clustered wireless networks. We believe that this thesis is a significant step towards the realization of energy- and delay-efficient large-scale sensor networks.

Appendices

APPENDIX A

OPTIMAL CLUSTERING LEMMAS

A.1 Proof of the existence of a unique real-valued root of $p(x) = 2cx^3 - x^2 - 1$ with range (0,1) when $c > 1$

The discriminant of the cubic polynomial $p(x) = 2cx^3 - x^2 - 1$ is less than zero. Hence, $p(x) = 0$ has one real and two complex conjugate solutions. From Rouche's bound on the real-valued root, $\mid x \mid \leq max\{1, \frac{1}{c}\}$, i.e., $\mid x \mid \leq 1 \quad \forall c \geq 1$. Further, $x \leq 0 \implies p(x) < 0 \quad \forall c \geq 0$. Also, $x = 1 \implies c = 1$ when $p(x) = 0$. Therefore, $p(x)$ has a single real-valued root that lies in (0,1) when $c > 1$.

A.2 Proof of the existence of a unique real-valued root of $p(x) = 4\alpha_2^2 d^2 x^7 + \alpha_1^2 x^5 - 2\alpha_1^3 x^4 + 2\alpha_1^2 x^3 - 4\alpha_1^3 x^2 + \alpha_1^2 x - 2\alpha_1^3$ with range (0,1) when $\alpha_2^2 d^2 > \alpha_1^2(2\alpha_1 - 1)$

Under the assumptions of $\alpha_1, \alpha_2 > 1$, $d > 0$ and $\alpha_2^2 d^2 > \alpha_1^2(2\alpha_1 - 1)$, in the following Lemmas 1-2 we show that $p(x)$ has a real-valued root in $(0, 1)$. In Lemmas 3-4 we show that this root is distinct and unrepeated, thus proving the claim.

Lemma 1. *$p(x)$ has at-least one real-valued root in (0,1) when $\alpha_2^2 d^2 > \alpha_1^2(2\alpha_1 - 1)$.*

Proof. Since $p(x)$ is a polynomial, it is continuous and differentiable everywhere. $p(0) = -2\alpha_1^3 < 0 \; \forall \alpha_1 > 0$ and $p(1) = 4\alpha_2^2 d^2 + 4\alpha_1^2 - 8\alpha_1^3 > 0$ for $\alpha_2^2 d^2 > \alpha_1^2(2\alpha_1 - 1)$. By the intermediate value theorem, $\exists\, c \in (0, 1)$ s.t. $p(c) = 0$. ■

Lemma 2. *All the real-valued roots of $p(x)$ lie in $(0, 1)$ when $\alpha_2^2 d^2 > \alpha_1^2(2\alpha_1 - 1)$.*

Proof. Consider the three intervals for $x \in \mathbb{R}$:

$$\begin{aligned}
x \leq 0 \quad &\implies \quad p(x) < 0 \quad \forall \alpha_1, \alpha_2, d > 0 \\
x \geq 1 \quad &\implies \quad x^n \geq x^m \quad \forall n, m \in \mathbb{N},\ n > m \\
&\implies \quad x^5 + 2x^3 + x \geq x^4 + 2x^2 + 1,\ 4x^7 \geq x^4 + 2x^2 + 1 \\
&\implies \quad p(x) \geq (x^4 + 2x^2 + 1)(\alpha_2^2 d^2 + \alpha_1^2 - 2\alpha_1^3) \\
&\qquad \forall \alpha_1, \alpha_2, d > 0 \\
&\implies \quad p(x) > 0 \quad \forall \alpha_2^2 d^2 > \alpha_1^2 (2\alpha_1 - 1)
\end{aligned}$$

Hence, all the real-valued roots of $p(x) \in (0, 1)$. ∎

Lemma 3. *$p(x)$ has exactly one distinct real-valued root in $[0, 1]$ when $\alpha_2^2 d^2 > \alpha_1^2(2\alpha_1 - 1)$.*

Proof. Sturm's theorem states: Given a univariate polynomial p of order m and the sequence of polynomials

$$\begin{aligned}
p_0(x) &= p(x) \\
p_1(x) &= p'(x) \\
p_2(x) &= -rem(p_0, p_1) \\
p_3(x) &= -rem(p_1, p_2) \\
&\ldots \\
p_m(x) &= -rem(p_{m-2}, p_{m-1}),
\end{aligned}$$

denote the number of sign changes in the sequence $p(\xi)$, $p_1(\xi)$, $p_2(\xi)$, ... ,$p_m(\xi)$ as $\sigma(\xi)$. Then, for $a < b$, both real numbers such that $p(a), p(b) \neq 0$, the number of distinct real-valued roots in $[a, b]$ is given by $\sigma(a) - \sigma(b)$.

For $\alpha_2^2 d^2 > \alpha_1^2(2\alpha_1 - 1)$, the sign sequence of $p(x)$ at $x = 0$ is - + + - + + + - $\implies \sigma(0) = 4$. For $\alpha_2^2 d^2 > \alpha_1^2(2\alpha_1 - 1)$, the sign sequence of $p(x)$ at $x = 1$ is + + + - +

$+ + - \implies \sigma(1) = 3$. Hence, There is only one distinct real-valued root in $[0, 1]$. We can further show that this is a non-repeating root. ■

Lemma 4. *$p(x)$ is square free in $\mathbb{R}$ i.e., there are no real-valued repeated roots.*

Proof. Let r be a root of $p(x)$ i.e, $p(r) = 0$. Then, $\exists$ a sixth order polynomial $q(x)$ such that,

$$\begin{aligned} p(x) &= (x - r)q(x) \\ p'(x) &= q(x) + (x - r)q'(x) \\ p'(r) &= q(r) \end{aligned}$$

Hence the derivative $p'(r) = 0$ if r is a repeated root. We have

$$\begin{aligned} p'(r) &= 28\alpha_2^2 d^2 r^6 + 5\alpha_1^2 r^4 - 8\alpha_1^3 r^3 + 6\alpha_1^2 r^2 - 8\alpha_1^3 r + \alpha_1^2 \\ rp'(r) &= rp'(r) - 7p(r) \\ &= \alpha_1^2(-2r^5 + 6\alpha_1 r^4 - 8r^3 + 20\alpha_1 r^2 - 6r + 14\alpha_1) \end{aligned}$$

Since $r \in (0, 1)$ (Lemmas 1-2), $r^{n+1} < r^n \; \forall n \in \mathbb{N}$. Therefore,

$$\begin{aligned} 0 < r < 1 \quad &\implies \quad 6r^4 > 2r^5,\ 20r^2 > 8r^3,\ 14 > 6r \\ &\implies \quad rp'(r) > 0 \quad \forall \alpha_1 \geq 1 \end{aligned}$$

Hence, $p'(r) \neq 0 \; \forall r \in (0, 1)$ i.e, $p(x)$ does not have a real-valued repeated root. ■

A.3 Proof of the boundedness of $p_1^\star$

Lemma 5. *If r is a root of $p(x) = 4\alpha_2^2 d^2 x^7 + \alpha_1^2 x^5 - 2\alpha_1^3 x^4 + 2\alpha_1^2 x^3 - 4\alpha_1^3 x^2 + \alpha_1^2 x - 2\alpha_1^3$ and $s = \frac{\alpha^2(r^2+1)}{2\beta d r^3}$, then $s \in (0, 1)$ given $\alpha_1 > 1$.*

Proof. From Lemmas 1-4, $p(x) = 0$ has a unique real-valued solution r such that $0 < r < 1$. Therefore, $r^{n+1} < r^n \ \forall n \in \mathbb{N}$. Hence, $2r^5 + 4r^3 + 2r < 2r^4 + 4r^2 + 2$ i.e., $\alpha_1^2(2r^5+4r^3+2r) < \alpha_1^3(2r^4+4r^2+2) \ \forall \alpha_1 \geq 1$. Since $p(r) = 0$, $\alpha_1^2(r^5+2r^3+r) < 4\alpha_2^2 d^2 r^7$ which implies $\alpha_1^2(r^2+1)^2 < 4\alpha_2^2 d^2 r^6$ given $r > 0$. Hence, $s = \frac{\alpha_1(r^2+1)}{2\alpha_2 dr^3} < 1$. Also, $\alpha_1, \alpha_2, d > 0 \implies s > 0$. ∎

A.4 Proof of threshold inequality

Lemma 6. *$th_{23}\{p_2\} < th_{23}\{p_3\}$ when $\alpha < \beta$. Here $\alpha, \beta > 1$.*

Proof. $th_{23}\{p_3\}$ and $th_{23}\{p_2\}$ are given by Eqn. 2.30 and Eqn. 2.31. We need to show,

$$
\begin{aligned}
& \frac{\alpha^2\left[2\alpha^5 - \alpha^4 - 2\alpha^2\beta^2 + 4\alpha^3\beta^2 - \beta^4 + 2\alpha\beta^4\right]}{4\rho^2\gamma^2\beta^4} \\
& \qquad < \frac{\beta^2\left[2\alpha(2\beta-\alpha)\sqrt{\frac{2\beta-\alpha}{\alpha}} + \alpha - 2\beta\right]}{\rho^2\gamma^2\alpha} \\
\Longleftarrow \quad & \alpha^3(2\alpha^5 - \alpha^4 - 2\alpha^2\beta^2 + 4\alpha^3\beta^2 - \beta^4 + 2\alpha\beta^4) \\
& \qquad < 4\beta^6\left[2\alpha(2\beta-\alpha)\sqrt{\frac{2\beta-\alpha}{\alpha}} + \alpha - 2\beta\right] \\
\Longleftarrow \quad & 2\alpha^8 + 4\alpha^6\beta^2 + 2\alpha^4\beta^4 + 8\alpha^2\beta^6 + 8\beta^7 < 16\alpha\beta^7 + 4\alpha\beta^6 + \alpha^7 + 2\alpha^5\beta^2 + \alpha^3\beta^4 \\
\Longleftarrow \quad & (2\alpha-1)(4\alpha\beta^6 + \alpha^3\beta^4 + 2\alpha^5\beta^2 + \alpha^7) < 8\beta^7(2\alpha-1) \\
\Longleftarrow \quad & (4\alpha\beta^6 + \alpha^3\beta^4 + 2\alpha^5\beta^2 + \alpha^7) < 8\beta^7 \quad \forall\alpha > 1
\end{aligned}
$$

The last statement is true since $4\alpha\beta^6 < 4\beta^7$, $\alpha^3\beta^4 < \beta^7$, $2\alpha^5\beta^2 < 2\beta^7$ and $\alpha^7 < \beta^7$ $\forall\alpha < \beta$. ∎

APPENDIX B

HOP-DELAY D GIVEN THE PACKET ARRIVAL RATE G

Evaluation of the hop-delay D given the packet arrival rate G for a CSMA/CD channel is presented in closed form in [71]. To gain clarity, we walk-through the procedure and present the equations associated with the infinite population case.

From Little's result, the mean delay is given by

$$\overline{D} = \frac{\overline{B}\lambda_p}{G}$$

where $\overline{B}$ is the average number of active users, $\frac{1}{\lambda_p}$ is the mean packet length and G is the packet arrival rate. $\overline{B} = \sum_{n=1}^{\infty} n\overline{P}(n)e = \overline{P}(1)e + \overline{P}(2)(2I - R)(I - R)^{-2}e$ [71, Eqn. 63] where $\overline{P}(n)$ is the vector of limiting probabilities for n users and $e = [11 \ldots 1]^T$. Matrix R is given by $R = -A_0[A_1 + Ge1_{(0)}]^{-1}$, where

$$A_0 = \begin{bmatrix} 0 & 0 & 0 & G & 0 \\ 0 & G & 0 & 0 & 0 \\ 0 & 0 & 0 & G & 0 \\ 0 & 0 & 0 & G & 0 \\ G & 0 & 0 & 0 & 0 \end{bmatrix}$$

$$A_1 = \begin{bmatrix} -(G+\gamma+\lambda_p+\lambda_c) & \lambda_d & \lambda_p & \gamma & 0 \\ 0 & -(G+\lambda_p) & 0 & 0 & 0 \\ 0 & 0 & -(G+\gamma+\lambda_d) & \gamma & 0 \\ 0 & 0 & 0 & -(G+\lambda_c) & \lambda_c \\ \gamma & 0 & 0 & 0 & -(G+\gamma) \end{bmatrix}$$

$$1_{(0)} = \begin{bmatrix} 0 & 0 & 0 & 0 & 1 \end{bmatrix}$$

$\frac{1}{\lambda_c}$ is the mean conflict truncation time and $\frac{1}{\lambda_d}$ is the mean transmission detection time. The limiting probabilities can be obtained by solving the system of equations below.

$$\begin{bmatrix} \overline{P}(0)\overline{P}(1)\overline{P}(2) \end{bmatrix} \begin{bmatrix} -G & B_0 & 0 & 1 \\ B & B_1 & B_3 & e \\ 0 & B_2 & A_1 + RA_2 & (I-R)^{-1}e \end{bmatrix} = \begin{bmatrix} 0 & 0 & 0 & 1 \end{bmatrix}$$

where the component block matrices are

$$B = \begin{bmatrix} 0 & \lambda_p & \lambda_d & 0 \end{bmatrix}^T$$

$$B_0 = \begin{bmatrix} G & 0 & 0 & 0 \end{bmatrix}$$

$$B_1 = \begin{bmatrix} -(G+\lambda_p+\lambda_c) & \lambda_d & \lambda_p & 0 \\ 0 & -(G+\lambda_p) & 0 & 0 \\ 0 & 0 & -(G+\lambda_d) & 0 \\ \gamma & 0 & 0 & -(G+\gamma) \end{bmatrix}$$

B_2 is obtained by deleting the 4^{th} column of A_2 and B_3 is obtained by deleting the 4^{th} row of A_0.

APPENDIX C

INTER-LEVEL ROUTING ALGORITHM

C.1 Structure of the routing packets.

Bytes	1	4	4	4	1	2
Field	Type	Origin	Destination	Source	Class of Origin	Hops from Origin
Clustering and Routing Commands	RREQ	CHId	(Broadcast)	myId	(CH)	hopcount
	RREP	DeviceId	CHId	myId	ED/EG	hopcount
	CMD (1)	L2CHId	L2mEGId	(myId)	(CH)	(hopcount)
	L2RREQ	L2mEGId	(Broadcast)	myId	(EG)	hopcount
	L2RREP	DeviceId	L2mEGId	myId	(EG)	(hopcount)

Optional fields are enclosed in parentheses.

C.2 Distributed clustering, classification and routing : Level-1

Request-Timer T_A expire event()
if $ch\_hops \neq 1$ **then**
  ▷ Merge CHs within one hop
  $ch\_assigned$ = TRUE; my_class = CH; $my\_chId = my\_id$; $ch\_hops = 0$;
  Broadcast < $RREQ$, my_chId, my_id, $hop = 1$ >

Reply-Timer T_B expire event()
$origin\_id = my\_id$;
$dest\_id = my\_chId$;
$reply\_scheduled$ = FALSE;
Unicast < RREP, $origin\_id$, $dest\_id$, my_id, my_class, ch_hops >

Inputs: p_1, k_1, T_{k_1}, T_{REQ}, T_{REP} and T_{wait}

```
▷ Default End Device
ch_assigned = FALSE;  my_class = ED;  my_chId = inf;  ch_hops = inf;
min_hop = inf;  rand = Uniform(0,1);
if rand < p1 then
    ▷ Volunteered CH
    Start timer TA = Uniform(0,TREQ)
while clock < current_time + 2 × Tk1 + TREQ + TREP do
    Listen for messages
    if a message < RREQ, chId, srcId, hop > is received then
        EDtoEG_now = FALSE;
        if | ch_hops − hop |≤ 1 and chId < my_chId and ch_hops ≠ 0 then
            ▷Edge-Node
            my_class = EG;  EDtoEG_now = TRUE;
        if ch_assigned ≠ TRUE or hop < ch_hops then
            ch_assigned = TRUE;  my_chId = chId;  ch_hops = hop;
            if EDtoEG_now = FALSE then
                ▷Re-classification of Re-assigned nodes
                my_class = ED;
            ▷Forward Route to CH
            Add Route < Dest: my_chId, Next hop: srcId >
            if reply_scheduled = FALSE then
                Start timer TB = Twait + Uniform(0,TREP);
                reply_scheduled = TRUE;
            if hop < k1 then
                hop = hop + 1;
                Broadcast < RREQ, my_chId, my_id, hop >;
    if a message < RREP, origin, dest, src, class, hop > is received then
        ▷Backward Routes to Connected Nodes
        Add Route < Dest: origin, Next hop: src >
        if dest = my_id then
            if class = EG and hop < min_hop then
                ▷Edge-Node with minimum hops from CH
                mEG_id = origin;  min_hop = hop;
        else
            Unicast < RREP, origin, dest, my_id, class, hop >
if ch_assigned ≠ TRUE then
    ▷ Forced Edge-Node
    my_class = EG;
```

C.3 Distributed clustering and routing : Level-2

Inputs: p_2, k_2, T_{k_2}, and T_{REP}

```
L2ch_assigned = FALSE;   my_L2chId = inf;
L2ch_hops = inf;   rand = Uniform(0,1)
if my_class = CH and rand < p2 then
    ▹ Volunteered Level-2 CH
    origin_id = my_id;   dest_id = mEG_id;
    Unicast < CMD=1, origin_id, dest_id >
while clock < current_time + 2 × Tk2 + TREP do
    ▹ Representative Edge-CH
    Listen for messages
    if a message < CMD = 1, origin, dest > is received then
        if dest = my_id then
            L2ch_assigned = TRUE;   my_L2chId = my_id;
            L2ch_hops = ch_hops;   origin_id = my_id;
            Broadcast < L2RREQ, my_L2chId, my_id, L2ch_hops + 1 >
        else
            Unicast < CMD=1, origin, dest >
    if a message < L2RREQ, L2chId, srcId, hop > is received then
        if my_class = EG and (L2ch_assigned ≠ TRUE or hop < L2ch_hops)
        then
            L2ch_assigned = TRUE;   my_L2chId = L2chId;
            L2ch_hops = hop;
            ▹Forward Route to Level-2 Edge-CH
            Add Route < Dest: my_L2chId, Next hop: srcId >
            Start timer TC = Uniform(0,TREP)
            if hop < k2 then
                hop = hop + 1;
                Broadcast < L2RREQ, my_L2chId, my_id, hop >
    if a message < L2RREP, origin, dest, src > is received then
        ▹Backward Routes to Connected Level-2 Edge-Nodes
        Add Route < Dest: origin, Next hop: src >
        if dest ≠ my_id then
            Unicast < L2RREP, origin, dest, my_id >
```

Reply-Timer T_C expire event()
$origin\_id = my\_id$;
$dest\_id = my\_L2chId$;
Unicast < L2RREP, $origin\_id$, $dest\_id$, my_id >

Output Data path: $ED \rightarrow CH \rightarrow mEG \rightarrow L2mEG \rightarrow L2CH$

REFERENCES

[1] C.-Y. Chong and S. P. Kumar, "Sensor networks: evolution, opportunities, and challenges," *Proceedings of the IEEE*, vol. 91, no. 8, pp. 1247–1256, 2003.

[2] K. Sohraby, D. Minoli, and T. Znati, *Wireless sensor networks: technology, protocols, and applications*. John Wiley & Sons, 2007.

[3] J. Yick, B. Mukherjee, and D. Ghosal, "Wireless sensor network survey," *Computer networks*, vol. 52, no. 12, pp. 2292–2330, 2008.

[4] B. Warneke, M. Last, B. Liebowitz, and K. S. Pister, "Smart dust: communicating with a cubic-millimeter computer," *Computer*, vol. 34, no. 1, pp. 44–51, 2001.

[5] J. M. Rabaey, M. J. Ammer, J. L. da Silva, D. Patel, and S. Roundy, "Picoradio supports ad hoc ultra-low power wireless networking," *Computer*, vol. 33, no. 7, pp. 42–48, 2000.

[6] G. J. Pottie and W. J. Kaiser, "Wireless integrated network sensors," *Communications of the ACM*, vol. 43, no. 5, pp. 51–58, 2000.

[7] Y. Liu, Y. He, M. Li, J. Wang, K. Liu, and X. Li, "Does wireless sensor network scale? a measurement study on greenorbs," *Parallel and Distributed Systems, IEEE Transactions on*, vol. 24, no. 10, pp. 1983–1993, 2013.

[8] P. Dutta, J. Hui, J. Jeong, S. Kim, C. Sharp, J. Taneja, G. Tolle, K. Whitehouse, and D. Culler, "Trio: enabling sustainable and scalable outdoor wireless sensor network deployments," in *Proceedings of the 5th international conference on Information processing in sensor networks*, ACM, 2006, pp. 407–415.

[9] I. Chatzigiannakis, S. Fischer, C. Koninis, G. Mylonas, and D. Pfisterer, "Wisebed: an open large-scale wireless sensor network testbed," in *Sensor Applications, Experimentation, and Logistics*, Springer, 2009, pp. 68–87.

[10] C. B. Des Rosiers, G. Chelius, E. Fleury, A. Fraboulet, A. Gallais, N. Mitton, and T. Noël, "Senslab," in *Testbeds and Research Infrastructure. Development of Networks and Communities*, Springer, 2011, pp. 239–254.

[11] A. Arora, R. Ramnath, E. Ertin, P. Sinha, S. Bapat, V. Naik, V. Kulathumani, H. Zhang, H. Cao, M. Sridharan, *et al.*, "Exscal: elements of an extreme scale wireless sensor network," in *Embedded and Real-Time Computing Systems and Applications,*

2005. Proceedings. 11th IEEE International Conference on, IEEE, 2005, pp. 102–108.

[12] P. Rawat, K. D. Singh, H. Chaouchi, and J. M. Bonnin, "Wireless sensor networks: a survey on recent developments and potential synergies," *The Journal of supercomputing*, vol. 68, no. 1, pp. 1–48, 2014.

[13] I. F. Akyildiz, W. Su, Y. Sankarasubramaniam, and E. Cayirci, "A survey on sensor networks," *Communications magazine, IEEE*, vol. 40, no. 8, pp. 102–114, 2002.

[14] P. Huang, L. Xiao, S. Soltani, M. W. Mutka, and N. Xi, "The evolution of mac protocols in wireless sensor networks: a survey," *Communications Surveys & Tutorials, IEEE*, vol. 15, no. 1, pp. 101–120, 2013.

[15] X. Chen, K. Makki, K. Yen, and N. Pissinou, "Sensor network security: a survey," *Communications Surveys & Tutorials, IEEE*, vol. 11, no. 2, pp. 52–73, 2009.

[16] A. A. Abbasi and M. Younis, "A survey on clustering algorithms for wireless sensor networks," *Computer communications*, vol. 30, no. 14, pp. 2826–2841, 2007.

[17] K. Akkaya and M. Younis, "A survey on routing protocols for wireless sensor networks," *Ad hoc networks*, vol. 3, no. 3, pp. 325–349, 2005.

[18] J. N. Al-Karaki and A. E. Kamal, "Routing techniques in wireless sensor networks: a survey," *Wireless communications, IEEE*, vol. 11, no. 6, pp. 6–28, 2004.

[19] N. Pantazis, S. A. Nikolidakis, and D. D. Vergados, "Energy-efficient routing protocols in wireless sensor networks: a survey," *Communications Surveys & Tutorials, IEEE*, vol. 15, no. 2, pp. 551–591, 2013.

[20] J. Li and P. Mohapatra, "Analytical modeling and mitigation techniques for the energy hole problem in sensor networks," *Pervasive and Mobile Computing*, vol. 3, no. 3, pp. 233–254, 2007.

[21] E. M. Royer and C.-K. Toh, "A review of current routing protocols for ad hoc mobile wireless networks," *Personal Communications, IEEE*, vol. 6, no. 2, pp. 46–55, 1999.

[22] S. K. Singh, M. Singh, and D. Singh, "A survey of energy-efficient hierarchical cluster-based routing in wireless sensor networks," *International Journal of Advanced Networking and Application (IJANA)*, vol. 2, no. 02, pp. 570–580, 2010.

[23] D. J. Baker and A. Ephremides, "The architectural organization of a mobile radio network via a distributed algorithm," *Communications, IEEE Transactions on*, vol. 29, no. 11, pp. 1694–1701, 1981.

[24] M. Chatterjee, S. K. Das, and D. Turgut, "Wca: a weighted clustering algorithm for mobile ad hoc networks," *Cluster computing*, vol. 5, no. 2, pp. 193–204, 2002.

[25] S. Basagni, "Distributed clustering for ad hoc networks," in *Parallel Architectures, Algorithms, and Networks, 1999.(I-SPAN'99) Proceedings. Fourth International-Symposium on*, IEEE, 1999, pp. 310–315.

[26] A. D. Amis, R. Prakash, T. H. Vuong, and D. T. Huynh, "Max-min d-cluster formation in wireless ad hoc networks," in *INFOCOM 2000. Nineteenth Annual Joint Conference of the IEEE Computer and Communications Societies. Proceedings. IEEE*, IEEE, vol. 1, 2000, pp. 32–41.

[27] W. B. Heinzelman, A. P. Chandrakasan, and H. Balakrishnan, "An application-specific protocol architecture for wireless microsensor networks," *IEEE Transactions on wireless communications*, vol. 1, no. 4, pp. 660–670, 2002.

[28] W. R. Heinzelman, A. Chandrakasan, and H. Balakrishnan, "Energy-efficient communication protocol for wireless microsensor networks," in *System sciences, 2000. Proceedings of the 33rd annual Hawaii international conference on*, IEEE, 2000, 10–pp.

[29] S. Lindsey, C. Raghavendra, and K. Sivalingam, "Data gathering in sensor networks using the energy* delay metric," in *null*, IEEE, 2001, 30188b.

[30] C.-F. Chiasserini, I. Chlamtac, P. Monti, and A. Nucci, "Energy efficient design of wireless ad hoc networks," in *NETWORKING 2002: Networking Technologies, Services, and Protocols; Performance of Computer and Communication Networks; Mobile and Wireless Communications*, Springer, 2002, pp. 376–386.

[31] O. Younis and S. Fahmy, "Heed: a hybrid, energy-efficient, distributed clustering approach for ad hoc sensor networks," *Mobile Computing, IEEE Transactions on*, vol. 3, no. 4, pp. 366–379, 2004.

[32] P. Ding, J. Holliday, and A. Celik, "Distributed energy-efficient hierarchical clustering for wireless sensor networks," in *Distributed computing in sensor systems*, Springer, 2005, pp. 322–339.

[33] V. Mhatre and C. Rosenberg, "Homogeneous vs heterogeneous clustered sensor networks: a comparative study," in *Communications, 2004 IEEE International Conference on*, IEEE, vol. 6, 2004, pp. 3646–3651.

[34] Y. Jin, L. Wang, Y. Kim, and X. Yang, "Eemc: an energy-efficient multi-level clustering algorithm for large-scale wireless sensor networks," *Computer Networks*, vol. 52, no. 3, pp. 542–562, 2008.

[35] S. Bandyopadhyay and E. J. Coyle, "Minimizing communication costs in hierarchically-clustered networks of wireless sensors," *Computer Networks*, vol. 44, no. 1, pp. 1–16, 2004.

[36] M. Haenggi, J. G. Andrews, F. Baccelli, O. Dousse, and M. Franceschetti, "Stochastic geometry and random graphs for the analysis and design of wireless networks," *Selected Areas in Communications, IEEE Journal on*, vol. 27, no. 7, pp. 1029–1046, 2009.

[37] G. Chen, C. Li, M. Ye, and J. Wu, "An unequal cluster-based routing protocol in wireless sensor networks," *Wireless Networks*, vol. 15, no. 2, pp. 193–207, 2009.

[38] H. Li, Y. Liu, W. Chen, W. Jia, B. Li, and J. Xiong, "Coca: constructing optimal clustering architecture to maximize sensor network lifetime," *Computer Communications*, vol. 36, no. 3, pp. 256–268, 2013.

[39] R. V. Kulkarni and G. K. Venayagamoorthy, "Particle swarm optimization in wireless-sensor networks: a brief survey," *Systems, Man, and Cybernetics, Part C: Applications and Reviews, IEEE Transactions on*, vol. 41, no. 2, pp. 262–267, 2011.

[40] D. Karaboga, S. Okdem, and C. Ozturk, "Cluster based wireless sensor network routing using artificial bee colony algorithm," *Wireless Networks*, vol. 18, no. 7, pp. 847–860, 2012.

[41] S. Hussain, A. W. Matin, and O. Islam, "Genetic algorithm for hierarchical wireless sensor networks," *Journal of Networks*, vol. 2, no. 5, pp. 87–97, 2007.

[42] I. Gupta, D. Riordan, and S. Sampalli, "Cluster-head election using fuzzy logic for wireless sensor networks," in *Communication Networks and Services Research Conference, 2005. Proceedings of the 3rd Annual*, IEEE, 2005, pp. 255–260.

[43] T. Rault, A. Bouabdallah, and Y. Challal, "Energy efficiency in wireless sensor networks: a top-down survey," *Computer Networks*, vol. 67, pp. 104–122, 2014.

[44] Z Chair and P. K. Varshney, "Optimal data fusion in multiple sensor detection systems," *Aerospace and Electronic Systems, IEEE Transactions on*, no. 1, pp. 98–101, 1986.

[45] S. S. Pradhan, J. Kusuma, and K. Ramchandran, "Distributed compression in a dense microsensor network," *Signal Processing Magazine, IEEE*, vol. 19, no. 2, pp. 51–60, 2002.

[46] T. Bass, "Intrusion detection systems and multisensor data fusion," *Communications of the ACM*, vol. 43, no. 4, pp. 99–105, 2000.

[47] G. Bontempi and Y Le Borgne, "An adaptive modular approach to the mining of sensor network data," in *Proceedings of 1st International Workshop on Data Mining in Sensor Networks as part of the SIAM International Conference on Data Mining*, SIAM Press Newport Beach, CA, 2005, pp. 3–9.

[48] J.-L. Rougier, D. Kofman, and A. Gravey, "Optimization of hierarchical routing protocols," *Performance Evaluation*, vol. 41, no. 2, pp. 227–245, 2000.

[49] N. Bansal, T. Sharma, M. Misra, and R. C. Joshi, "Ftep: a fault tolerant election protocol for multi-level clustering in homogeneous wireless sensor networks," in *Networks, 2008. ICON 2008. 16th IEEE International Conference on*, IEEE, 2008, pp. 1–6.

[50] E. M. Belding-Royer, "Multi-level hierarchies for scalable ad hoc routing," *Wireless Networks*, vol. 9, no. 5, pp. 461–478, 2003.

[51] S. Yi, J. Heo, Y. Cho, and J. Hong, "Peach: power-efficient and adaptive clustering hierarchy protocol for wireless sensor networks," *Computer communications*, vol. 30, no. 14, pp. 2842–2852, 2007.

[52] Z. Yu, X. Fu, Y. Cai, and M. C. Vuran, "A reliable energy-efficient multi-level routing algorithm for wireless sensor networks using fuzzy petri nets," *Sensors*, vol. 11, no. 3, pp. 3381–3400, 2011.

[53] R. Ramanathan and M. Steenstrup, "Hierarchically-organized, multihop mobile wireless networks for quality-of-service support," *Mobile networks and applications*, vol. 3, no. 1, pp. 101–119, 1998.

[54] L. Kleinrock and F. Kamoun, "Hierarchical routing for large networks performance evaluation and optimization," *Computer Networks (1976)*, vol. 1, no. 3, pp. 155–174, 1977.

[55] ——, "Optimal clustering structures for hierarchical topological design of large computer networks," *Networks*, vol. 10, no. 3, pp. 221–248, 1980.

[56] S. Bandyopadhyay and E. J. Coyle, "An energy efficient hierarchical clustering algorithm for wireless sensor networks," in *INFOCOM 2003. Twenty-Second Annual Joint Conference of the IEEE Computer and Communications. IEEE Societies*, IEEE, vol. 3, 2003, pp. 1713–1723.

[57] F Baccelli, K Tchoumatchenko, and S Zuyev, "Markov paths on the poisson-delaunay graph with applications to routeing in mobile networks," *Advances in Applied Probability*, pp. 1–18, 2000.

[58] S. Foss and S. Zuyev, "On a voronoi aggregative process related to a bivariate poisson process," *Advances in Applied Probability*, pp. 965–981, 1996.

[59] S. Bandyopadhyay, Q. Tian, and E. J. Coyle, "Spatio-temporal sampling rates and energy efficiency in wireless sensor networks," *IEEE/ACM Transactions on Networking (TON)*, vol. 13, no. 6, pp. 1339–1352, 2005.

[60] J. D'Errico, *Bounded minimum search*, Retrieved Jan 2016.

[61] J. C. Lagarias, J. A. Reeds, M. H. Wright, and P. E. Wright, "Convergence properties of the nelder–mead simplex method in low dimensions," *SIAM Journal on optimization*, vol. 9, no. 1, pp. 112–147, 1998.

[62] P. Santi and D. M. Blough, "The critical transmitting range for connectivity in sparse wireless ad hoc networks," *IEEE transactions on Mobile Computing*, vol. 2, no. 1, pp. 25–39, 2003.

[63] F. Xiangning and S. Yulin, "Improvement on leach protocol of wireless sensor network," in *Sensor Technologies and Applications, 2007. SensorComm 2007. International Conference on*, IEEE, 2007, pp. 260–264.

[64] D. Phanish and E. J. Coyle, "Application-based optimization of multi-level clustering in ad hoc and sensor networks," *IEEE Transactions on Wireless Communications*, 2017.

[65] K. Akkaya and M. Younis, "An energy-aware qos routing protocol for wireless sensor networks," in *Distributed Computing Systems Workshops, 2003. Proceedings. 23rd International Conference on*, IEEE, 2003, pp. 710–715.

[66] T. Clausen and P. Jacquet, "Optimized link state routing protocol (olsr)," Tech. Rep., 2003.

[67] C. Perkins, E. Belding-Royer, and S. Das, "Ad hoc on-demand distance vector (aodv) routing," Tech. Rep., 2003.

[68] B. Karp, "Geographic routing for wireless networks," PhD thesis, Harvard University, Cambridge, MA, Oct. 2000.

[69] S. Biswas and R. Morris, "Opportunistic routing in multi-hop wireless networks," *ACM SIGCOMM Computer Communication Review*, vol. 34, no. 1, pp. 69–74, 2004.

[70] F. Baccelli, B. Błaszczyszyn, and P. Mühlethaler, "Time–space opportunistic routing in wireless ad hoc networks: algorithms and performance optimization by stochastic geometry," *The Computer Journal*, vol. 53, no. 5, pp. 592–609, 2009.

[71] E Coyle and B. Liu, "A matrix representation of csma/cd networks," *IEEE Transactions on Communications*, vol. 33, no. 1, pp. 53–64, 1985.

[72] S. L. Beuerman and E. J. Coyle, "The delay characteristics of csma/cd networks," *IEEE Transactions on Communications*, vol. 36, no. 5, pp. 553–563, 1988.

[73] L. D. Elsgolc, *Calculus of variations*. Courier Corporation, 2012.

[74] T. R. Henderson, M. Lacage, G. F. Riley, C Dowell, and J Kopena, "Network simulations with the ns-3 simulator," *SIGCOMM demonstration*, vol. 14, no. 14, p. 527, 2008.

[75] *Network simulator 3*, Retrieved Sept 2017.

[76] F. Xue and P. R. Kumar, "The number of neighbors needed for connectivity of wireless networks," *Wireless networks*, vol. 10, no. 2, pp. 169–181, 2004.

[77] M. Haenggi, "Mean interference in hard-core wireless networks," *Communications Letters, IEEE*, vol. 15, no. 8, pp. 792–794, 2011.

[78] B. Matérn, *Spatial variation*. Springer Science & Business Media, 2013, vol. 36.

[79] E. Spodarev, *Stochastic geometry, spatial statistics and random fields: asymptotic methods*. Springer, 2013, vol. 2068.

[80] F. Voss, C. Gloaguen, V. Schmidt, *et al.*, "Scaling limits for shortest path lengths along the edges of stationary tessellations," *Advances in Applied Probability*, vol. 42, no. 4, pp. 936–952, 2010.

[81] C. Gloaguen, F. Voss, and V. Schmidt, "Parametric distance distributions for fixed access network analysis and planning," in *Teletraffic Congress, 2009. ITC 21 2009. 21st International*, IEEE, 2009, pp. 1–8.

[82] E. J. Coyle, J. P. Allebach, and J. G. Krueger, "The vertically-integrated projects (vip) program in ece at purdue: fully integrating undergraduate education and graduate research," in *Proceedings of the 2006 ASEE Annual Conference and Exposition*, Citeseer, 2006, pp. 18–21.

[83] J. P. Lynch, K. H. Law, A. S. Kiremidjian, E. Carryer, C. R. Farrar, H. Sohn, D. W. Allen, B. Nadler, and J. R. Wait, "Design and performance validation of a wireless sensing unit for structural monitoring applications," *Structural Engineering and Mechanics*, vol. 17, no. 3-4, pp. 393–408, 2004.

[84] Y. Wang, J. P. Lynch, and K. H. Law, "A wireless structural health monitoring system with multithreaded sensing devices: design and validation," *Structure and Infrastructure Engineering*, vol. 3, no. 2, pp. 103–120, 2007.

[85] J. Rodrigues and P. Almeida, "Modeling of action induced by crowds on brazilian football stadium," in *Conference: IMAC XXIV–Conference & Exposition on Structural Dynamics*, 2006.

[86] F. N. Catbas, M. Gul, and H. O. Sazak, "Dynamic testing and analysis of a football stadium," in *Dynamics of Civil Structures, Volume 4*, Springer, 2011, pp. 195–203.

[87] J. Hill, M. Horton, R. Kling, and L. Krishnamurthy, "The platforms enabling wireless sensor networks," *Communications of the ACM*, vol. 47, no. 6, pp. 41–46, 2004.

[88] G. Werner-Allen, P. Swieskowski, and M. Welsh, "Motelab: a wireless sensor network testbed," in *Proceedings of the 4th international symposium on Information processing in sensor networks*, IEEE Press, 2005, p. 68.

[89] N. Xu, S. Rangwala, K. K. Chintalapudi, D. Ganesan, A. Broad, R. Govindan, and D. Estrin, "A wireless sensor network for structural monitoring," in *Proceedings of the 2nd international conference on Embedded networked sensor systems*, ACM, 2004, pp. 13–24.

[90] Texas Instruments, *SimpliciTI compliant RF protocol stack vCCS-1.1.1*, `http://www.ti.com/tool/simpliciti`, accessed 06-Dec-2014.

[91] X Dong, D Zhu, Y Wang, J. P. Lynch, and R. A. Swartz, "Design and validation of acceleration measurement using the martlet wireless sensing system," *ASME Smart Materials, Adaptive Structures and Intelligent Systems (SMASIS), Newport, RI*, 2014.

[92] *GNURadio*, `http://www.gnuradio.org/`, accessed 06-Dec-2014.

[93] J. Malsbury, *Gr-mac*, `https://github.com/jmalsbury/gr-mac`, accessed 06-Dec-2014.

[94] VIP eStadium, *Vibration data at Bobby Dodd stadium*, `http://sensornets.vip.gatech.edu/sensornets_data.html`, accessed 06-Dec-2014.

[95] B. Sundararaman, U. Buy, and A. D. Kshemkalyani, "Clock synchronization for wireless sensor networks: a survey," *Ad Hoc Networks*, vol. 3, no. 3, pp. 281–323, 2005.

VITA

Deepa Phanish received the Bachelor of Engineering degree in Electronics and Communication from Visvesvaraya Technological University, Karnataka, India, in 2009. From 2009 to 2011, she worked in the embedded systems industry on software development and optimization of multimedia codecs. She received the M.S. degree in Electrical and Computer Engineering from Georgia Institute of Technology, Atlanta, GA in 2013. She is currently pursuing the Ph.D. degree and she is a lead researcher on the eStadium VIP team, which designs, develops, tests, deploys, and operates an IoT in the football stadium at Georgia Tech. Her research interests include design of networking protocols, embedded systems and high performance scientific computing.